

**SYNTHESIS, CHARACTERIZATION AND
INVESTIGATION OF METHYL ORANGE DYE
DEGRADATION USING Ag/MoO₃/TiO₂
NANOCOMPOSITE UNDER UV-IRRADIATION**

SHAHINA KADER

A thesis submitted to the Department of Chemical Engineering in partial
fulfillment of the requirements for the degree of
MASTER OF SCIENCE IN ENGINEERING (CHEMICAL)



DEPARTMENT OF CHEMICAL ENGINEERING
BANGLADESH UNIVERSITY OF ENGINEERING AND
TECHNOLOGY (BUET)
DHAKA, BANGLADESH

MARCH, 2021

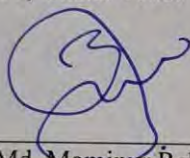
CERTIFICATION OF THESIS WORK

We the undersigned, glad to certify that **Shahina Kader**, candidate for the degree of Master of Science in Engineering (Chemical) has presented her thesis work title “**Synthesis, Characterization and Investigation of Methyl Orange Dye Degradation using Ag/MoO₃/TiO₂ Nanocomposite under UV-Irradiation**”. The thesis is acceptable in form and content. The student demonstrated satisfactory knowledge of the field covered by this thesis in an oral examination held on 13 March, 2021.



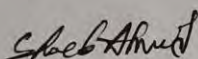
Dr. Md. Shahinoor Islam
Associate Professor
Department of Chemical Engineering
BUET, Dhaka-1000.

**Chairman
(Supervisor)**



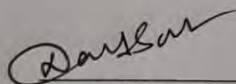
Dr. Md. Mominur Rahman
Professor and Head
Department of Chemical Engineering
BUET, Dhaka-1000.

**Member
(Ex-Officio)**



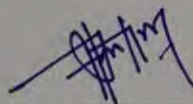
Dr. Shoeb Ahmed
Associate Professor
Department of Chemical Engineering
BUET, Dhaka-1000.

Member



Dr. Nahid Sanzida
Associate Professor
Department of Chemical Engineering
BUET, Dhaka-1000.

Member



Dr. Shakhawat Hossain Firoz
Professor and Head
Department of Chemistry
BUET, Dhaka-1000.

**Member
(External)**

CANDIDATE'S DECLARATION

It is hereby, declared that this thesis paper or any part of it has not been submitted anywhere else for the award of any degree or diploma.

Signature of the Candidate



Shahina Kader

Student ID: 0416022009

13 March, 2021

ABSTRACT

Advanced oxidation processes (AOPs) are considered as the most efficient and highly attractive process for the degradation of azo dyes from textile wastewater. In this process, a strong oxidizing radical known as hydroxyl radical ($\cdot\text{OH}$) is produced, which can react with organics unselectively until mineralization. Titanium dioxide (TiO_2) based photocatalytic process has been utilized widely in last few decades because of its higher photocatalytic activity to degrade organics from textile wastewater. Doping of TiO_2 with noble metals (Ag, MoO_3) can increase the performance of TiO_2 . Therefore, the major objectives of this study were to synthesize Ag/ MoO_3 / TiO_2 nanocomposite, design and construction of UV-Ag/ MoO_3 / TiO_2 nanocomposite immobilized reactor using borosilicate glass (BG), and finally investigation and optimization of the UV-Ag/ MoO_3 / TiO_2 nanocomposite reactor performance for the treatment of methyl orange (MO) dye. The photocatalysts of TiO_2 , MoO_3 / TiO_2 , Ag/ TiO_2 , and Ag/ MoO_3 / TiO_2 were synthesized by sol-gel and heat treatment methods. The physico-chemical properties of all the photocatalysts were analyzed by applying X-ray diffraction (XRD), Scanning electron microscopy (SEM), Fourier transform infrared spectroscopy (FT-IR), UV-Vis diffuse reflectance spectroscopy (UV-Vis/DRS), and Brunauer–Emmett–Teller (BET). The XRD showed the increased amount of anatase phase of Ag/ MoO_3 / TiO_2 nanocomposite compared to TiO_2 nanoparticles and MoO_3 / TiO_2 and Ag/ TiO_2 nanocomposites. The photocatalytic removals of MO dye (10 ppm) were found 59.5%, 63.1%, 70.6% and 75.8%, for TiO_2 , MoO_3 / TiO_2 , Ag/ TiO_2 , and Ag/ MoO_3 / TiO_2 , respectively, for a particular dose of photocatalyst (0.120 g) at pH 7.0 with 5.5 h of contact time. The impact of operating parameters such as initial dye concentration, pH and hydrogen peroxide (H_2O_2) dose was evaluated. The photocatalytic performance was decreased with increase of pH and initial dye concentration, and increased with the addition of photocatalyst and H_2O_2 in the reactor. The reaction kinetics were consistent with the first-order kinetic model and rate constant values were 0.003 min^{-1} , 0.002 min^{-1} , 0.003 min^{-1} , and 0.004 min^{-1} for TiO_2 , MoO_3 / TiO_2 , Ag/ TiO_2 , and Ag/ MoO_3 / TiO_2 , respectively, for 0.120 g of photocatalyst dose. Thus, the outcomes from the current study suggest that the synthesized Ag/ MoO_3 / TiO_2 nanocomposite has a great potential for the treatment of organics present in textile wastewater under UV-radiation.

ACKNOWLEDGEMENT

I would like to convey my heartfelt appreciation and gratitude to them whose blessing and cooperation was important to bring this work in light. Firstly, I would like to praise the name of the almighty Allah, for giving me patience and courage to carry out the research work successfully.

I wish to express profound sense of gratitude to my supervisor **Dr. Md. Shahinoor Islam**, Associate professor, Dept. of Chemical Engineering, Bangladesh University of Engineering and Technology (BUET) for his guidance, sincere, valuable comments, encouragement, enthusiasms and all round support. It is a great pleasure to thank him for his generous contribution to the conception and creation of the thesis dissertation.

I am grateful to the authority of BUET for providing financial support for this research work.

I would like to thank the project partner **Sanzeeda Baig Shuchi, Md. Burhan Kabir Suhan** and **Md. Rashid Al-Mamun** for their contribution, friendly attitude, and help throughout the research work.

In addition, my sincere thanks go to all my friends, seniors and husband for their continuous inspirations, moral supports who have patiently extended all sorts of help for accomplishing this undertaking.

Finally, I could never accomplished any of my successes including this particular work till date without my loving parents. I still believe that I owe them a lot for their unconditional love, support and sacrifice.

TABLE OF CONTENTS

	Page
	No.
<i>ABSTRACT</i>	i
<i>ACKNOWLEDGEMENT</i>	ii
<i>LIST OF FIGURES</i>	vi-vii
<i>LIST OF TABLES</i>	viii
CHAPTER 1	
INTRODUCTION	
1.1 Background	01
1.2 Significance of the study	03
1.3 Objectives of the study	05
1.4 Organizational outline of thesis	05
CHAPTER 2	
LITERATURE REVIEW	
2.1 Photochemical advanced oxidation processes	07
2.2 Heterogeneous photocatalysis	08
2.3 Advanced semiconductor photocatalyst	09
2.3.1 Titanium dioxide (TiO ₂) photocatalyst	09
2.4 Preparation of photocatalytic materials	11
2.4.1 Sol-gel process	11
2.4.2 Sol-gel chemistry	13
2.5 Modified and unmodified TiO ₂ based photocatalyst	13
2.5.1 Bulk modification of TiO ₂ photocatalyst	14
2.5.2 Electronic properties and optical response of TiO ₂ photocatalyst	15
2.6 Mechanism and Reaction Kinetics of TiO ₂ Photocatalysis	16
2.7 Reactor configuration of photocatalysis	18
2.7.1 Immobilization procedure of TiO ₂ based photocatalyst	20
2.8 Photocatalytic model dye compound	20
2.8.1 Azo dyes	20
2.8.2 Methyl orange	21

2.9	Selection of radiation sources	21
2.10	Factors affecting photocatalytic activity	22
2.11	Characterization techniques of photocatalyst materials	26

CHAPTER 3

MATERIALS AND METHODOLOGY

3.1	Materials	30
3.1.1	Chemicals	30
3.1.2	Equipment and analytical instruments	30
3.2	Experimental Methods	31
3.3	Synthesis of photocatalysts using sol-gel and heat treatment method	31
3.4	Characterization Techniques of TiO ₂ Based photocatalyst	32
3.4.1	X-Ray diffraction (XRD)	32
3.4.2	Scanning electron microscope (SEM)	33
3.4.3	Fourier transform infrared spectroscopy (FTIR)	33
3.4.4	UV-Vis diffuse reflectance spectrophotometer (UV-Vis/DRS)	33
3.4.5	Brunauer–emmett–teller isotherm (BET)	34
3.5	Design and construction of TiO ₂ immobilized materials	34
3.5.1	Immobilization of TiO ₂ based photocatalyst on BG	34
3.6	Experimental Set-up	35
3.7	Photocatalytic degradation of MO dye under UV radiation	36
3.7.1	Preparation of desired concentrated methyl orange solution	36
3.7.2	Calibration curve	37
3.7.3	Photocatalytic reactor activity and batch adsorption	37
3.7.4	Optimization of reactor performance	38
3.7.5	Reaction kinetics and mathematical equations	39

CHAPTER 4

RESULTS AND DISCUSSION

4.1	Characterization of photocatalysts	41
4.1.1	X-ray Diffraction (XRD) of photocatalyst	41
4.1.2	Scanning electron microscope (SEM) of photocatalyst	44
4.1.3	Fourier transform infrared spectroscopy (FT-IR) of photocatalyst	46

4.1.4	UV-Vis diffuse reflectance spectroscopy (UV-Vis/DRS) of photocatalyst	47
4.1.5	Nitrogen physisorption measurement (BET) of photocatalyst	49
4.2	Photocatalytic activity assessment	50
4.2.1	Reactors performance evaluation	51
4.2.2	Reaction kinetics study	51
4.2.3	Impact of pH	53
4.2.4	Impact of photocatalyst dose	54
4.3	Impact of dye concentration and hydrogen peroxide concentration on reactor performance	56
4.3.1	Impact of dye concentration	56
4.3.2	Impact of hydrogen peroxide (H ₂ O ₂) concentration	57
CHAPTER 5		
CONCLUSION		
5.1	Conclusion	60
REFERENCES		
APPENDIX		
Appendix A	Experimental UV reactor with apparatus	80
Appendix B	BET isotherm study	81
Appendix C	Reaction kinetic study	83

LIST OF FIGURES		Page
		No.
Figure 2.1	Generalized scheme of sol-gel synthesis	12
Figure 2.2	The bonding diagram of a perfect TiO ₂ crystal	16
Figure 2.3	Schematic demonstration of the photochemical steps in semiconducting TiO ₂	18
Figure 2.4	Configuration of photocatalytic membrane reactors	19
Figure 2.5	Chemical structure of MO	21
Figure 3.1	A set-up of UV-TiO ₂ immobilized photocatalytic reactor	36
Figure 3.2	Calibration curve of MO for dye degradation	37
Figure 4.1	XRD plot of all synthesized photocatalysts (a) TiO ₂ , (b) MoO ₃ /TiO ₂ , (c) Ag/TiO ₂ , and (d) Ag/MoO ₃ /TiO ₂	43
Figure 4.2	SEM image of all synthesized photocatalysts (a) TiO ₂ , (c) MoO ₃ /TiO ₂ , (e) Ag/TiO ₂ , and (g) Ag/MoO ₃ /TiO ₂ ; and particle size diameter of photocatalysts (b) TiO ₂ , (d) MoO ₃ /TiO ₂ , (f) Ag/TiO ₂ , and (h) Ag/MoO ₃ /TiO ₂	45
Figure 4.3	FT-IR analysis of all synthesized photocatalysts; (a) TiO ₂ , (b) MoO ₃ /TiO ₂ , (c) Ag/TiO ₂ , and (d) Ag/MoO ₃ /TiO ₂	46
Figure 4.4	UV/Vis response of synthesized photocatalysts; (a) absorbance graphs, and (b) reflectance graphs	47
Figure 4.5	Bandgap energy of all photocatalysts (a) TiO ₂ , (b) MoO ₃ /TiO ₂ , (c) Ag/TiO ₂ , and (d) Ag/MoO ₃ /TiO ₂ nanocomposites	49
Figure 4.6	MO dye removal under UV irradiation (Experimental condition: Ag/Mo/TiO ₂ immobilized on BG reactors: 120 mg, pH: 7.0, initial MO dye conc.: 10 ppm)	51
Figure 4.7	Pseudo first-order reaction kinetics of MO dye degradation in presence of UV irradiation (Experimental condition: dose of Ag/Mo/TiO ₂ immobilized on BG reactors: 120 mg, pH: 7.0, initial MO dye conc.: 10 ppm)	52
Figure 4.8	Impact of pH on MO degradation efficiency; (a) TiO ₂ , (b) Mo/TiO ₂ , (c) Ag/TiO ₂ , and (d) Ag/Mo/TiO ₂ photocatalyst under UV irradiation (Experimental condition: 0.120 g of photocatalyst on immobilized reactor, dye concentration: 10 ppm, pH: 3.0, 7.0, and 11.0)	54

Figure 4.9	MO dye degradation under UV irradiation (Experimental condition: dose of Ag/Mo/TiO ₂ immobilized on BG reactors: 120 mg, pH: 3.0, initial MO dye conc.: 10 ppm)	55
Figure 4.10	Impact of initial MO concentration on the degradation efficiency (Experimental condition: dose of Ag/Mo/TiO ₂ immobilized on BG reactors: 120 mg, pH: 3.0, initial MO dye conc.: 10 ppm)	57
Figure 4.11	Impact of H ₂ O ₂ concentration on the degradation efficiency (Experimental condition: dose of Ag/Mo/TiO ₂ immobilized on BG reactors: 120 mg, pH: 3.0). (a) 10 ppm initial dye concentration with addition of 0.1 and 0.25 mL H ₂ O ₂ concentration, (b) 30 ppm initial dye concentration with addition of 0.1 and 0.25 mL H ₂ O ₂ concentration, and (c) 50 ppm initial dye concentration with addition of 0.1 and 0.25 mL H ₂ O ₂ concentration.	59

LIST OF TABLES

		Page
		No.
Table 2.1	Bandgap energy of some metal oxide photocatalysts	09
Table 2.2	Crystallographic and physical properties of TiO ₂ photocatalyst	10
Table 4.1	Summary of theoretical physicochemical properties of TiO ₂ nanoparticles	42
Table 4.2	The bandgap energy (eV) of all TiO ₂ based nanocomposites prepared with sol-gel by using Kubelka-Munk equation.	48
Table 4.3	Surface area and pore volume measurement of all composites	50

CHAPTER 1

INTRODUCTION

This chapter reveals the importance of the study with respect to the current situation of the industry. The scope and significance of the research work have been discussed concerning to industrial and commercial aspects. Finally, the chapter includes the research objectives and organization of the thesis.

1.1 Background

In recent years, water pollution has been considered a major issue because a large number of unwanted contaminants are being discharged into the surface water from different industrial sources such as textile, dyeing, food, pharmaceuticals, plastics, leather, pulp and paper, sugar, petroleum and metal works [1, 2]. Among these sources, textile industries are found to be the highest polluting source since a large quantity of wastewater is generated every day [3, 4]. The wastewater generated from the textile industry contains a higher concentration of inorganics and organics compared to wastewaters generated from other industries. Typically, the textile wastewater contains dyes, suspended solids, dissolved solids and heavy metals, which correspond to high BOD, COD, and intense color that are discharged after partial treatment [1, 5]. Textile azo dyes are mostly bio-persistent, carcinogenic, mutagenic, and toxic to the environment that can cause serious damage to human health such as skin irritation, nausea, headache, and congenital malformation [6, 7]. A common type of azo dye is methyl orange (MO), which has shown many detrimental consequences on the environment. Typically, it resists bio-degradation because of its fused aromatic ring structure. It can also be easily reduced to toxic amines because of the presence of the azo group in the structure. This indicates a potential treatment strategy is badly needed to manage this wastewater for sustainable development of the textile sector.

Various treatment technologies such as physical (filtration, adsorption, ion exchange), biological (bio-sorption, bioaccumulation, biodegradation), and chemical processes (oxidation, ozonation, and electrochemical) have been developed for the treatment of textile wastewater. All conventional treatment technologies have some limitations for the degradation of organic dye compounds such as high energy consumption, high chemical consumption, operating cost, sludge production, toxic gas release and thus, considered as a

ineffective treatment process [6, 8, 9]. In the last few decades, the researchers have suggested that the best possible solution might be formulated with several existing techniques together. The recommended arrangement was the physico-chemical treatment followed by advanced tertiary treatment techniques [10]. The advanced tertiary treatment techniques are of three major categories including physical, physico-chemical, and chemical techniques such as advanced oxidation processes (AOPs). In AOPs, a highly reactive hydroxyl radical ($\cdot\text{OH}$) is generated that can degrade a broad range of pollutants non-selectively and quickly into carbon dioxide (CO_2), and water (H_2O) [6, 11]. Recently, the semiconductor photocatalysts including TiO_2 [12], CdS [13], ZnO [14], ZnS [15], SnO_2 [16], SiO_2 [17], Al_2O_3 [18], ZrO_3 [19], and WO_3 [20] have received greater attention for the treatment of textile dye-containing wastewater.

Among those semiconductor photocatalysts, TiO_2 has received as one of the most emerging photocatalyst for effective remediation of contaminated water due to its low cost, low operating temperature, biologically inert nature, low energy consumption, water insolubility, high chemical stability, less toxicity, narrow bandgap ($\sim 3.0 - 3.2 \text{ eV}$), wide spectrum, environmentally benign, and safety toward both environment and human [6]. In photocatalytic process, the degradation is observed when the semiconductor photocatalyst absorbs UV-radiation. Generally, UV-radiation itself is not capable to generate $\cdot\text{OH}$ to degrade dye or organics in water, but combination with TiO_2 semiconductor it can generate $\cdot\text{OH}$ to degrade organics [21]. When semiconductor TiO_2 absorbs UV-radiation at wavelength $< 400 \text{ nm}$, the electrons (e^-) are excited by photon energy and forms charge carriers of conduction band electron (e_{CB}^-) and valance band hole (h_{VB}^+), respectively. This charge carriers are recombined and scavenged with OH^- , H_2O , and organic compounds in presence of O_2 and forms $\cdot\text{OH}$, and superoxide radical anions (O_2^-) on TiO_2 surface that are capable of degrading a large variety of organic compounds [6, 22]. In the last decade, several strategies have been focused namely chemical and morphological modification to enhance charge separation and visible light region of TiO_2 which would permit the use of UV-radiation [23]. The morphological modification was developed by increasing the surface area, pore-volume, and porosity of semiconductor materials. Several research have conducted study on chemical modification of TiO_2 such as metal doping [24], non-metal doping [25], co-doping with metal/metal [26], co-doping with non-metal/non-metal [23], and co-doping with metal/non-metal [27] in the treatment of dye solution. Doping or co-doping of metal/non-metals [28]

with TiO₂ crystal structure under UV-radiation has been demonstrated as the most potential path towards bandgap energy reduction in order to increase the active catalyst site [6, 29]. Metal doping or co-doping can be easily introduced into the TiO₂ lattice crystal structure due to their comparable ionic radius [6]. The uses of noble metals have properties to increase charge carrier separation, which consequently increases the photo-induced electron transmit rate at the edge [30]. Among all the noble metals, silver has received greater potential in TiO₂ photocatalyst's surface that can enhance the photocatalytic activity. This enhancement is mainly due to its distinctive surface plasmon resonance property which acts as an electron sink and assists to reduce electron recombination [31]. The next suitable semiconductor is MoO₃ (n-type semiconductor with a bandgap of 2.9 eV), which has also shown positive aspect and considered a comparatively cheap and less consumable that can replace the WO₃ [30].

In photocatalytic degradation, the semiconductor photocatalyst is used as a suspension and thin-film/immobilization. However, the major disadvantage of the suspension method of application of TiO₂ photocatalyst is the separation/filtration of the TiO₂ from the treated wastewater that increases the total treatment cost [32]. To address this issue, TiO₂ based nanocomposites are immobilized on various supporting materials such as glass, ceramics, polymeric material, stainless steel, silica, cellulose, etc. that have greater potential for enhancing the photocatalytic process performance [33, 34]. The most commonly used supporting material is glass due to its high transparency to the UV-radiation, chemical inertness, low cost, good adherence capability, resistance to the corrosive environment, and high calcination temperature [35].

Several techniques have been employed for the synthesis of TiO₂ crystal structure such as sol-gel method [3], precipitation method [3], sonochemical method [36], chemical vapor deposition method [3], hydrothermal [37], solvothermal method [3], and thermal decomposition of alkoxide method [3]. Among those synthesis techniques, sol-gel is a very simple, effective, economical, and eases of maintenance for preparing nanoparticles [3].

1.2 Significance of the Study

The textile industry is one of the largest growing and profitable sectors in Bangladesh. More than 4500 textile industries grew up in the country, and the export stood around \$30 billion per year from this sector. The textile, in particular, contributes around 80% of all the exports, which contributes 20% of GDP. Moreover, around 4 million people are working in this sector

which contributes about 45 percent of all industrial employment and contributes 5% to the total national income [38]. Therefore, textile sector is playing a key role in Bangladesh's economy by earning foreign currency and providing employment opportunity.

Although textile provides significant economic benefits both employment and government revenue, it also faces the environmental and social impacts associated with the generations of toxic wastewaters from its wet processing operations. Consequently, a huge amount of wastewater is generated every day. The wastewater is discharged to the environment after ineffective conventional treatment techniques. The discharge of this ineffectively treated wastewater gives rise to an alarming environmental concern related to water pollution. The possible solution can be done by the modification of existing wastewater treatment processes using TiO₂ based photocatalysts. The addition of AOPs with conventional treatment schemes seems to be the right step to make the treatment system more efficient and effective. Therefore, this current research was an attempt to synthesize TiO₂ based photocatalysts for enhancing visible light photocatalytic performance. The synthesized photocatalyst will be able to degrade model textile MO dye (model azo dye) using TiO₂ photocatalyst-immobilized on BG reactor under a self-designed UV photocatalytic reactor. However, in Bangladesh, the TiO₂ based photocatalytic wastewater treatment application is still not being considered. Thus, the proposed research will reveal the comprehensive and fundamental assessments of the photocatalytic concept for the treatment of textile and other industrial wastewaters. The knowledge from this research will contribute to applying the technique on a large scale for the treatment of wastewater to achieve the zero discharge.

Recently, the foreign investors are creating pressure on the textile industry for proper treatment of wastewater before disposal to the water intake body. Based on the foreign pressure, the Department of Environment (DoE), Bangladesh has imposed a road map of zero liquid discharge on every industry to be implemented. However, the existing ETPs in local industries are not adequately equipped for attaining zero discharge. Therefore, the main purpose of the proposed study was to investigate a modified TiO₂ based photocatalyst for the treatment of textile wastewater in presence of UV-radiation. Thus, the proposed technology in combined with the existing conventional technology will assist to remove toxic and biopersistent dye contaminants effectively and the treated effluent will be mineralized completely which will in turn lead to zero liquid discharge. This is not achievable by using the existing technology alone. The process illustrated in this paper will be able to provide knowledge on laboratory scale research and further need to scale-up for industrial

application. Thus, it is expected that the outcome from the current research will assist to improve the conventional wastewater treatment technology and will help to develop sustain economic growth of the textile sector in Bangladesh.

1.3 Objectives of the Study

The main objective of this study was to investigate the UV-photocatalytic reactor performance using laboratory synthesized TiO_2 photocatalyst, and $\text{MoO}_3/\text{TiO}_2$, Ag/TiO_2 , and $\text{Ag}/\text{MoO}_3/\text{TiO}_2$ nanocomposites on MO dye degradation. The specific aims under the main objective to be covered were listed below:

- Synthesis of TiO_2 photocatalyst, and $\text{MoO}_3/\text{TiO}_2$, Ag/TiO_2 , and $\text{Ag}/\text{MoO}_3/\text{TiO}_2$ nanocomposites using sol-gel technique and heat treatment method.
- Characterization of TiO_2 photocatalyst, and $\text{MoO}_3/\text{TiO}_2$, Ag/TiO_2 , and $\text{Ag}/\text{MoO}_3/\text{TiO}_2$ nanocomposites using X-ray diffraction (XRD, for crystal structure), Scanning electron microscopy (SEM, for surface morphology), Fourier transform infrared spectroscopy (FT-IR, for the surface functional group), Ultra-violet visible spectroscopy (UV-Vis, for absorption edge and bandgap energy) and Brunauer–Emmett–Teller (BET, for the surface area).
- Assessment of borosilicate glass-photocatalysts (TiO_2 , $\text{MoO}_3/\text{TiO}_2$, Ag/TiO_2 , and $\text{Ag}/\text{MoO}_3/\text{TiO}_2$) immobilized reactor performance in the degradation of MO dye.
- Optimization of UV-reactor performance based on dye degradation by changing pH, dye concentration, and w/o addition of H_2O_2 .

1.4 Organization of the Thesis

The thesis paper has five distinct chapters. The outline of each chapter is given below:

Chapter 1 provides the introductory background, significance, and objectives of this study.

Chapter 2 reviews past work related to the general knowledge of photochemical advanced oxidation process, heterogeneous photocatalysis, and advances photocatalyst materials. It also gives an overview of photocatalytic reaction mechanisms, synthesis techniques and modification, photocatalyst immobilization, and factors affecting the photocatalytic activity. Finally, this chapter was associated with characterization techniques of photocatalysts.

Chapter 3 provides all the experimental methods, principles and procedures employed during this study. Firstly, the sol-gel preparation technique of TiO₂ based photocatalyst nanocomposites has been presented in the chapter. Secondly, the chapter includes all characterization techniques of TiO₂ based nanocomposites. Thirdly, the chapter includes the immobilization of TiO₂ photocatalyst and photocatalytic experimental setup diagram with detailed experimental procedures for the degradation of MO dye under UV-radiation.

Chapter 4 provides the results and discussion of the research work. Firstly, it discusses all the characterization techniques and compared the outcomes with relevant literature. Secondly, it discusses the photocatalytic performance of immobilized-Ag/MoO₃/TiO₂ on BG surface., Finally, optimization of the reactor performance by changing initial dye concentration, pH, photocatalyst dose, and the addition of H₂O₂ have been presented in the Chapter.

Chapter 5 summarizes the results from the present research work and provides a future outlook for continued research.

CHAPTER 2

LITERATURE REVIEW

Photocatalysis is a well-known and novel technology for the treatment of textile wastewater. A significant amount of research interest was shown in this process in the last decade. This Chapter represents the past works related to the fundamental background of TiO₂ based photocatalyst. It gives an overview of photocatalytic reaction mechanism and kinetics, preparation techniques of TiO₂ based nanocomposites with modification, dyes degradation techniques on the surface of photocatalyst, selection of dyes and radiation sources. Finally, the Chapter includes the factors that affect the photocatalytic reactor performance and characterization techniques of TiO₂ photocatalyst.

2.1 Photochemical Advanced Oxidation Processes

A group of chemical oxidative technologies classified as advanced oxidation processes (AOPs) has garnered a significant level for the treatment of textile wastewater over the last three decades. All AOPs are characterized by the production of highly reactive and non-selective hydroxyl radicals ($\cdot\text{OH}$), which are the strongest oxidants in an aqueous medium [39]. The $\cdot\text{OH}$ are capable of oxidizing nearly all organic compounds to water, carbon dioxide, and mineral salts through a process termed mineralization [40]. The conventional AOPs can be divided into homogeneous and heterogeneous based on the reaction phase [41]. Homogeneous catalysts are present in the same phase as reactants and products, usually liquid, while heterogeneous catalysts are present in a different phase, usually the solid and liquid or gaseous phases. Ultraviolet (UV) radiation in conjunction with other chemical additives like UV/H₂O₂, UV/O₃, UV/TiO₂, and UV/Fenton has been shown an effective process for the degradation of dye. When no UV source is used the technology can be termed as a dark oxidative process, such as: ozonation (O₃), fenton's reagent, sono-fenton, photo-fenton, electro-fenton, ultrasound, and microwaves. Among all developed AOPs, three have garnered the most study and use industrially: ozonation, UV/H₂O₂, and photocatalysis utilizing either ultraviolet (UV) or solar irradiation with titanium dioxide (TiO₂) [42].

The major advantages of the advanced photocatalytic oxidation process are as follows[43]:

- It offers a good route for the use of broadly available energy.
- This process does not have waste disposal problems.
- The photocatalytic process is a non-selective oxidation process for most organic pollutants; therefore, it can destroy a variety of hazardous organic compounds in different influents.
- It can transform organic pollutants into innocuous products by redox reactions and complete the mineralization of the organic pollutants.
- It is inexpensive. Thus, the photocatalytic degradation of environmental pollutants is an interesting topic for study.

2.2 Heterogeneous Photocatalysis

Heterogeneous photocatalysis is a process of enhancing the rate of chemical reactions by means of light in a catalytic system. It is the most widely applied photocatalytic process. In this process, both the photocatalyst and chemical reactants are in different phases [6]. Basic concepts of the heterogeneous photocatalytic system involve steps as follows [44]:

1. Transfer of reactants in water to the surface of photocatalysts.
2. Adsorption of reactants on the surface.
3. Photonic activation of the surface of photocatalyst and reaction in the adsorbed phase.
4. Desorption of reaction products.
5. Elimination of reaction products from the interface region.

It is generally accepted that when photocatalyst (TiO_2) absorbs the light with energy equal to or greater than the bandgap energy of photocatalyst, the formation of electron-hole pairs occurs [45]. The electron-hole pairs dissociate into positively charged holes (h^+) in valence band (VB) and electrons (e^-) in conduction band (CB). These charge carriers in the CB and VB reduce and oxidize compounds adsorbed on the surface of photocatalyst, respectively. However, recombination of these charge carriers can occur causing absence of chemical reaction. Often in the literature, decrease or increase of photocatalytic activity is explained by enhanced or suppressed electron-hole recombination, respectively [46].

2.3 Advanced Semiconductor Photocatalyst

Photocatalysis has received much attention in recent decades as a promising environmental remediation technique because of its ability to complete degradation of organic and inorganic toxins from textile wastewater [47, 48]. The photocatalytic heterogeneous wastewater treatment processes which use various groups of solid semiconductors such as oxides titanium dioxide (TiO_2), cerium oxide (CeO_2), zinc oxide (ZnO), zirconium oxide (ZrO_2), iron oxide (Fe_2O_3), tungsten oxide (WO_3), vanadium pentoxide (V_2O_5), sulfide (ZnS), and cadmium sulfide (CdS) were investigated [6]. Although the metal oxides are less powerful catalysts (higher bandgap energies) than the noble metals, these are more suitable as photocatalytic semiconductors because of their resistive behavior to deactivation and poisoning [49]. However, many of these semiconductors have enough bandgap energies which need to overcome for the photocatalytic chemical reactions. By doping the metal oxide with impurities reduces the bandgap energy and electromagnetic radiation with lower energy (to be fit in the visible light region) and can be utilized to activate the catalyst, possibly increasing photocatalytic activity [50]. The bandgap energy of various metal oxides is listed in Table 2.1.

Table 2.1: Bandgap energy of some metal oxide photocatalysts

Photocatalyst	Bandgap energy (eV)	Photocatalyst	Bandgap energy (eV)
TiO_2 (rutile)	3.0	CdS	2.4
TiO_2 (anatase)	3.2	WO_3	2.7
ZnS	3.7	Fe_2O_3	2.2
ZnO	3.3	MoS_2	1.8
SnO_2	3.6	SrTiO_3	3.2
SnO	$\sim 2.5\text{-}3.0$	WSe_2	1.2

2.3.1 Titanium dioxide (TiO_2) photocatalyst

Titanium dioxide (TiO_2) is a semiconductor material, which is extensively used due to its superior photoreactivity, long-term stability, chemically and biologically inert, non-toxicity, low operating cost, radically low level of energy consumption, and not dangerous for humans and the environment [6]. The photocatalytic activity of TiO_2 depends on various factors, including surface area, crystallinity, impurities and density of the surface hydroxyl groups. Among all

properties of TiO₂, the photodecomposition of the organic pollutants in an aqueous environment and the photoelectrochemical water splitting are of the main interest of this work [51].

TiO₂ is an n-type semiconductor. Naturally, it occurs in three available crystal forms known as anatase, rutile and brookite, in which well-crystallized anatase and rutile have been widely studied owing to their practical uses. Both anatase and rutile phase of TiO₂ crystal structures are comprised of TiO_6 - octahedrons that each Ti atom is surrounded octahedrally by six oxygen atoms [6]. The basic crystallographic and physical properties of anatase, rutile, and brookite phase of TiO₂ photocatalyst are listed in Table 2.2.

Table 2.2: Crystallographic and physical properties of TiO₂ photocatalyst

Property	Anatase	Rutile	Brookite
Crystallographic structure	Tetragonal	Tetragonal	Orthorhombic
Space group	$I4_1/amd$	$P4_2/mmm$	Pbca
Lattice parameters (nm)	a = 0.3784 b = 0.9515	a = 0.4594 b = 0.2959	a = 0.5447 b = 0.9184 c = 0.5145
Volume of the unit cell/molecule ($10^{-3}nm^3$)	34.172	31.216	25.75
Density (g/cm^3), T= 298 K	3.894	4.250	3.99
Bandgap energy (E_g) [eV]	3.2	3.03	3.10-3.40
Electron effective mass (m^*)	$1m_o$	$20m_o$	---
Hall mobility of electron [cm^2/Vs], T = 298 K	4	0.1	---

Electrons in the crystalline semiconductors are confined to certain energy levels, which are also known as electron movement orbitals, and forbidden from another region. The highest range of energy levels that electrons occupy at absolute zero degree is called the valence band and the range of energy levels higher than that is called conduction band. Each energy band has a large number of quantum states. The valence band describes a state of electrons tightly bound to the atomic nuclei and the conduction band reflects the electrons escaped from the materials to move entirely free in the crystal lattice. Rutile phase TiO₂ has a direct bandgap of 3.0 eV while the anatase phase has an indirect bandgap of 3.2 eV [52]. To extend the light absorption spectrum

toward the visible light range, intense efforts have been made in order to modify the optical absorption properties of TiO₂ phases, including ions doping and compositing TiO₂ with other semiconductors of narrower bandgap. The most feasible modification method seems to be doping TiO₂ with metal and nonmetal atoms to tune the band structures [52, 53].

There are several ways to overcome these drawbacks like doping of cationic sublattice of TiO₂ with either donor-type ions such as W⁶⁺, Mo⁶⁺ and Nb⁵⁺ or acceptor-type ions such as Cr³⁺, Fe³⁺. These so-called second-generation photocatalysts are particularly interesting to increase the electrical conductivity, which in most cases results in a decrease of the recombination losses, as well as to modify the electronic structure of the photocatalysts leading to an improvement of their optical properties. The third generation of photocatalysts is the anion-doped TiO₂ has attracted considerable attention due to its enhanced photocatalytic activity in the visible light. In this case, N-doped TiO₂ seems to be the most interesting due to the noticeable red-shift of light absorption [53].

2.4 Preparation of Photocatalytic Materials

In photocatalysis, the photocatalyst is the most important part that is mostly dependent on its synthesis technique. Various techniques are applied for the preparation of TiO₂ nanoparticles or thin films of TiO₂ including sol-gel method, chemical precipitation method, hydrolysis, spray deposition method, chemical vapor deposition, sputtering, micro-emulsion method, aerosol-assisted chemical vapor deposition, hydrothermal method, electro-deposition, flame combustion method, microwave-assisted hydrothermal synthesis, thermal plasma, solvothermal method, and sonochemical method, etc. [54]. Among all synthesis technique, sol-gel is an inexpensive and moderately low-temperature procedure. This technique allows almost comprehensive control over the product's chemical ingredient compositions. The technique also permits trouble-free addition of very minute dopant in terms of impurities. In most cases, the dopant is considered to be uniformly distributed in the ultimate desired product. In addition, sol-gel method also has other remunerations like micro-structured crystals and pure product [55, 56].

2.4.1 Sol-gel Process

The Sol-gel method is a wet chemical route for the synthesis of colloidal dispersions of metal alkoxides or organic salts which can be altered to powders, fibers, thin films and monoliths [57].

In general, the sol-gel method consists of hydrolysis and condensation reactions. TiO_2 can also be made using alkoxide precursors, most commonly metal alkoxides, such as titanium isopropoxide and titanium propoxide [58, 59]. Sol-gel coating is a process of preparation of single or multicomponent oxide coating which may be glass, glass ceramic or crystalline ceramic depending on the process as shown in Figure 2.1. Also, the nanomaterials used in modern ceramic and device technology require high purity and facilitate to control over composition and structure. The sol-gel coating is one of the interesting methods because it has many advantages are listed below.

- The chemical reactants for the sol-gel process can be conveniently purified by distillation and crystallization.
- All starting materials are mixed at the molecular level in the solution so that a high degree of homogeneity of films can be expected.
- Organic or inorganic salts can be added to adjust the microstructure or to improve the structural, optical and electrical properties of oxide films.

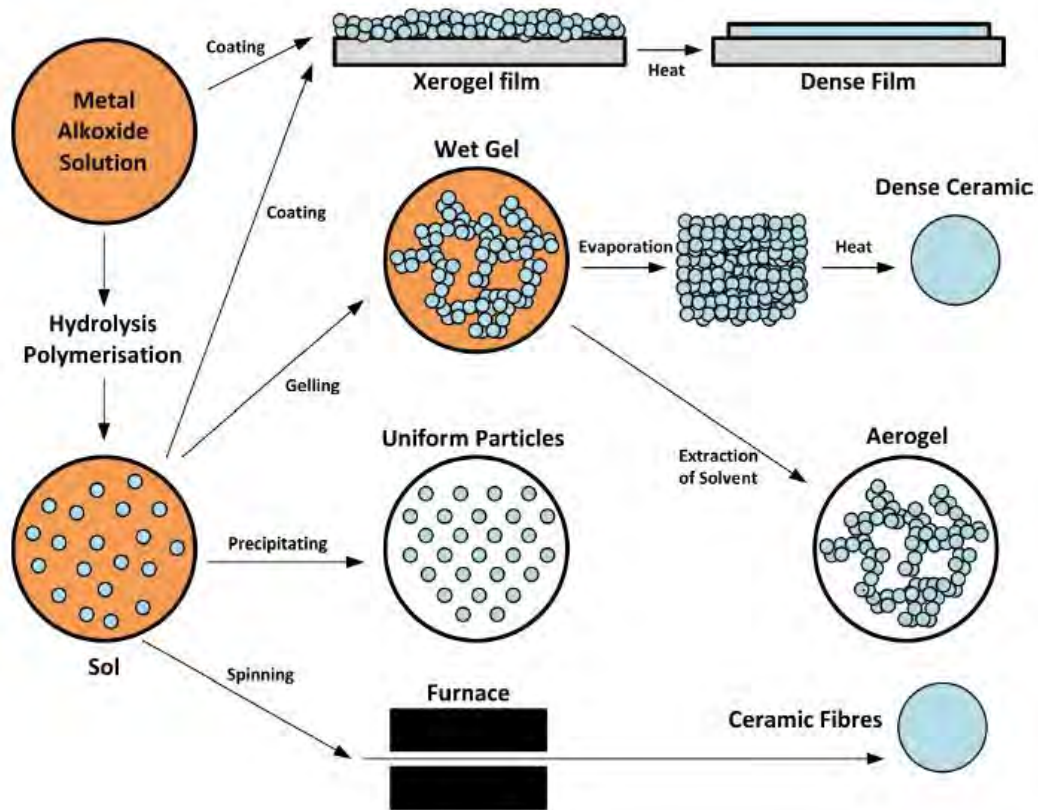
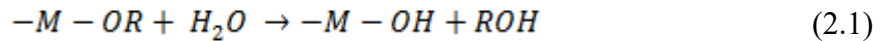


Figure 2.1: Generalized scheme of sol-gel synthesis [59]

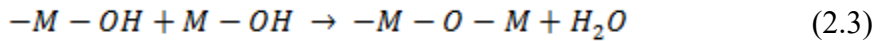
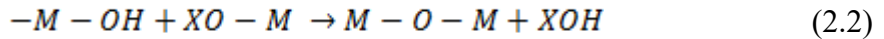
2.4.2 Sol-gel Chemistry

The sol-gel process consists of a colloidal solution called “sol” that acts as the precursor for an integrated network known as “gel” of either discrete particles or network polymers. A variety of precursors for TiO₂ including titanium halides (Titanium tetrachloride, TiCl₄) and titanium alkoxides (methoxide, ethoxide, isopropoxide and tert-butoxide) can be used for the preparation of TiO₂ nanoparticles [60]. The TiO₂ nanoparticles are formed using the precursors which undergo various forms of hydrolysis and condensation reactions. Prior to these two reactions, the metal alkoxides are prepared in a solution by adding it to alcohol. The alcohol preference is done based on their miscibility property. Once the solution is ready, it goes through two types of chemical reactions represented by Eq. (2.1-2.3). For the case of hydrolysis process, M represents Ti and R represents group of CH₃ or C₂H₅. In condensation process X represents either H or alkyl group [61].

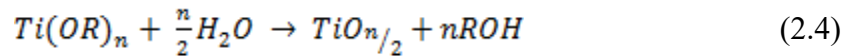
Hydrolysis reaction:



Condensation reaction:



A stable sol is formed by using the steps of hydrolysis and condensation of the alkoxide. Then the sol is dried further, condensing to form a gel of amorphous TiO₂ [62]. Final heat treatment, typically >400°C, crystallizes the amorphous TiO₂ into the anatase phase, which is usually the desirable crystal phase for photocatalysis. The overall reaction is shown in Eq. (2.4) [63], where R is the alkyl group.



2.5 Modified and Unmodified TiO₂ Based Nanocomposites

Modification of TiO₂ can lead to desired photocatalytic activity under visible light. The performance of TiO₂ nanomaterials in textile wastewater treatment strongly relies on their physicochemical characteristics such as crystallinity, crystallite size, crystal structure, specific surface area, thermal stability and quantum efficiency [64]. Generally, the modification of TiO₂

nanomaterials can be divided into two main groups, (i) bulk modification and (ii) surface modification. In bulk modification, foreign-element-doping is one of the well-known methods to enhance the performance of TiO₂ nanomaterials [65]. It also increases the thermal stability, surface area and shifts the absorption edge over a broad range [66]. In some cases, simultaneous cation and anion doping of TiO₂ also helps in improving the desirable bulk properties of TiO₂. Similarly, in surface modification, sensitizing TiO₂ with colored inorganic or organic compounds can improve its optical absorption in the visible light region [67]. In addition, modification of the surface of the TiO₂ nanomaterials with other semiconductors can alter the charge-transfer properties between TiO₂ and the surrounding environment [68].

2.5.1 Bulk Modification of TiO₂ Nanomaterials

Recently, numerous studies have focused on shifting the bandgap of TiO₂ to the visible spectral region which would potentially allow more efficient utilization [69]. The transition metal ions such as Fe, Cr, V, Mn and Co can be added as dopants [6]. The deposition of noble metals on the surface of TiO₂ also acts as an electron trap. The noble metal electron trapping technique helps to delay the recombination process. The common doping noble metals used with TiO₂ are Ag, Au and Pt. The noble metals also have properties of increasing charge carrier separation. The charge carrier separation is increased by the photo-induced electron transmit rate at the edge. This type of doping also increases the photoinduced electron/hole charge recombination lifetimes by acting as an electron-hole trap site [70, 71].

A separate approach to shifting the absorption edge over a broader range is by modifying TiO₂ with anions such as C, N, S, and F [66]. The non-metal nitrogen doping onto the TiO₂ photocatalyst is extensively considered due to their electronic properties including high stability, small ionization and comparable atomic size with oxygen that is better than standard TiO₂. It can be easily incorporated into nano TiO₂ structures as interstitials and substitutional [6].

The coupled semiconductors like CdS, WO₃, ZnO and MoO₃ have shown a very high-quality visible light enhancement of TiO₂. The enhancement is due to efficient charge separation, prolonged excitement of charge-carrier and enhanced interfacial charge transfer. All these major aspects are the consequence of the reduction in the usual bandgap energy of TiO₂. The semiconductor doping helps in creating smaller artificial bandgap energy. The smaller artificial

bandgap energy is found to be only possible when comparatively lower leveled bandgap semiconductors are coupled [70, 72]. Some of the current research has shown MoO₃ (n-type semiconductor with a bandgap of 2.9 eV) acquires similar positive aspects of WO₃. MoO₃ can be seen as a comparatively cheap and less consumable replacement of WO₃. Though, till now very few articles on MoO₃-TiO₂ have been published and thus leaves a gap to be explored [71, 73].

A suitable metal dopant can lead to improvement of the textural properties of TiO₂, an increase in the acidity of its surface, acceleration of phase transfer, and an increase in the degree of separation of any photogenerated charges. These factors are controlled by changes in the preparation method, loading of a catalyst, and type of dopant element [74]. Most of the research has mainly focused on the surface area, the crystalline structure and anatase to rutile phase transformation. In addition to crystal structure, the hybrid material's structural properties/morphology is also important. This can affect the transport of reactants and products to or from the catalytic active sites, the light absorbance for the photo-excitation of the catalyst, and the generation of electron–hole pairs.

2.5.2 Electronic Properties and Optical Response of TiO₂ Photocatalysts

The optical response of any material is largely dependent on its underlying electronic structure. The electronic structure of a nanomaterial is closely related to its chemical composition, arrangement, and physical dimensions. The electronic states of TiO₂ are generally considered to consist of three parts are shown in Figure 2.2, such as (i) valence band, (ii) lower conduction band, and (iii) upper conduction band [75].

- i. Valence band: The VB consists of three parts: σ bonding of the O $p\sigma$ and Ti e_g states in the lower energy region; the π bonding of the O $p\pi$ and Ti e_g states in the middle energy region; and the O $p\pi$ states in the higher energy region.
- ii. Lower conduction band: The bottom of the lower conduction band (CB) consists of the Ti_{d_{xy}} orbital, which contributes to the metal metal interactions due to the σ bonding of the Ti t_{2g} -Ti t_{2g} states. At the top of the lower CB, the remaining Ti_{1_{2g}} states are antibonding with the O $p\pi$ states.
- iii. Upper conduction band: The upper CB consists of the σ antibonding orbitals between the O $p\sigma$ and Ti_{1_{eg}} states. The chemical composition of TiO₂ applicable for solar applications

can be altered by incorporating a dopant. Specifically, the metal (Ti) or the nonmetal (O) component can be replaced by the dopant material in order to alter the optical properties. The following section shows the effects of metal and nonmetal doping on both the electronic properties and the optical response of TiO₂ nanomaterials.

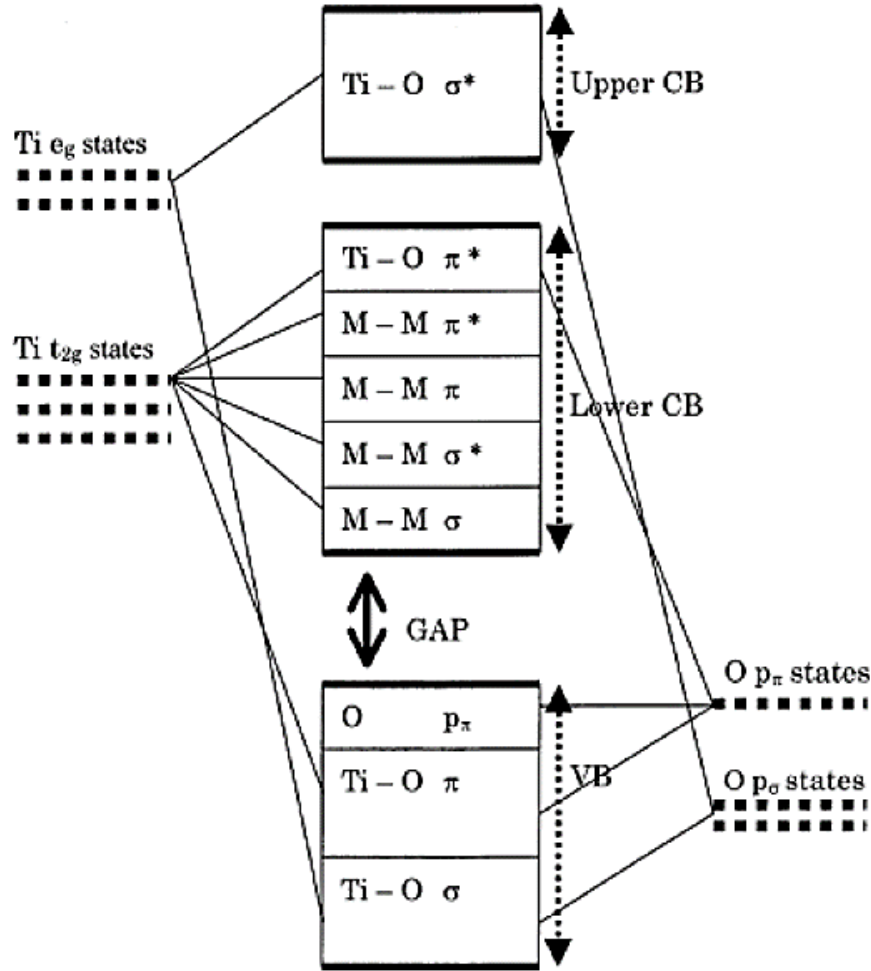
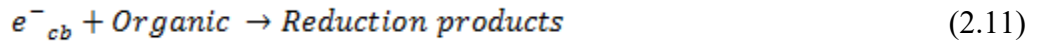
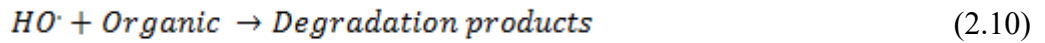
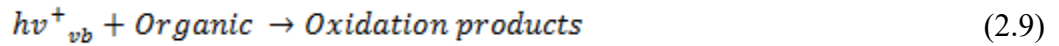


Figure 2.2: The bonding diagram of a perfect TiO₂ crystal [75].

2.6 Mechanism and Reaction Kinetics of TiO₂ Photocatalysis

The UV-TiO₂ treatment process is an indirect but effective heterogeneous photocatalytic process, which uses energy from UV radiation to break down various organic and inorganic substances in the wastewater [76]. For a semiconductor to be an active photocatalyst in the degradation of organic pollutants, the redox potential of the photogenerated holes should be sufficiently positive to generate the ·OH radicals. Further the redox potential of the photogenerated electrons must be

sufficiently negative to be able to reduce the adsorbed O₂ to superoxide. In photocatalysis, under light irradiation (photons), electrons and positive holes are generated in the conduction (e^-_{cb}) and valence band (hv^+_{vb}) of titanium dioxide according to Eq. (2.5) [77]. The holes can either react directly with organic molecules (Eq. 2.9) or form ·OH (Eq.2.7) that subsequently oxidize organic molecules (Eq.2.10) [78]. The electrons can also react with organic compounds to provide reduction products (Eq.2.5-2.11). The role of oxygen is important because it can react with the photogenerated electrons.



This mechanism is widely considered to describe the photocatalytic degradation of organic compounds using the UV-TiO₂ process [12]. The mechanism of the degradation of organic compounds by UV-TiO₂ process in textile wastewater has been explained by Figure 2.3.

In photocatalytic studies, first-order kinetics is found sufficient to model the photo mineralization of organic compounds. It is reported that first-order kinetics is only valid for low concentration dye. One of the most favorable models to describe the dye degradation reaction is Langmuir–Hinshelwood (L-H) kinetic model [44].

$$r = -\frac{dc}{dt} = k_r \theta_x = \frac{k_r KC}{1+KC} \quad (2.12)$$

According to L-H model represented by Eq. (2.12), the photocatalytic reaction rate (r) is proportional to the fraction of surface coverage by the organic substrate (θ_x). Here k_r is the reaction rate constant, C is the concentration of dye and K is the Langmuir adsorption constant.

L-H model depends on several assumptions, which include:

- i. The reaction system should be in dynamic equilibrium

- ii. The reaction should be surface-mediated
- iii. The competition for photocatalyst's active site is negligible

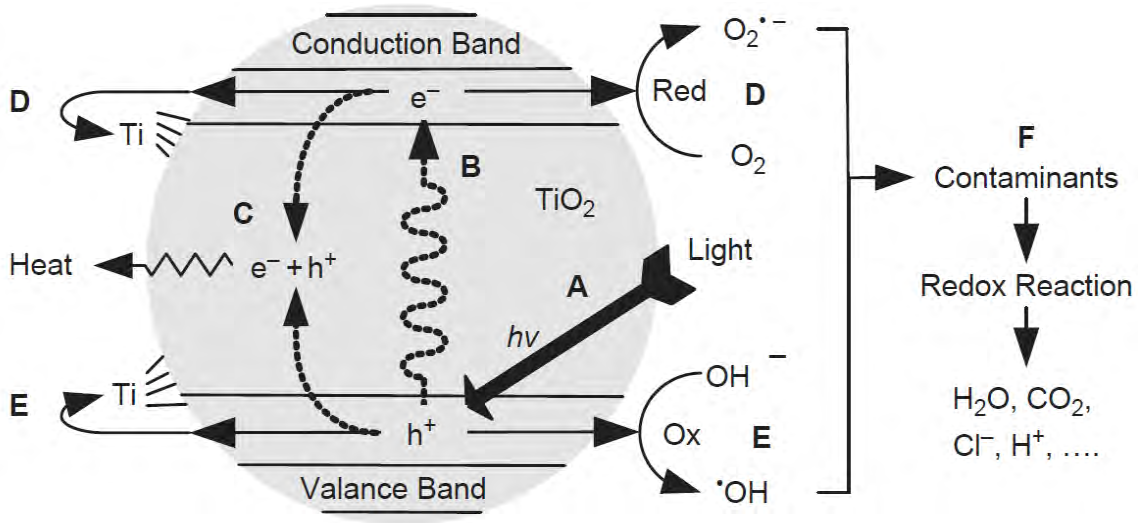


Figure 2.3: Schematic demonstration of the photocatalytic reaction for TiO₂ photocatalyst; (A) light irradiation to TiO₂ surface, (B) generation of electrons and holes as charge carriers, (C) recombination of the electrons and holes, (D) and (E) reductive and oxidative pathways of substances absorbed on TiO₂ sites, and (F) redox reaction to decompose organic contaminants in water [12].

Literature studied that the real K-value is significantly smaller [79]. This is explained by the differences in adsorption and desorption phenomena during the dark and illuminated period. Considering all these assumptions, the Eq. (2.12) can be converted to a typical pseudo-first-order model. The pseudo-first-order model is represented by Eq. (2.13).

$$C = C_0 e^{-kt} \tag{2.13}$$

Where C₀ is initial concentration, t is time and k is an apparent first-order rate constant.

2.7 Reactor Configuration of Photocatalysis

Photocatalytic reactors for water purification processes can be classified into two main configurations, depending on the location of the photocatalysts: (1) slurry-type photocatalytic reactors with suspended photocatalyst particles, and (2) reactors with the photocatalyst immobilized onto an inert carrier [80]. In slurry type photocatalytic reactor, the catalyst is evenly

dispersed in the solution. The uniform catalyst distribution provides very high surface area to volume ratios with low mass transfer limitations. Even though there have been several patents pertaining to the catalyst in suspension, there has been very little application at a larger scale for water treatment [70]. Similarly, in immobilized type photocatalytic reactor, the catalyst is immobilized or fixed on a supporting material. Different surfaces such as glass, sand, etc. can be used in the reactor [81]. Coating the catalyst on the surface can reduce the active surface area and limit the mass transfer in the reactor. Since the catalyst is in a continuous operation, fouling of the active sites on the coated support can reduce the rate over time [82]. The difference between the slurry-type photocatalytic reactors and photocatalyst-immobilized reactors is that the former requires a posttreatment separation process for the recovery of photocatalyst particles (batch process), while the latter allows a continuous operation. As illustrated in Figure 2.4, photocatalytic membrane reactors can be generalized as exhibiting (1) irradiation of the membrane module with an immobilized photocatalyst, and (2) irradiation of a feed tank containing a photocatalyst in suspension [83].

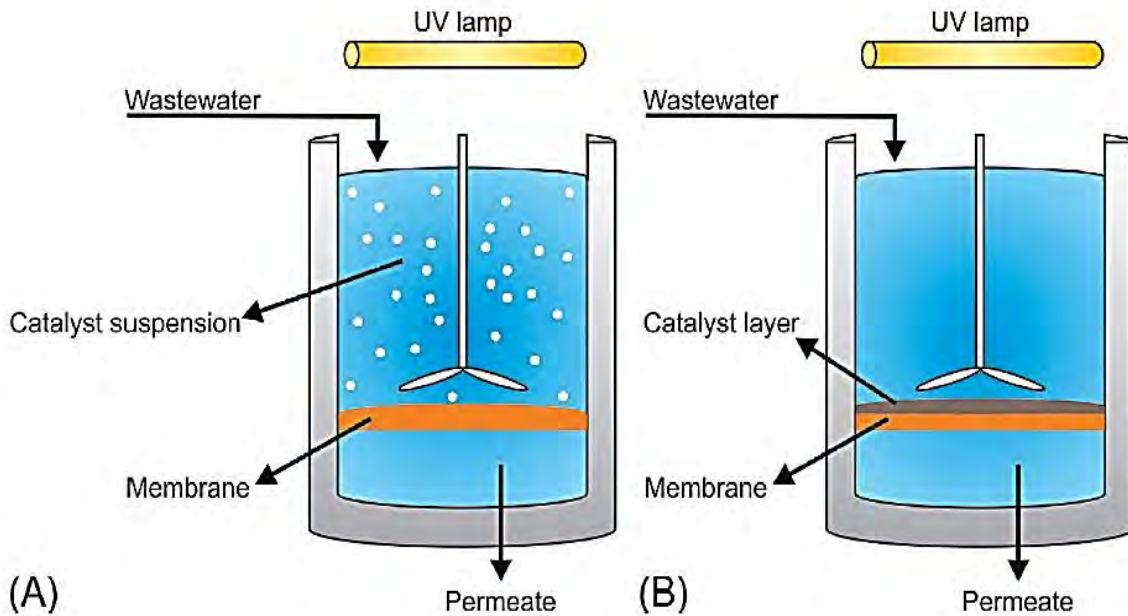


Figure 2.4: Configuration of photocatalytic membrane reactors: (A) slurry-type photocatalytic membrane reactors (photoreactors with a photocatalyst in a liquid suspension) and (B) immobilized photocatalytic membrane reactors (photoreactors with the photocatalyst immobilized in/on the membrane) [83].

2.7.1 Immobilization Procedure of TiO₂ Based Photocatalyst

Different methods such as heat treatment, spin-coating; dip coating, electrophoretic coating, and spray coating have been developed for immobilization of TiO₂ on surface. Among those, the heat treatment is the most common and widely used technique for immobilization. The immobilization is followed by high-temperature treatment for a better bond to the supporting materials. Dip coating is the easiest of all the coating methods and produces non-uniform films that require several dipping cycles [84]. The immobilized film is produced by dip-coating is not mechanically robust and can easily be wiped off or damaged during the photocatalytic experiment. On the contrary, the other coating produced by different methods is relatively stable but could be difficult to produce at larger scales [85]. It is essential to choose a preparation and immobilization technique that is compatible with the support in the reactor during the experiment.

2.8 Photocatalytic Degradation of Dye

A dye is a colored substance that has an affinity to the substrate to which it is being applied. The dye is generally applied in an aqueous solution, and requires a mordant to improve the fastness of the dye on the fiber [86]. Various classes and types of dyes are listed; acid dyes, natural dyes, basic (cationic) dyes, synthetic dyes, direct (substantive) dyes, disperse dyes, sulfur dyes and pigment dyes. Synthetic dyes are ingredients often derived from carcinogenic petrochemical derivatives and are used as colouring agents for many different products on the market. Common types of synthetic dyes are known as “azo dyes”. The natural textile dyes are mainly from vegetable and animal resources. The synthetic dyes are normally aromatic compounds produced by process of chemical synthesis [87].

2.8.1 Azo Dyes

Azo dyes are the major colourants used in the textile industry, allowing for a large spectrum of colours and increased colour fastness. They are a large group of synthetic organic dyes that contain nitrogen as the azo group (-N=N-) [89, 90]. The azo group is often bound to an aromatic ring, and the dye can then be broken down to an aromatic amine and arylamine. This can take place either chemically, through 'reductive cleavage', or through the body's own enzyme system. Some azo dyes can also be broken down to arylamines during storage due to light and high

temperature. The majority of azo dyes are water-soluble and are therefore easy for the body to absorb, and this takes place through inhalation and swallowing of dust as well as through skin contact. Azo dyes may also be toxic to aquatic organisms and cause long-term adverse effects in the aquatic environment [91, 92].

2.8.2 Methyl Orange

Methyl orange (MO) is a widely used azo dye and anionic in nature. The chemical formula of MO is $C_{14}H_{14}N_3NaO_3S$. There is a presence of $-N=N-$ as shown in the molecular structural arrangement represented in Figure 2.5.

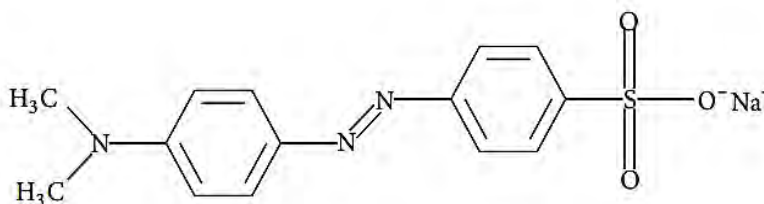


Figure 2.5: Chemical structure of MO [91].

Methyl orange is a pH indicator frequently used in titrations because of its clear and distinct colour change. Recently, MO degradation using photocatalyst has received massive interest from environmental scientists. The quest is to find the best photocatalytic reaction mechanism to enhance the photocatalytic degradation of MO [91, 92].

2.9 Selection of Radiation Sources

In photocatalysis, light must be absorbed on the molecules. It has been exhibited the practice of different light sources for carrying out dissimilar photodegradation studies and many investigations emphasis on the use UV light [93]. Various types of radiation sources are applied for photocatalysis in textile wastewater treatment that are described below.

2.9.1 The Mercury Lamps

Mercury lamps have widely used for suitability and when the photodegradation of the compounds is low [94]. Its own adequate energy to produce electron hole ($e^- - h^+$) pairs within the catalyst, which activate the formation of radicals and result in the oxidative degradation of the contaminants. The UV photoreactor λ region is higher than the X-ray λ region which is ≤ 100

nm, but is shorter than the visible λ region which is > 400 nm of the electromagnetic radiation [93].

2.9.2 Resonance Lamps

Cadmium (Cd)-vapour resonance lamp has been used for the photosensitized luminescence of many substances. This source emits radiation mainly at 326.1 and 228.8 nm. Sodium (Na) vapor resonance lamps are available commercially, and lamps using the other alkali metals can be either purchased or constructed easily. They usually offer little interest in photochemical use since the electronic transition involved is of such small energy [95].

2.9.3 Discharge Lamps

A windowless source from a low-pressure discharge in hydrogen is very rich in the 800-200 nm region. High-intensity noble-gas discharges have been described using low pressures of Krypton (116.5, 123.6 nm). Hot-cathode low pressure discharges using hydrogen, helium, argon, or nitrogen provide radiation in the 50-165 nm region [96].

2.9.4 The Vacuum Ultraviolet Region

In gas phase photochemistry, the vacuum ultraviolet region is the most important because highly energetic processes can occur in this process that involving photoionization and higher excited states. The light source used in this process as synchrotron radiation. The radiation is also produced in bursts, with pulse lengths as short as 100 ps so that time-resolved experiments are possible.

2.10 Factors Affecting Photocatalytic Activity

The photocatalytic performance of the catalyst is influenced by several factors; extrinsic and intrinsic. Extrinsic factors are those that are not part of the reaction but are an external influence towards the reaction by either improving or decreasing the end result. The extrinsic parameters are temperature, light intensity, pH, reaction time, catalyst loading and initial concentration of pollutant. Similarly, intrinsic factors are those that are not part of the reaction but are an internal influence on the reaction by either improving or decreasing the end result. The intrinsic factors

include crystal structure, crystallinity and the morphology particle size, surface hydroxyls, and surface area [97, 98].

2.10.1 Effect of Initial Dye Concentration

The most critical factor governing photodegradation of organic pollutants is the formation of $\cdot\text{OH}$ on the catalyst's surface and their interaction with the dye. High initial concentration of dyes shows low degradation efficiency and hence dilutions are necessary [99]. In highly concentrated effluents an increased number of dye molecules are adsorbed on the catalyst surface, covering most active sites. Additionally, concentrated dye solution decreases the path length of photon entering the solution [100]. The light is absorbed by the pollutant, shielding it from reaching the catalyst and reducing the formation of hydroxyl radicals leading to decreased photocatalytic activity [101]. The concentration of dye molecules is affected by the available catalyst active sites and thus the concentration of dye should increase with increasing catalyst loading for the optimal results.

2.10.2 Effect of Catalyst Loading

Catalyst loading plays a major role in photocatalytic degradation as it is the absorbent of the dye molecules. The increase in catalyst loading increases the surface area, thus increasing active sites and formation of $\cdot\text{OH}$ responsible for the degradation [101]. However, when catalyst loading exceeds the optimal value it becomes detrimental to the photodegradation reaction. The catalyst particles tend to aggregate, decreasing the surface area, and increasing light scattering causing difficulty in light penetration through the solution [102]. Increased catalyst concentration decreases photo absorption which sequentially reduces the dye adsorption onto the catalyst surface and thus reducing the reaction rates [103].

2.10.3 Effect of Temperature

Reaction temperature is an important process parameter. Usually, the photocatalytic systems are operated at room temperature. In the range of 20–80°C, a weak dependence of the degradation rates on temperature has been observed [107]. Temperature alters the crystal structure of the photocatalyst, therefore, the surface defects are changed, which decreases the reaction of the recombination of electron/hole pairs, eventually improving photocatalytic activity [108].

However, heating above 80°C requires cooling as this may reduce the rate of reaction leading to the decrease in the adsorption of pollutant on the catalyst surface [107].

2.10.4 Effect of Irradiation Time

The photocatalytic reaction has a proportional relationship with irradiation time. But after sometimes it shows an inverse relationship with irradiation time due to evaporation. Thus, the reaction rate of dye is increased until evaporation starts. With the increase of evaporation of water, the degradation rate of original dye compounds decreases as the concentration of dye increased with irradiation time. As the time increase, more and more intermediate products such as small chain aliphatic compounds are produced and these aliphatic compounds react with $\cdot\text{OH}$ that causes the slow kinetics of dye degradation after the certain reaction time [109].

2.10.5 Effect of Light Source

The light source used for the degradation of the organic pollutants is essential as it determines performance of the catalyst used. The threshold wavelength corresponds to the bandgap energy for the semiconductor catalyst; e.g. for the TiO_2 catalyst having a bandgap energy of 3.02 eV, thus the ideal wavelength is at 400 nm [99] i.e. UV light region. Sunlight and visible light have also been used as an effective light source as reported by [103]. The degradation of sulforhodamine-B in aqueous TiO_2 dispersions was investigated under three lighting regimes: UV light, visible and sunlight. The results revealed that UV and sunlight showed better degradation efficiency compared to visible light [110].

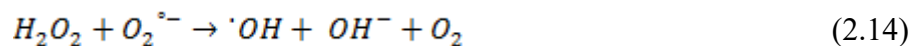
2.10.6 Effect of pH

The pH of the dye solution also has an important effect on the photocatalytic performance and the stability of the catalyst during the degradation process. pH effect is typically dependent on the point charge of the semiconductor used in the degradation reaction (electrostatic interaction of the catalyst with the pollutant) and on the type of pollutant used in the study [99]. Titanium dioxide has an amphoteric character with a zero-point charge pH of 6.25; its surface is positively charged under acidic conditions and negatively charged under alkaline conditions [111]. The maximum oxidizing capacity of the titania is at lower pH, however, the reaction rate may decrease at low pH due to excess H^+ . The adsorption of the pollutant and photocatalytic

performance is enhanced near the zPc of the catalyst [112]. The effect of pH is not only dependent on surface charge, but also on the generation of $\cdot\text{OH}$. It was studied the degradation of benzamide (BA) and para-hydroxybenzoic acid (4-HBZ) using TiO_2 in a pH range of 3–11 and chloride anions (range 0–0.8 mol /l) [113]. The degradation rate of 4-HBZ increased with decreasing pH, but BA was affected by the chloride anions concentration. This phenomenon is dependent on the nature of the pollutant being investigated [47].

2.10.7 Effect of Oxidant

There are various oxidants including H_2O_2 , BrO_3^- and $\text{S}_2\text{O}_8^{2-}$ are added to TiO_2 catalyst that has a great influence on the degradation of organic compounds such as (i) to increase the $\cdot\text{OH}$ concentration, (ii) to prevent the hole-electron recombination, and (iii) to generate other oxidizing elements (O_2° , $^\circ\text{SO}_4^-$) to enhance the degradation of intermediate compounds. In photocatalytic reaction, the intermediate oxidants perform dual functions such as strong oxidants and electron scavengers. These intermediate products can inhibit the hole-electron recombination of the TiO_2 surface according to the following equations [92].



The addition of peroxide acts as an oxygen supplier that increases the reaction rate. The effect of H_2O_2 on the degradation of textile wastewater is significant. The oxidation rates have been increased with the addition of H_2O_2 since more hydroxyl radicals could be generated by removing surface trapped electrons [114]. However, the oxidative conversion of photocatalytic efficiency would be uniformly increased by the addition of H_2O_2 . As a result, $\cdot\text{OH}$ are produced from the oxidation of hydroxide ions are given in the reactions.

2.10.8 Effect of Particle Size and Surface Area

Surface area has a great impact of dye degradation. Nanotechnology has been developed to improve the surface area for enhanced photodegradation performance. It has been proven that the smaller the particle size, the more the surface area observed and thus more $\cdot\text{OH}$ are available to surface for degrading organic pollutants [115, 116].

2.10.9 Effect of Surface Morphology

Surface morphology has a great impact on catalyst performance. Crystalline morphology has been reported to have enhanced photodegradation performance compared to amorphous morphologies. Heat treatment has been used to transform amorphous titania to crystalline titania [117].

2.11 Characterization Techniques of Photocatalyst Materials

According to the literature, several analytical techniques are used for the characterization of TiO₂ based photocatalysts. These analytical techniques are used to understand the surface morphology and other physical-chemical properties of nanoparticles. Some of the universally reliable and splendid analytical techniques are listed below:

1. X-Ray Diffraction (XRD)
2. Scanning Electron Microscopy (SEM)
3. Energy Dispersive X-ray Spectroscopy (EDX)
4. Fourier Transform Infrared Spectroscopy (FT-IR)
5. Ultraviolet-Visible (UV-Vis) Absorption Spectroscopy
6. BET Surface Area Analysis

2.11.1 X-Ray Diffraction (XRD)

X-Ray Diffraction (XRD) is a laboratory-based technique commonly used for identification of crystalline materials and analysis of unit cell dimensions. One of two primary types of XRD analysis (X-ray powder diffraction and single-crystal XRD) is commonly applied to samples to obtain specific information about the crystalline material under investigation.

In XRD, the X-rays are generated by a cathode ray tube, filtered to produce monochromatic radiation, collimated to concentrate, and directed toward the sample. The interaction of the incident rays with the sample produces constructive interference (and a diffracted ray) when conditions satisfy Bragg's Law. This law relates the wavelength of electromagnetic radiation to the diffraction angle and the lattice spacing in a crystalline sample [118]. These diffracted X-rays are then detected, processed, and counted. By scanning the sample through a range of 2θ angles, all possible diffraction directions of the lattice are attained due to the random orientation of the powdered material. Conversion of the diffraction peaks to d-spacing allows identification of the

mineral because each mineral has a set of unique d-spacing. Typically, this is achieved by comparison of d-spacing with standard reference patterns. The value of d-spacing is obtained from Bragg's law-

$$2d \sin\theta = n\lambda \quad (2.17)$$

Where d is an interlayer spacing, θ is the X-ray angle of incidence (and of diffraction) measured concerning the crystalline planes, n is an integer value and λ is the wavelength of the incident beam. Crystallite size of crystals are calculated from Scherrer formula-

$$D = \frac{k\lambda}{\beta \cos\theta} \quad (2.18)$$

Where D is the crystallite size, k is a dimensionless shape factor (typical value 0.9), λ is the X-ray wavelength, β is the line broadening at halfway of the maximum intensity (FWHM) and θ is the Bragg angle (in degrees). Sample preparation is one of the most important steps in a successful XRD analysis [119].

2.11.2 Scanning Electron Microscopy (SEM)

Since the invention of Scanning Electron Microscopy (SEM), it has become an indispensable tool in research and has significantly contributed towards biology, medicine, environment, and material sciences research [120]. SEM analysis is employed to determine the size, shape and morphologies of particles. The working principle of SEM is similar to an optical microscope, but it measures the electrons scattered from the sample rather than photon. Magnification of images up to 200000 times can be performed using SEM. It can measure the particle size and shape of any conductive or sputter coated sample and the sensitivity is down to 1 nm [121]. There are various advantages of SEM including its wide array of applications, the detailed two-dimensional and topographical imaging, and the versatile information garnered from different detectors. SEMs are also easy to operate with the proper training and advances in computer technology and associated software have made the operation user-friendly.

2.11.3 Energy Dispersive X-ray Spectroscopy (EDX)

Energy-dispersive X-ray (EDX) spectroscopy is used to characterize the sample chemically [122]. It relies on the investigation of a sample through interactions between electromagnetic radiation and matter, analyzing X-rays emitted by the matter in response to being hit with charged particles. A high-energy beam of charged particles such as electrons or protons, or a beam of X-rays, is focused on the sample being studied. At rest, an atom within the sample contains ground state (or unexcited) electrons in discrete energy levels or electron shells bound to the nucleus. The incident beam may excite an electron in an inner shell, ejecting it from the shell while creating an electron hole where the electron was. An electron from an outer, higher-energy shell then fills the hole, and the difference in energy between the higher-energy shell and the lower energy shell may be released in the form of an X-ray. The number and energy of the X-rays emitted from a specimen can be measured by an energy-dispersive spectrometer. As the energy of the X-rays is characteristic of the difference in energy between the two shells, and of the atomic structure of the element from which they were emitted, this allows the elemental composition of the specimen to be measured [120].

2.11.4 Fourier Transform Infrared Spectroscopy (FT-IR)

Fourier Transform Infrared Spectroscopy (FTIR) is an analytical technique used to identify the functional groups on the surface. The FTIR analysis method uses infrared light to scan test samples and observe chemical properties. The principle of FTIR is related to the vibrations of the atoms in a molecule. The infrared zone of the electromagnetic radiation is utilized to determining what fraction of the incident radiation is transmitted or absorbed at a particular energy [123]. Each peak in the absorption spectrum corresponds to the vibration of a molecule part. FT-IR involves the energy region of EMR corresponding to the wavenumber of $14000 \sim 4 \text{ cm}^{-1}$. It can be divided into near-infrared region ($14000 \sim 4000 \text{ cm}^{-1}$), mid-infrared region ($4000 \sim 400 \text{ cm}^{-1}$) and far-infrared region ($400 \sim 4 \text{ cm}^{-1}$). The commonly used region for FTIR is ($4000 \sim 400 \text{ cm}^{-1}$) because the absorption radiation of most functional groups and bonds in organic and inorganic materials is within this region. FTIR spectroscopy is an established technique for quality control when evaluating industrially manufactured material, and can often serve as the first step in the material analysis process. A change in the characteristic pattern of absorption bands clearly indicates a change in the composition of the material or the presence of contamination [124].

2.11.5 Ultraviolet-Visible (UV-Vis) Absorption Spectroscopy

UV-Vis refers to absorption spectroscopy or reflectance spectroscopy in the ultraviolet-visible spectral region. This means it uses light in the visible and adjacent (near-UV and near-infrared (NIR)) ranges. The absorption or reflectance in the visible range directly affects the perceived color of the chemicals involved. In this region of the electromagnetic spectrum, molecules undergo electronic transitions. This technique is complementary to fluorescence spectroscopy, in that fluorescence deals with transitions from the excited state to the ground state, while absorption measures transitions from the ground state to the excited state [125]. The transitions or interaction of light is illustrated in various different forms.

For solid like semiconductors, the reflectance against wavelength curve is easily being observed. The values of reflectance are used to calculate the absorbance. The absorbance curve is utilized to observe the absorbance edge shift. In addition, Tauc plot is a commonly applied to determine bandgap with respect to reflectance. For liquids, the light absorbance depends on constituted chemical compounds in liquid. This absorbance property is used to identify particular compounds within liquid mixture. Simultaneously, Beer's law can be applied to calculate the concentration of that particular compound [126]. The Beer's law is represented by equation (2.19) which states absorbance quantity (A) of a solution is directly proportional to concentration of absorbing species (c). Taking into consideration that path length (b) and constant of proportionality (ϵ) are kept constant.

$$A = \epsilon bc \quad (2.19)$$

2.11.6 Nitrogen Physisorption Measurement (BET analysis)

The physisorption technique is one of the most common methods used to measure surface area, pore-volume, pore size, and its statistical distribution. The technique uses an inter gas as adsorbate, especially nitrogen. The process of adsorption and desorption is carried out with different amounts of nitrogen. The corresponding readings in terms of pressure or thermal conductivity are measured. The recorded measurements are used in gas adsorption equation models to estimate microstructure characteristics like porosity. According to literature, the Brunauer–Emmett–Teller (BET) multi-point model is one of the finest available techniques [127].

CHAPTER 3

MATERIALS AND METHODOLOGY

This chapter represents the research methodology that has been adopted. Firstly, preparation techniques of TiO₂ based photocatalysts are presented. Secondly, all characterization techniques used in this research are discussed. The chapter also includes the immobilization procedure, and photocatalytic experimental schematic with detailed experimental procedures.

3.1 Materials

3.1.1 Chemicals

The major reagents and chemicals used for experiments in the laboratory include the precursor titanium (IV) isopropoxide (C₁₂H₂₈O₄Ti) (Sigma-Aldrich, 97%), silver nitrate (AgNO₃) (Sigma-Aldrich, 99%), absolute ethanol (C₂H₅OH) (Tradia, USA), methyl orange (Sigma-Aldrich, dye content 85%), molybdenum tetra-hydrate ((NH₄)₆Mo₇O₂₄·4H₂O) (Sigma-Aldrich, 99%), nitric acid (HNO₃) (Merck, 69% extra pure), hydrochloric acid (HCl) (Sigma-Aldrich, 37%), acetone (C₃H₆O) (Mark, India, 97%), sodium hydroxide (NaOH) (Merck, Germany), hydrofluoric acid (HF, 48% extra pure) (Sigma-Aldrich), and hydrogen peroxide (H₂O₂) (Sigma-Aldrich, 30%), and distilled water.

3.1.2 Equipment and Analytical Instruments

The major equipments used for analysis in the laboratory include the UV-Visible spectrophotometer (UV-Vis) (DR-6000, DR-4000, UV-2600, Shimadzu, Japan), Fourier transport infrared spectroscopy (FT-IR) (FT-IR-470, Shimadzu, Japan), Scanning electron microscope (SEM) (JSM-6700F, JEOL, Japan), X-ray diffraction (XRD) (PANalytical Empyrean Series 2 X-ray Diffraction), Brunauer–Emmett–Teller isotherm (BET), Digital balance (Precisa, Switzerland), Drier (Germany), Muffle furnace (Navertherm, England), and Magnetic stirrer (China).

3.2 Experimental Methods

The experimental design and procedures were determined by taking research objectives into consideration. The major parts of this particular research were divided into six categories.

- i. Synthesis of TiO₂ based nanocomposites using sol-gel method
- ii. Characterization of TiO₂ based photocatalysts
- iii. Immobilization of TiO₂ photocatalysts on borosilicate glass
- iv. Experimental set-up of photocatalysis
- v. Photocatalytic degradation of methyl orange
- vi. Optimization of reactor performance

3.3 Synthesis of Photocatalysts using Sol-gel and Heat Treatment Method

All chemicals that were used to perform the experiments were analytical grade. The laboratory apparatus was washed using distilled water, acetone, and hydrochloric acid followed by drying in a micro-oven at 70°C for 30 min. In the typical sol-gel synthesis process, at first, the solvents absolute ethanol and distilled water were mixed in a molar ratio of 6:3 with vigorous stirring at 800 rpm for 10 min. In the following steps, 7.0 ml precursor solution of titanium (IV) isopropoxide (TTIP) was added dropwise to the solvent and stirred vigorously at above rpm for 3 hours at room temperature to enrich the stability and homogeneity of the gel at an adjusted pH 3 using HNO₃ (0.1 M) and NaOH (0.1 M) [3,30,128]. The higher quantity of solvent mixture was used to suppress the fast condensation, which enhance the nucleophile attack of TTIP species to yield TiO₂ nanocrystals [129]. The resulting gel was allowed to be aged at room temperature for 24 h. Then the obtained gel was dried in a micro-oven (controlled environment) at 90 °C, 100°C, and 110 °C for 2 h at each condition to evaporate water and other organic materials to the maximum extent [130]. Thus, the dried TiO₂ clustered solid was calcined at 400 °C and 500 °C (heating rate was 6.66 °C/min to raise temp 400 °C and then at 3.33 °C/min to raise temp 500 °C) for 2 h. The heated sample was cooled naturally to room temperature for 24 h. Finally, the obtained calcined sample was marked as pure TiO₂ nanoparticles.

A similar procedure was applied to prepare Ag/TiO₂, MoO₃/TiO₂, and Ag/MoO₃/TiO₂ nanocomposites. The only exception was the addition of silver nitrate and ammonium molybdenum into the solution. In the preparation of Ag/TiO₂ nanocomposite, a solution of silver

nitrate (AgNO_3) was prepared by using deionized water. AgNO_3 solution was prepared after the addition of 0.134 g of AgNO_3 in 20 ml of deionized water. The AgNO_3 solution was added dropwise to titanium precursor solution under vigorous stirring to maintain silver (Ag) in the final product at 1 wt% [131, 132]. The rest of all synthesis procedures were exactly similar to the synthesis of TiO_2 nanoparticles. The obtained final product was marked as Ag/TiO_2 nanocomposite.

For $\text{MoO}_3/\text{TiO}_2$ nanocomposite preparation, about 0.52 g of ammonium molybdenum mixed with 20 ml deionized water and stirred for 10 min. Similarly, this solution was added dropwise to the titanium precursor solution under vigorous stirring. This was done to maintain at 3 wt% of molybdenum (MoO_3) in the final product [133], and the rest of all synthesis procedures were exactly similar to the synthesis of TiO_2 nanoparticles. The obtained final product was marked as $\text{MoO}_3/\text{TiO}_2$ nanocomposite.

In the case of silver and molybdenum doping, at first, AgNO_3 and MoO_3 solutions were prepared separately and stirred for 10 minutes. All the other preparation steps were similar to the Ag/TiO_2 and $\text{MoO}_3/\text{TiO}_2$ preparation techniques. The concluding product was marked as $\text{Ag/MoO}_3/\text{TiO}_2$ nanocomposite.

3.4 Characterization Techniques of TiO_2 Based Nanocomposites Photocatalysts

3.4.1 X-Ray Diffraction (XRD)

X-ray Diffraction (XRD) was conducted on a PANalytical Empyrean Series 2 X-ray diffraction system at a wavelength ($\lambda = 0.154 \text{ nm}$) (Cu $K\alpha$ wavelength), at 40 mA, and at 40 keV. XRD diffractograms were acquired at 25 °C over a 2θ range of 20–75° with a step size of 0.020° and a step time of 1 s. The corresponding results of all samples were observed from computer at 2θ in terms of intensity. The average crystalline size of photocatalysts was calculated according to the Debye-Scherrer formula [30] that is represented in Eq. (3.1), where θ , β and λ are Bragg angle, shape factor, and wavelength, respectively. The lattice parameters were measured and described using tetragonal system equation as given in Eq. (3.2), where, hkl are the miller index, d is the lattice spacing, and a, c are the lattice parameter. The mass fraction of anatase and rutile phase was calculated that is stated as Eq. (3.3), where, W_R is the mass fraction of rutile phase, and A_R and A_A are the areas of rutile and anatase diffraction, respectively.

$$D = 0.9\lambda/\beta C \cos \theta \quad (3.1)$$

$$\frac{1}{d^2} = \frac{h^2 + k^2}{a^2} + \frac{l^2}{c^2} \quad (3.2)$$

$$W_R = \frac{A_R}{0.866 A_A + A_R} \quad (3.3)$$

3.4.2 Scanning Electron Microscope (SEM)

Scanning Electron Microscopy (SEM) (JSM-6700F, JEOL, Japan) images were taken to visualize the surface morphology, shape, and size of the photocatalysts. For SEM analysis, the samples were dried and de-moisturized. A minute amount of de-moisturized samples was taken on a both-side conductive carbon-based tape. The sample containing carbon tape was placed in the sample holder. In this particular analytical technique, images of different positions were taken at the micro and nano level. The different magnification (30,000-50,000x), working voltage (5.0 kV), and working distance (8 mm) respectively were visualized at the micro and nano level. For each and every sample, corresponding images were generated at the same condition for consistency.

3.4.3 Fourier Transform Infrared Spectroscopy (FTIR)

Fourier Transform Infrared Spectroscopy (FTIR) was used to analyze the functional group of different TiO₂ based nanocomposites (IRPrestige-21@Shimadzu at Centre for Advanced Research in Science in University of Dhaka) within a range of 4000-400 cm⁻¹. The spectra of the solid samples were frequently obtained by mixing and grinding a small amount of materials with dry and pure KBr crystals. The discs were prepared by first mixing 1 mg of dried sample with 500 mg of KBr (Merck, for spectroscopy) in an agate mortar and then pressing the resulting mixture at 10 tonnes cm⁻² for 15 min under vacuum.

3.4.4 UV-Vis Diffuse Reflectance Spectrophotometer (UV-Vis/DRS)

The UV-Vis spectral analysis of the photocatalysts was performed in slurry form. water was used as solvent to make separate suspensions of the photocatalysts. A double beam spectrophotometer (Spectrophotometer, UV-Vis-2600) was used to perform the experiments at pH 6 in the visible region (200-800 nm [134]). A 1 mg sample of TiO₂ nanocomposite was dissolved in a 10 ml distilled water. The UV-Visible spectrum of TiO₂ was obtained for 10 μM solutions in the range

of 200 nm to 800 nm. All the other samples were analyzed using an analogous way without any notable change.

The graphical pattern of the absorbance against wavelength plot was used to estimate absorbance edge shift. As calculation of bandgap energy of composite materials is very significant. The bandgap energy (E_g) of all samples was determined by employing the Kubelka-Munk formulae and Tauc's plot, which are stated in Eq. (3.4-3.5), where α is the absorption coefficient (cm^{-1}), $h\nu$ (eV) is the energy of excitation (photon energy), K is a featuring constant, R is the diffuse reflectance, and E_g is the bandgap energy. The value of n was considered 2 as a representation of direct transition [30]. The calculation of the E_g can be performed by plotting ($[f(R)h\nu]^n$ or α^n versus $h\nu$) and extrapolating the absorption edge to zero [30].

$$f(R) = \frac{(1-R)^2}{2R} \quad (3.4)$$

$$[f(R)h\nu]^2 = \alpha^2 = K(h\nu - E_g) \quad (3.5)$$

3.4.5 Brunauer–Emmett–Teller Isotherm (BET)

Brunauer–Emmett–Teller (BET) analysis was performed to determine the specific surface area (m^2/g) and total pore volume (cm^3/g) of catalyst. The BET analysis was conducted at the boiling temperature of N_2 (77 K). All the samples were dried at 250 °C for 30 min. The moisture-free samples were analyzed sequentially by nitrogen adsorption and desorption methods. Different compositions of nitrogen (15%, 30%, 50%, and 95%) were used to perform the experiment. The respective parameters of thermal conductivity were calculated using 48 Pulse Chemi Sorb 2705 (Micromeritics) [135]. The BET model is represented by the Eq. (3.6).

$$\frac{1}{\vartheta[(p_0/p) - 1]} = \frac{c-1}{\vartheta_m c} \left(\frac{p}{p_0} \right) + \frac{1}{\vartheta_m c} \quad (3.6)$$

3.5 Design and Construction of TiO_2 Immobilized Reactors

3.5.1 Immobilization of TiO_2 Based Nanocomposites on BG

The borosilicate glass (BG) was used as supporting material where TiO_2 based nanocomposites were immobilized. This supporting material was purchased from the local market. At the very beginning, the TiO_2 based nanocomposites were immobilized on BG using heat treatment

method. Before immobilization, the BG supporting material was cleaned with distilled water followed by cleaning using HF solution (1 M) overnight. After that the BG was washed with NaOH solution (0.1 M) for 2 h for ensuring a good fixation of TiO₂ photocatalyst on the BG plates [136]. 0.120 g TiO₂ photocatalyst was added in absolute ethanol solvent and the suspension was stirred by using a glass rod for 10 min to improve the dispersion of TiO₂ photocatalyst in the solvent [137]. The suspension was poured on a BG plate and then placed in room temperature for 1 hour. After that, it was placed in an oven at 110 °C for 1 hr. After drying, the BG plate was calcinated at 500 °C for 120 min and washed with distilled water for the removal of weakly attached TiO₂ [138]. This thermal treatment ensured the removal of the organic (ethanol) load and facilitated inter connection (sintering) between TiO₂. Similar procedures were applied for the immobilization of Ag/TiO₂, MoO₃/TiO₂, and Ag/MoO₃/TiO₂ nanocomposites on the BG plate.

3.6 Experimental Set-up

The experimental photocatalytic reactor system was designed with respect to certain criteria stated below:

- a. UV radiation penetration
- b. Pure surface
- c. Suitable sampling and parameters reading credentials
- d. Catalyst in immobilized form

The UV-Ag/MoO₃/TiO₂ nanocomposites immobilized experiments were carried out using batch reactors containing Ag/MoO₃/TiO₂-immobilized surface. Four types of BG supporting material was used to immobilize-Ag/MoO₃/TiO₂. Experiments and analysis were performed according to developed methods based on the dye degradation by changing initial dye concentration, pH, and with or without the addition of oxidant hydrogen peroxide. The experimental set-up of MO degradation by using Ag/MoO₃/TiO₂-immobilized supported material is shown in Figures 3.1.

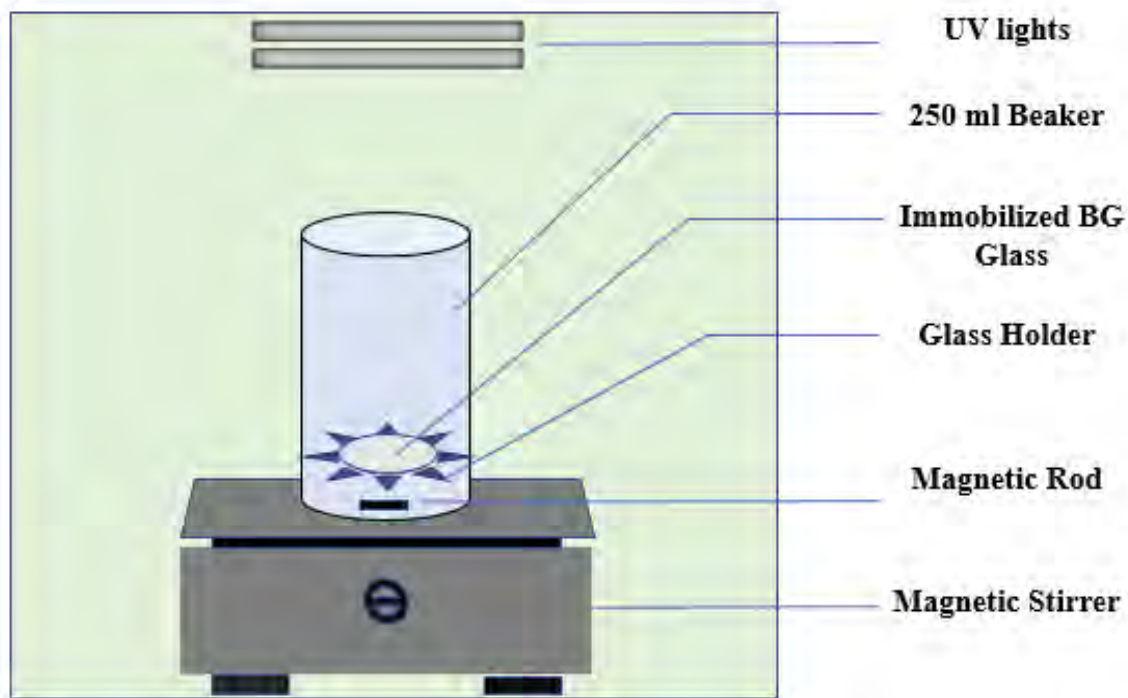


Figure 3.1: The schematic diagram of photocatalytic reactor system.

3.7 Photocatalytic Degradation of MO Dye under UV Radiation

The photocatalytic degradation of MO dye has been divided into five major parts stated below:

1. Preparation of desired MO solution
2. Preparation of calibration curve
3. Photocatalytic reactions and sample analysis
4. Optimization of reactor performance
5. Reaction kinetics

3.7.1 Preparation of Desired Methyl Orange Solution

At first, approximately 0.1 g of the powder MO was added to 1 L of deionized water to prepare 100 ppm MO solution. The solution was stirred for 20 min. The homogeneous solution (10 ppm, 30 ppm, and 50 ppm) was used for the experiments. Before using the dye solution for experiments, it was stirred for 10 min.

3.7.2 Calibration Curve

The molar absorption coefficient of the MO solutions was determined from a plot of absorbance against concentration (calibration curve) using Beer-Lambert law. For calibration curve, 5, 10, 15, 20, and 30 ppm MO solutions were prepared. Each and every sample including a blank was placed in SHIMADZU UV-2600 UV-VIS Spectrophotometer. The corresponding absorbance peak value was recorded at a wavelength of 464 nm. The recorded absorbance peak values against MO concentrations were plotted to generate calibration curve is shown in Figure 3.2.

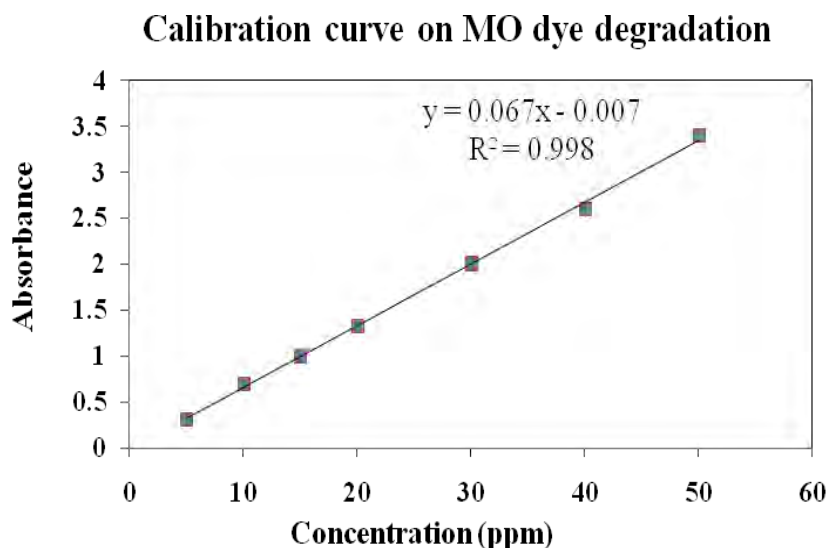


Figure 3.2: Calibration curve of MO for dye degradation

3.7.3 Photocatalytic Reactor Activity and Batch Adsorption

The photocatalytic activities of TiO_2 photocatalyst and Ag/TiO_2 , $\text{MoO}_3/\text{TiO}_2$, and $\text{Ag/MoO}_3/\text{TiO}_2$ nanocomposites were estimated by determining the degradation of MO dye in immobilized reactor under 5 h of UV light radiation. In our experiments, the self-designed immobilized batch reactor consists of 250 mL beaker (cylindrical Pyrex cell) and photocatalysts which may contain TiO_2 , Ag/TiO_2 , $\text{MoO}_3/\text{TiO}_2$, and $\text{Ag/MoO}_3/\text{TiO}_2$, respectively. In a typical experimental procedure, 4 sets of such immobilized reactors were employed together to investigate a comparative performance of those 4 reactors. Initially, a 125 mL of MO dye solution at a fixed concentration (e.g. 10 ppm) and a fixed pH (e.g. 6.8) was placed into each of 4 sets of reactors. The photocatalyst doses of each 4 set reactors was 0.120 g. Then the immobilized reactors were placed inside of a self-design wooden box covered with an aluminum

foil containing 100 W UV (5×20 W UV lamps) tube lamps (parallel arrangement). The experiment was carried out under UV radiation (365 nm wavelength) on a magnetic stirrer for 5 h at a dark condition. The aluminum foil cover was used to ensure the maximum light to fall on the reaction vessel by reflection. The mixture was stirred vigorously using a magnetic stirrer (China 78-Magnetic Stirrer) throughout the study to ensure uniform mixing. The batch studies were carried out from 11.00 am to 4.00 pm. At the end of 30 min time intervals, 5 mL samples were withdrawn and filtered. The supernatant was collected in a plastic bottle fitted with cap and was kept under cover to avoid any photo degradation. The various exposure times carried out were 0, 30, 60, 90, 120, 150, 180, 210, 240, 270, and 300 min. Finally, the filtered dye solutions were measured by using UV-Vis spectrophotometer (UV-Vis-2600 Spectrophotometer).

The molar absorption coefficient (calibration curve) of MO dye concentration was determined and the corresponding absorbance against with peak values of each curve were utilized. The maximum absorption wavelength of MO dye was found at 464 nm at pH 7.0. The photocatalytic degradation of dye was evaluated for each reactor to investigate the performance of TiO₂, Ag/TiO₂, MoO₃/TiO₂, and Ag/MoO₃/TiO₂ nanocomposites. The impact of initial dye concentration, pH, the addition of hydrogen peroxide was evaluated from the experiment. The pH was regulated by adding incremental amounts of either dilute HNO₃ or NaOH to the solution.

3.7.4 Optimization of Reactor Performance

The optimization of reactor performance was carried out by changing initial dye concentration, pH, and addition of H₂O₂. The optimization of these operating parameters are listed below:

Study of the Effect of Dye Concentration

The effect of dye concentration experiment was conducted for three different dye concentrations of 10 ppm, 30 ppm and 50 ppm at pH 3.0, 6.8, and 11.0. A 125 mL of MO solution was allowed to contact with fixed-dose (i.e., 0.120 g) of photocatalysts for a time interval of 5 h (11.00 am to 4.00 pm). The different dye concentrations of the MO solution were prepared by the addition of distilled water.

Study of the Effect of Photocatalyst Dose

To assess the impact of photocatalyst dose, the experiment was conducted at four different doses of 80 mg, 100 mg, 120 mg, and 140 mg, which were added in 125 mL 10 ppm of MO solution and were allowed to perform the experiment for a time interval of 5 h (11.00 am to 4.00 pm).

Study of the Effect of pH

The effect of pH was unraveled by conducting experiments at acidic pH 3, a basic pH 11 and at the neutral pH 6.8. In each case, 120 mg of the photocatalysts were added in a 125 mL of MO dye solution of 10, 30, and 50 ppm and allowed to perform the experiment for a time interval of 5 h (11.00 am to 4.00 pm). The pH of the MO solution was adjusted by the addition of dilute HNO₃ or NaOH solution.

Study of the Effect of H₂O₂

The effect of H₂O₂ was unraveled by adding 0.1 mL and 0.25 mL of H₂O₂ in a 125 mL of MO solution containing 10 ppm, 30 ppm and 50 ppm dye at acidic pH 3, a basic pH 11 and at the neutral pH of 6.8. In each case, 120 mg of the photocatalysts were added and allowed to perform the experiment for a time interval of 5 h (11.00 am to 4.00 pm).

3.7.5 Reaction Kinetics and Mathematical Equations

The dye degradation (%) was used as an indicator to evaluate and compare the photocatalytic performances of the Ag/MoO₃/TiO₂ immobilized BG reactor.

The percentage (%) degradation was determined by using the following equation [139]:

$$\% \text{ Degradation} = \frac{C_0 - C_t}{C_0} \times 100 \quad (3.7)$$

Where C₀ is initial concentration of dye solution, ppm, C_t is concentration of dye solution after irradiation, ppm.

The kinetics of the degradation of MO dye by photocatalytic reaction were studied for zero-order, first-order and second-order with respect to dye degradation with time [140]. The integrated form of expressions for kinetic models are presented by Eqs. (3.8-3.10)

Zero-order kinetics:

$$C_t - C_o = k_o t \quad (3.8)$$

First-order kinetics:

$$\ln \left(\frac{C_o}{C_t} \right) = k_1 t \quad (3.9)$$

Second-order kinetics:

$$\frac{1}{C_t} - \frac{1}{C_o} = k_2 t \quad (3.10)$$

Where k_0 ($\text{mgL}^{-1} \cdot \text{min}^{-1}$), k_1 (min^{-1}) and k_2 ($\text{Lmg}^{-1} \cdot \text{min}^{-1}$), represent the apparent kinetic rate constants for zero, first and second-order reaction kinetics, respectively. C_o and C_t are the initial dye concentration and dye concentration at time t (min), respectively [140].

CHAPTER 4

RESULTS AND DISCUSSION

In this Chapter, the results and discussion of the study have been presented systematically. The key parts of this Chapter include results and discussion on the characterization of photocatalysts and the photocatalytic degradation of MO dye in presence of UV-irradiation. The closing subsection contains optimization of photocatalytic activity of the modified TiO₂ photocatalysts.

4.1 Characterization of Photocatalysts

The analytical techniques used in this particular research were XRD for crystalline structure, SEM for surface morphology and particle size, FT-IR for surface functional group, UV-Vis/DRS for optical activity and bandgap energy, and BET for surface area and pore volume. The analytical results obtained are discussed in this particular section with respect to performed analysis in the laboratory.

4.1.1 X-ray Diffraction (XRD) of Photocatalyst

XRD was performed to determine, phase composition, crystallinity, and average crystalline size. The spectra of all synthesized samples (TiO₂ nanoparticles and MoO₃/TiO₂, Ag/TiO₂, and Ag/MoO₃/TiO₂ nanocomposites) are shown in Figure 4.1. As shown in Figure 4.1a, the 2θ peaks in XRD spectra were at 25.39°, 30.89°, 37.85°, 47.88°, 54.18°, 55.15°, 62.60°, 69.07°, 70.20°, and 75.06° corresponding to the diffractions from the crystal planes of {101}, {110}, {004}, {200}, {105}, {211}, {204}, {116}, {220} and {215} (JCPDS card no 21-32272), which indicates that the TiO₂ nanoparticles (NPs) were dominated by the anatase crystal structure [30,141]. It was observed that no distinguished peaks were observed for MoO₃/TiO₂, Ag/TiO₂, and Ag/MoO₃/TiO₂ nanocomposites as compared to TiO₂. This reveals that there was no change of crystal lattice structure of TiO₂ after modification using MoO₃ and Ag dopant due to the addition of a lower amount of MoO₃/Ag, the high crystalline structure of TiO₂, very low diffraction intensity from MoO₃ impurity, and uniform distribution of the Ag into the TiO₂ crystal structure [132, 133]. Only the key difference was observed in intensity level of the major anatase (101) plane peaks which depends on the rate of calcination temperature distribution. The

anatase phase was usually exhibited the best photocatalytic behavior, while the rutile phase was the most stable phase [142]. This was formed due to electron transport from the valence band to the conduction band in the anatase phase and thus, results in the increase of photocatalytic activity for dye degradation [143, 144].

More than 80% of anatase phase (Table 4.1) was obtained in Ag/MoO₃/TiO₂ nanocomposite and it was reported that the mixture of a large portion of anatase with an adjacent lower portion of rutile phase exhibited higher photocatalytic activity [142]. According to the literature, the dopant acts as a crystal structure defect and may suppress the rate of temperature distribution during the heating period on the surface of nanocomposites [30]. Besides, peaks with higher intensity were observed in doped nanocomposites as compared to TiO₂ nanoparticles indicating that the crystals were mostly amorphous [30]. The possible reason for amorphous nature is the presence of surface defects that are exhibited by dopants and surface oxygen vacancy [30,131,145]. For this particular case, the existence of MoO₃ and Ag has hindered the phase transformation, which resulted in amorphous phase rather than crystalline structure.

Table 4.1: Summary of theoretical physicochemical properties of TiO₂ nanoparticles

SI No.	Samples	Methods	Anatase phase, %	Rutile phase, %	Crystalline Size (nm)	d_{hkl} (Å)	Lattice Parameter (Å)	
							a	c
1.	TiO ₂	Sol-gel	70.44	29.55	11.52	3.52	3.786	9.518
2.	MoO ₃ /TiO ₂	Sol-gel	74.18	25.81	7.76	3.53	3.797	9.504
3.	Ag/TiO ₂	Sol-gel	80.59	19.40	6.13	3.51	3.784	9.495
4.	Ag/MoO ₃ /TiO ₂	Sol-gel	82.43	17.56	4.25	3.53	3.795	9.503

The peak intensities from the XRD analysis were used to measure the theoretical physicochemical properties of all samples and Table 4.1 shows those calculated data. The average crystalline size of the TiO₂, MoO₃/TiO₂, Ag/TiO₂, and Ag/MoO₃/TiO₂ nanocomposites were found to be 11.52 nm, 7.76 nm, 6.13 nm, and 4.25 nm, respectively. The crystalline size was reduced due to the lattice distortion that was employed with interface tension along with the stress field. The smaller crystalline size was responsible for the increased surface area of

Ag/MoO₃/TiO₂ and can have higher photocatalytic activity for the degradation of dye under the incident visible light exposure [146-147].

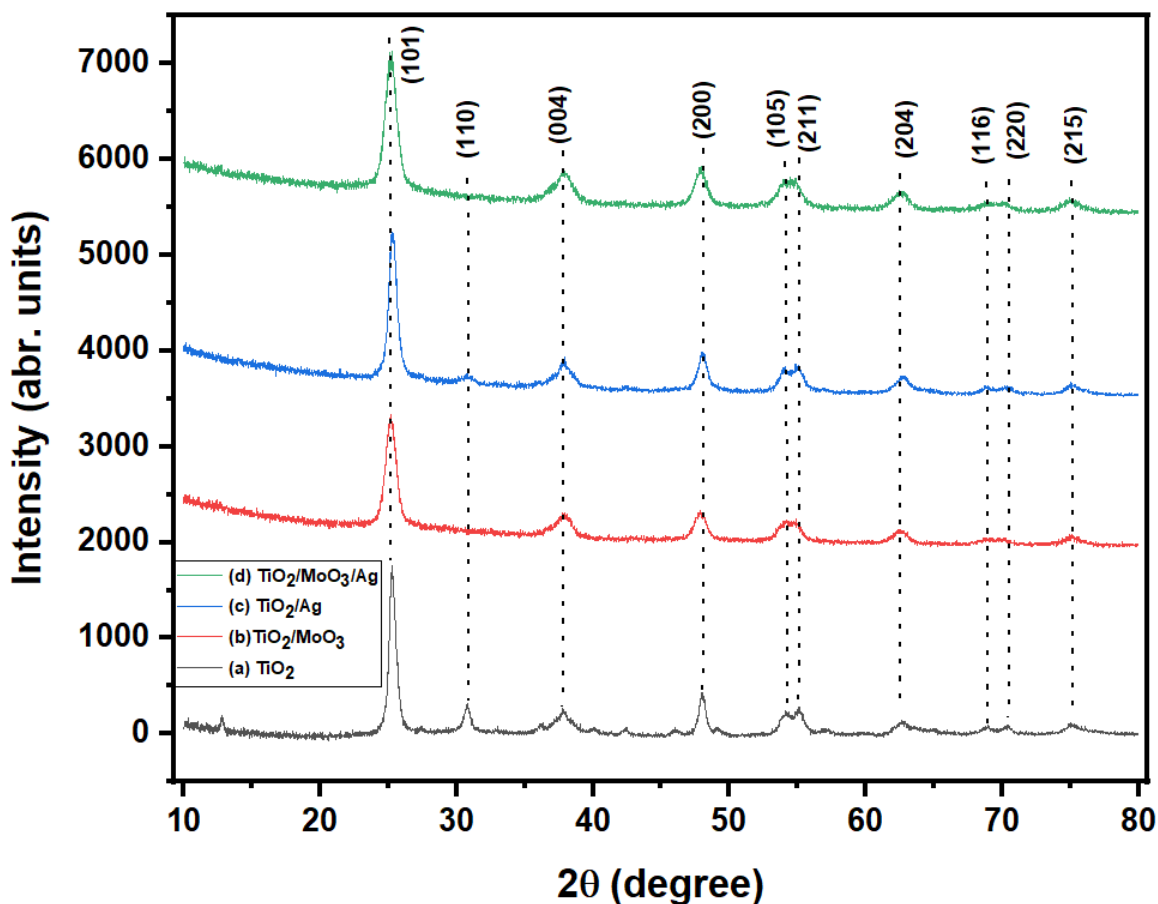


Figure 4.1: XRD plot of photocatalysts (a) TiO₂, (b) MoO₃/TiO₂, (c) Ag/TiO₂, and (d) Ag/MoO₃/TiO₂

Also, lattice parameters such as a , c , and d_{hkl} were determined for all samples (Table 4.1) and small difference were observed in doped TiO₂ with respect to TiO₂. These differences of axial parameters were formed due to anisotropic size dependent variation during preparation period [148]. Furthermore, those axial parameter deviations are very small to influence the photocatalytic activity of corresponding photocatalysts. As photocatalytic character was predominantly dependent on the availability of active surface area rather than slight amendments in axial parameters of the photocatalyst [149]. However, the smaller crystalline size in Ag/MoO₃/TiO₂ nanocomposite is an indication of increased surface area as we observed from

BET analysis and can have a higher photocatalytic activity to the degradation of dye under the incident visible light [146].

4.1.2 Scanning Electron Microscope (SEM) of Photocatalyst

SEM images, shown in Figure 4.2, demonstrate the shape and surface morphology of all the photocatalysts. A porous bulk structure along with quite uniform spherical morphology was observed for TiO₂ (Figure 4.2a). A similar morphology was obtained by other researchers with a slightly smaller particles size [150]. The surface ruggedness and roughness were increased slightly [151, 152] from the incorporation of MoO₃ in TiO₂ as shown in Figure 4.2c. This change of surface was executed due to the aggregation of MoO₃ and TiO₂ spherical particles. Figure 4.2e shows dense bubble pattern surface of Ag incorporated TiO₂, which has higher surface roughness due to aggregation of spherical Ag particles on TiO₂. This dense bubble pattern on support crystal due to particle aggregation that is frequently observed in literature of doping synthesis [153].

As shown in Figure 4.2g, it is clear that the aggregation of tiny particles was increased due to the addition of Ag on existing TiO₂/MoO₃. Therefore, the doping of Ag metal does not give any changes in the topology of the catalyst surface [30,154]. Moreover, the modification of TiO₂ photocatalyst using MoO₃ and Ag indicates an increased ruggedness, roughness and thus yielded a more porous surface area [155]. Based on the SEM image, the average diameters (Figure 4.2b, d, f, h) were found around 15-25 nm, 60-100 nm, 50-80 nm, and 12-18 nm for TiO₂, MoO₃/TiO₂, Ag/TiO₂, and Ag/MoO₃/TiO₂, respectively.

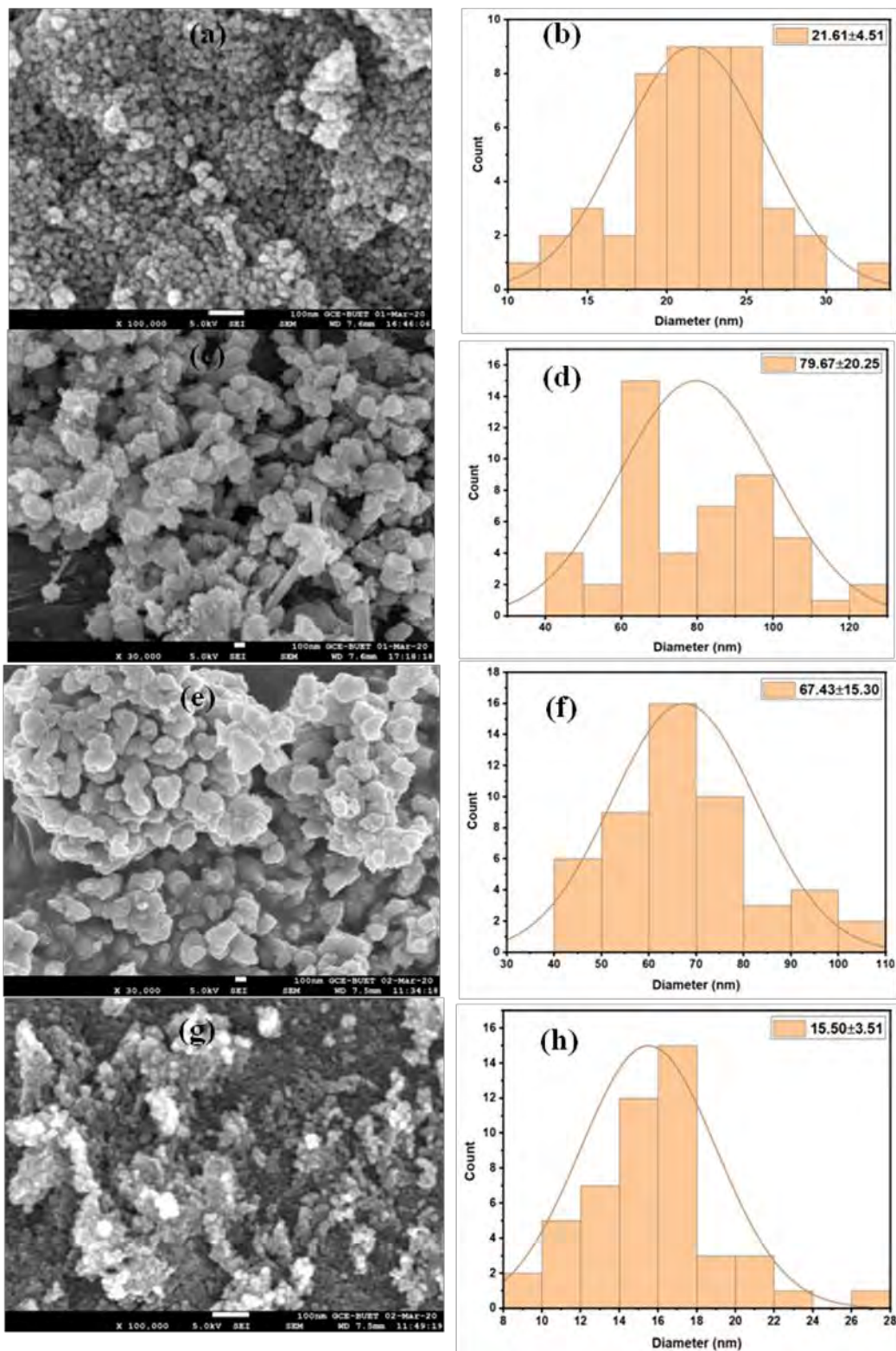


Figure 4.2: SEM image of nanocomposite photocatalysts (a) TiO₂, (c) MoO₃/TiO₂, (e) Ag/TiO₂, and (g) Ag/MoO₃/TiO₂; and particle size diameter of photocatalysts (b) TiO₂, (d) MoO₃/TiO₂, (f) Ag/TiO₂, and (h) Ag/MoO₃/TiO₂

4.1.3 Fourier Transform Infrared Spectroscopy (FT-IR) of Photocatalyst

FTIR spectroscopy was performed to study the surface functional groups on the photocatalysts and the spectra are shown in Figure 4.3. The absorption bands observed between $500\text{--}800\text{ cm}^{-1}$ (below 1000 cm^{-1}) represent the stretching vibrations of Ti–O–Ti, Ti–O–C, and Ti–O bonds in the TiO_2 lattice structure [8], which confirms the formation of titanium metal complex [156]. It has been reported that the presence of Ti–O–Ti bond enhances the photocatalytic performance of dye degradation [157].

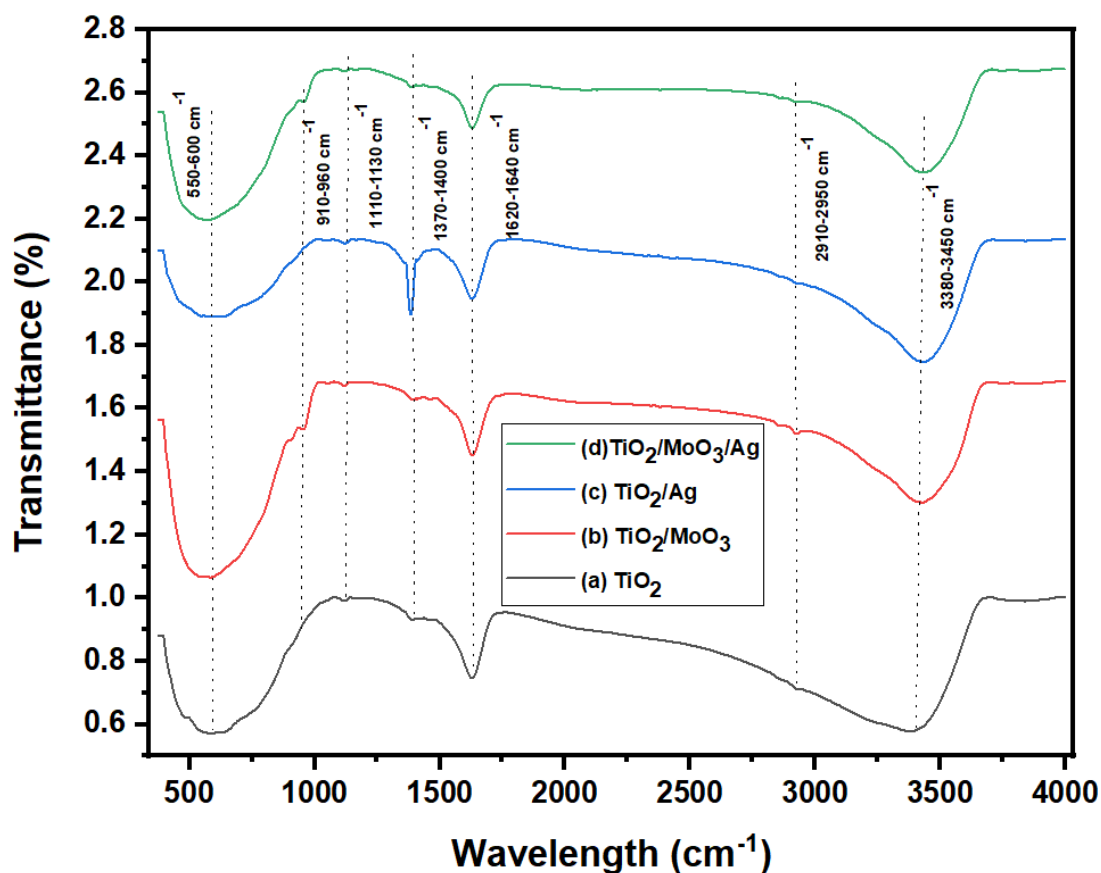


Figure 4.3: FT-IR analysis of synthesized photocatalysts; (a) TiO_2 , (b) $\text{MoO}_3/\text{TiO}_2$, (c) Ag/TiO_2 , and (d) $\text{Ag}/\text{MoO}_3/\text{TiO}_2$

The peak observed between $1620\text{--}1540\text{ cm}^{-1}$ corresponds to stretching vibrations of --C=C-- (alkenes) bond, indicating the presence of sp^2 hybridized carbon along with bending vibration of O–H bond, which results in higher intensity and shows potential photocatalytic activity. The sharp peaks observed between $1370\text{--}1400\text{ cm}^{-1}$ show stretching vibrations of Ti=O bond due to the addition of HNO_3 in material synthesis [158]. Similarly, the typical vibrations centered

absorption peaks around $3380\text{-}3450\text{ cm}^{-1}$ identify the broadband of O-H group that refers to alcohol (-OH) and carboxylic acid (-C=O-) groups and contributed to water molecules adsorption [159].

4.1.4 UV-Vis Diffuse Reflectance Spectroscopy (UV-Vis/DRS) of Photocatalyst

UV-Vis diffuse reflectance spectra (UV-Vis/DRS) of synthesized TiO_2 , $\text{MoO}_3/\text{TiO}_2$, Ag/TiO_2 , and $\text{Ag}/\text{MoO}_3/\text{TiO}_2$ photocatalysts were measured. As shown in Figure 4.4, it was observed that dopant (MoO_3 and Ag) assisted photocatalysts redshifted its absorption edge towards a higher wavelength that indicates the photogenerated electron/hole (e^-/h^+) pair and consequently enhance the photocatalytic activity [8,152]. This was formed due to a combinational effect of MoO_3 narrow and TiO_2 wide bandgap [30,160].

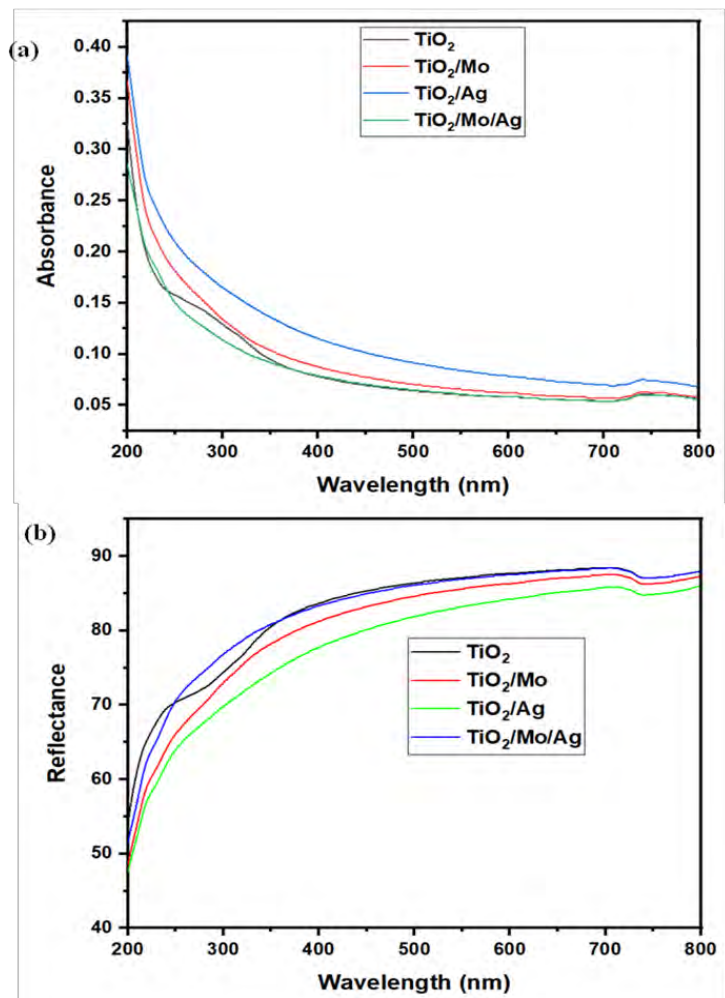


Figure 4.4: UV/Vis response of synthesized photocatalysts; (a) absorbance graphs and (b) reflectance graphs

Furthermore, the addition of Ag metal particles in TiO₂/MoO₃ nanocomposite acts as traps electron and reduces the e⁻/h⁺ pair recombination [8,152]. The absorption edge of Ag/MoO₃/TiO₂ nanocomposite undergoes a clear red shift along with broadband in visible range compared to TiO₂, MoO₃/TiO₂, and Ag/TiO₂ nanocomposites. This absorption was formed due to the surface plasmon resonance (SPR) and a drastic change in the dielectric constant of the surrounding medium of Ag nanoparticles [161, 162]. Additionally, it was clear that a slight increase of the reflectance spectrum of the dopant-assisted photocatalyst was found at a longer wavelength than TiO₂. Thus, an effective enrichment of visible light absorption capacity of Ag/MoO₃/TiO₂ nanocomposite has beneficial effect on the photocatalytic activity for the degradation of dye [8,152].

The bandgap energy (E_g) of all the photocatalysts were measured as it is an important parameter for photocatalytic degradation of dye. It reveals the amount of energy is to be absorbed by the photocatalyst to produce the e⁻/h⁺ pair [163]. The calculated E_g values by using Tauc plots (a graphical representation of Kubelka-Munk formulism) are tabulated in Table 4.2.

Table 4.2: The bandgap energy (eV) of all TiO₂ based nanocomposites prepared with sol-gel by using Kubelka-Munk equation

Sample	Method	Bandgap, E_g (eV)
TiO ₂	Sol-gel	3.24
MoO ₃ /TiO ₂	Sol-gel	3.15
Ag/TiO ₂	Sol-gel	2.95
Ag/MoO ₃ /TiO ₂	Sol-gel	2.89

The E_g values of TiO₂, MoO₃/TiO₂, Ag/TiO₂, and Ag/MoO₃/TiO₂ photocatalysts were found to be around 3.24 eV, 3.15 eV, 2.95 and 2.89 eV, respectively is shown in Figure 4.5. It has been reported that the typical bandgap energy of TiO₂ NPs for pure anatase phase is 3.2 eV and for pure rutile phase is 3.0 eV [164].

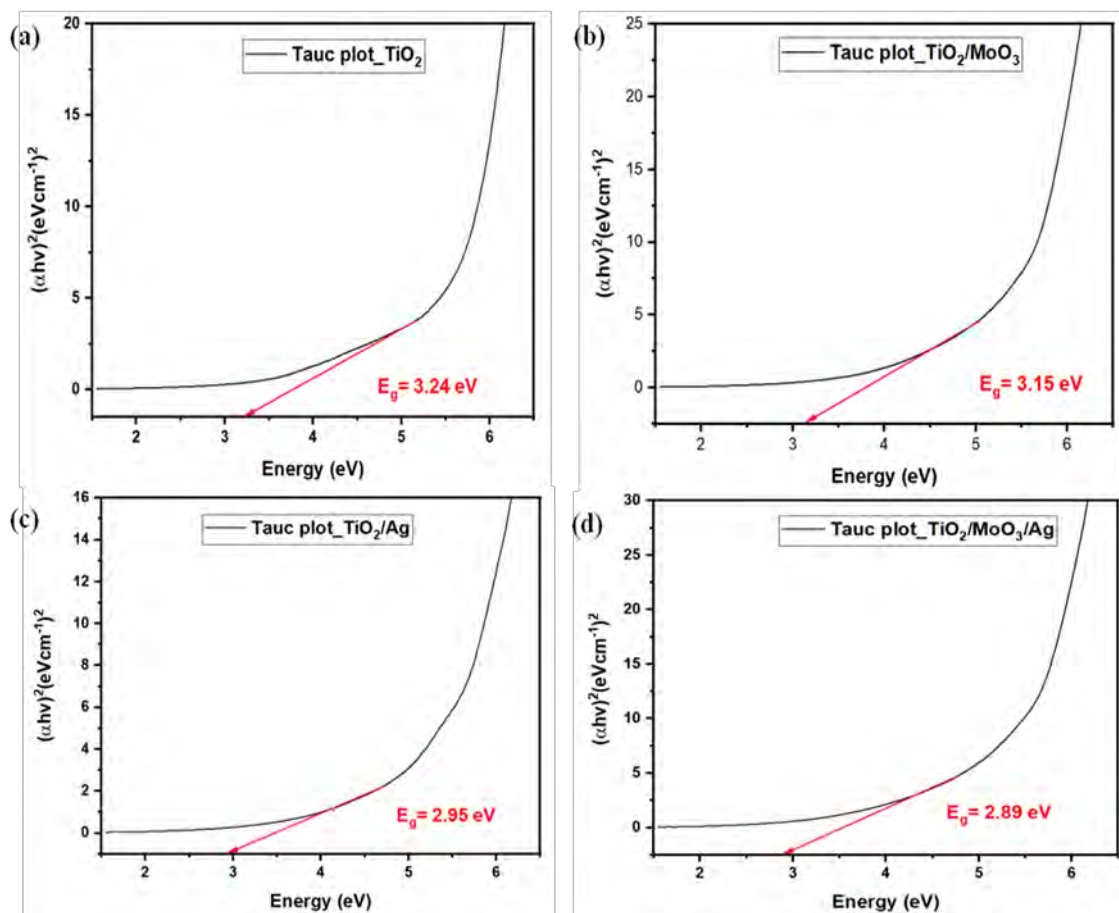


Figure 4.5: Bandgap energy of all photocatalysts (a) TiO₂, (b) MoO₃/TiO₂, (c) Ag/TiO₂, and (d) Ag/MoO₃/TiO₂ nanocomposites

It can be seen that the E_g values were relatively lower for nanocomposites due to the incorporation of dopants MoO₃ and Ag into the reaction medium, which attributed to the visible light absorption by SPR and suppression of the charge separation. This assists to easier formation of e^-/h^+ pair [2,165] on the photocatalysts. The photocatalysts having a smaller bandgap has higher photocatalytic activity for the degradation of organics.

4.1.5 Nitrogen Physisorption Measurement (BET) of Photocatalyst

The analysis of specific surface area and pore volume were carried out by N₂ adsorbate based adsorption-desorption mechanism. The experimental values were calculated using the BET adsorption method and are summarized in Table 4.3. The result of specific surface area shows a dramatic increase due to doping especially with MoO₃ and Ag. The specific surface area and pore volume of nanocomposites were increased as compared to undoped TiO₂. The specific

surface area of Ag/MoO₃/TiO₂ nanocomposite was increased by 6.6 times in comparison to TiO₂. It was observed that the surface area decreased with increasing the crystal size. The increase of specific surface area is consistent with the observed results as obtained from SEM image (Figure 4.2) analysis. The SEM images showed an increase in roughness of Ag and MoO₃ doped TiO₂ photocatalysts by means of bubbly surface. The specific surface area is a fundamental property of porous catalyst like TiO₂. The addition of Ag/MoO₃ has greater impact on specific surface area shown massive increase of surface area in comparison to MoO₃/TiO₂, and Ag/TiO₂ nanocomposites.

The pore volume was increased significantly with dopings of MoO₃ and Ag on TiO₂. This increase in pore volume was desired for photocatalytic reaction as suggested by the previous works related to photocatalysts especially TiO₂ [166, 167]. However, the increase of surface area can be very useful for contaminants to penetrate through and carry out the desired degradation reactions as it implies a larger contact surface exposed to the reagents. Similarly, the increase of pore volume can also be considered as an increase in mesopore volume [168]. The experimental results from the BET surface studies were justified by the results obtained from XRD (Table 4.1). In heterogeneous photocatalysis process, a higher surface area and pore volume can be useful in the formation of photogenerated e⁻/h⁺ pairs in photocatalyst. The heterogeneous photocatalytic activity can be influenced significantly by the surface area and pore volume [169].

Table 4.3: Surface area and pore volume measurement of all composites

SI No.	Sample	Method	Surface area (m ² /g)	Pore Volume (cm ³ /g)
1.	TiO ₂	Sol-gel	20.02±0.16	0.0673
2.	TiO ₂ /MoO ₃	Sol-gel	85.82±0.28	0.1555
3.	TiO ₂ /Ag	Sol-gel	58.11±0.35	0.1689
4.	Ag/MoO ₃ /TiO ₂	Sol-gel	136.40±1.63	0.0478

4.2 Photocatalytic Activity Assessment

The photocatalytic activity of immobilized TiO₂, Ag/TiO₂, MoO₃/TiO₂, and Ag/MoO₃/TiO₂ photocatalysts on BG plate was evaluated for the degradation of MO dye under UV (100 W)

irradiation (5.5 h) and compared each other. The impact of several operating conditions such as catalysts dosages, initial dye concentration, pH, and H₂O₂ were investigated.

4.2.1 Reactors Performance Evaluation

The dye degradation results for TiO₂, Ag/TiO₂, MoO₃/TiO₂, and Ag/MoO₃/TiO₂ photocatalysts are shown in Figure 4.6. It can be seen that the photocatalytic degradation of MO for TiO₂, MoO₃/TiO₂, Ag/TiO₂, and Ag/MoO₃/TiO₂ were found to be 59.5%, 63.1%, 70.6%, and 75.8%, respectively, which represents the evidence of enhancement of photocatalytic activity from doping. For Ag/MO₃/TiO₂, about 75% of MO was degraded within 5.5 h. According to the literature survey, glass is commonly used as the coating substrate, which has high transparency to UV-radiation and has the good adhesive property to support TiO₂ based nanocomposites without reduction of catalytic activity [170, 171]. Therefore, the high degradation rate was observed. The photocatalytic degradation orders were TiO₂ < MoO₃/TiO₂ < Ag/TiO₂ < Ag/MoO₃/TiO₂. The experimental result represents that the photodegradation efficiency can be enriched by the addition of Ag and MoO₃ nanoparticles onto the TiO₂ catalyst surface.

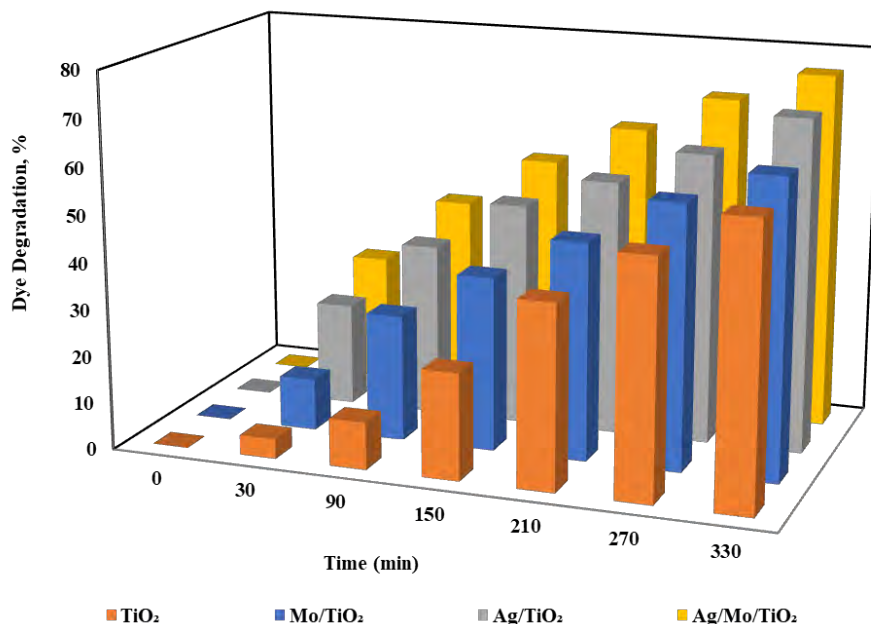


Figure 4.6: MO dye removal under UV irradiation (Experimental condition: Ag/Mo/TiO₂ immobilized on BG reactors: 120 mg, pH: 7.0, initial MO dye conc.: 10 ppm)

4.2.2 Reaction Kinetics Study

The pseudo-first-order model was fitted the best with the experimental data that indicate the straight lines almost fit the experimental values (Figure 4.7). The zero-order and the second-order models were less fitted with the experimental data and the reaction kinetic models are shown in Appendix C (Figure C1-C3). It can be seen from (Figure 4.7) that the rate constant values were increased with doping indicating the generation of e^-/h^+ pairs was increased with the doping of TiO_2 [30]. For instance, the rate constants were 0.003 min^{-1} , 0.002 min^{-1} , 0.003 min^{-1} , and 0.004 min^{-1} for TiO_2 , MoO_3/TiO_2 , Ag/TiO_2 , and $Ag/MoO_3/TiO_2$, respectively, for 0.120 g of photocatalyst dose. The regression values (R^2) values were 0.998, 0.968, 0.980, and 0.981 for TiO_2 , MoO_3/TiO_2 , Ag/TiO_2 , and $Ag/MoO_3/TiO_2$, respectively. This was executed due to the increase of generation of the number of e^-/h^+ pairs which consequently increased the $\cdot OH$ in solution and enhanced the dye degradation efficiency [172]. In constant, the decreasing trend of rate constant was observed with the increase of dye concentration in the treatment. This decrease in the rate of reaction might be executed from the reduction of active sites on the catalyst surface and interference of the UV-irradiation to reach the catalyst surface [30]. The slight deviations might be executed due to interference from oxygen or interfering from intermediates [30].

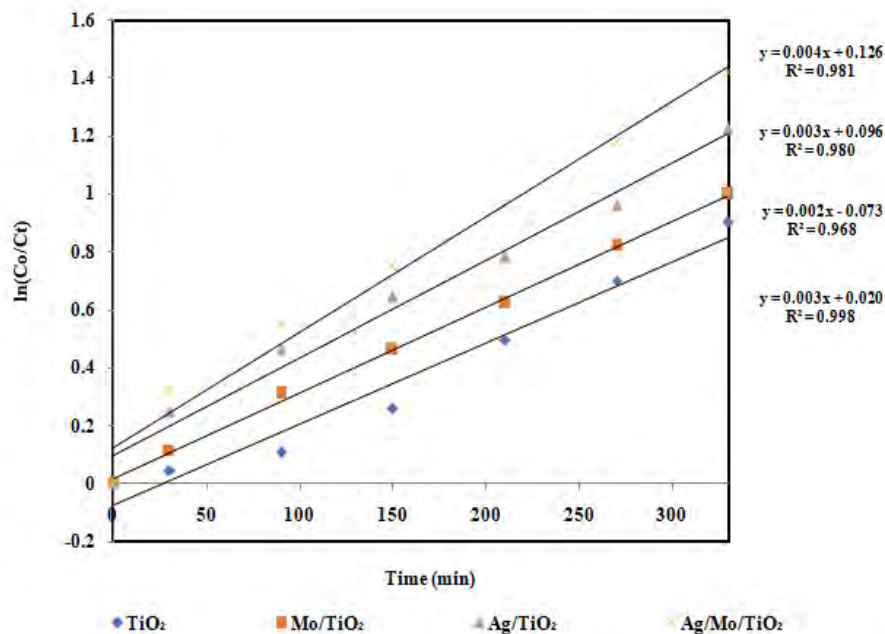


Figure 4.7: Pseudo first-order reaction kinetics of MO dye degradation in presence of UV-irradiation (Experimental condition: dose of $Ag/Mo/TiO_2$ immobilized on BG reactors: 120 mg, pH: 7.0, initial MO dye conc.: 10 ppm)

4.2.3 Impact of pH

The pH of the dye solution is an important factor in the photocatalytic process. To study the impact of the pH on photodegradation efficiency, experiments were carried out at pH 3.0, 7.0, and 11.0, respectively, with fixed initial dye concentration (10 ppm), and photocatalyst dose (0.120 g of TiO₂, Ag/TiO₂, MoO₃/TiO₂, and Ag/MoO₃/TiO₂ photocatalysts) for 5.5 h under UV-irradiation. The impact of pH on MO dye degradation is shown in Figure 4.8. As shown in Figure 4.8a, it was observed that the decrease of pH from 11.0 to 3.0 increases the photodegradation efficiency (from 54.3% to 78.1%). The degradation efficiency was 59.5% at pH 7.0. The experimental results showed that higher degradation efficiency was found in the acidic medium than in the neutral and alkaline medium. Similarly, for MoO₃/TiO₂ photocatalysts (Figure 4.8b), it can be seen that the decrease of pH from 11.0 to 3.0 increases the photodegradation efficiency from 59.5% to 81.2%. The impact of Ag/TiO₂ photocatalyst is shown in Figure 4.8c and a similar results were obtained for Ag/TiO₂. The highest removal (88.4%) was observed at pH 3.0. Finally, for Ag/MoO₃/TiO₂ photocatalyst (Figure 4.8d), it can be seen that the decrease of pH from 11.0 to 3.0, increases the photodegradation efficiency (from 62.6% to 96.5%).

The experimental results showed that the higher photocatalytic efficiency was found in the acidic medium than the neutral and alkaline medium. The order of the photodegradation efficiency was pH (11.0) < pH (7.0) < pH (3.0). The pH has a pronounced influence on photocatalytic degradation of MO dye. The optimal pH was acidic (pH 3). In an acidic condition, the surface of TiO₂ is positively charged, which stimulate TiO₂ to adsorb negative charged organic compounds. As a result, high photocatalytic activity is expected on the surface because of higher adsorption. In contrast, in an alkaline condition, significantly less interaction was caused by coulombic repulsion between the negative TiO₂ and organic compound anions, leading to a decline of photo-catalytic reaction [173, 174]. In addition, pH can also change the pathway of photocatalytic degradation for organic compounds. The adsorption of MO on TiO₂ surface at neutral or basic condition was very limited (3%) due to negatively charged sulfonate groups [175]. The experimental results of the present work suggest the synthesized Ag/MoO₃/TiO₂ nanocomposite has comparatively higher photodegradation efficiency for MO dye in aqueous solution under-UV irradiation.

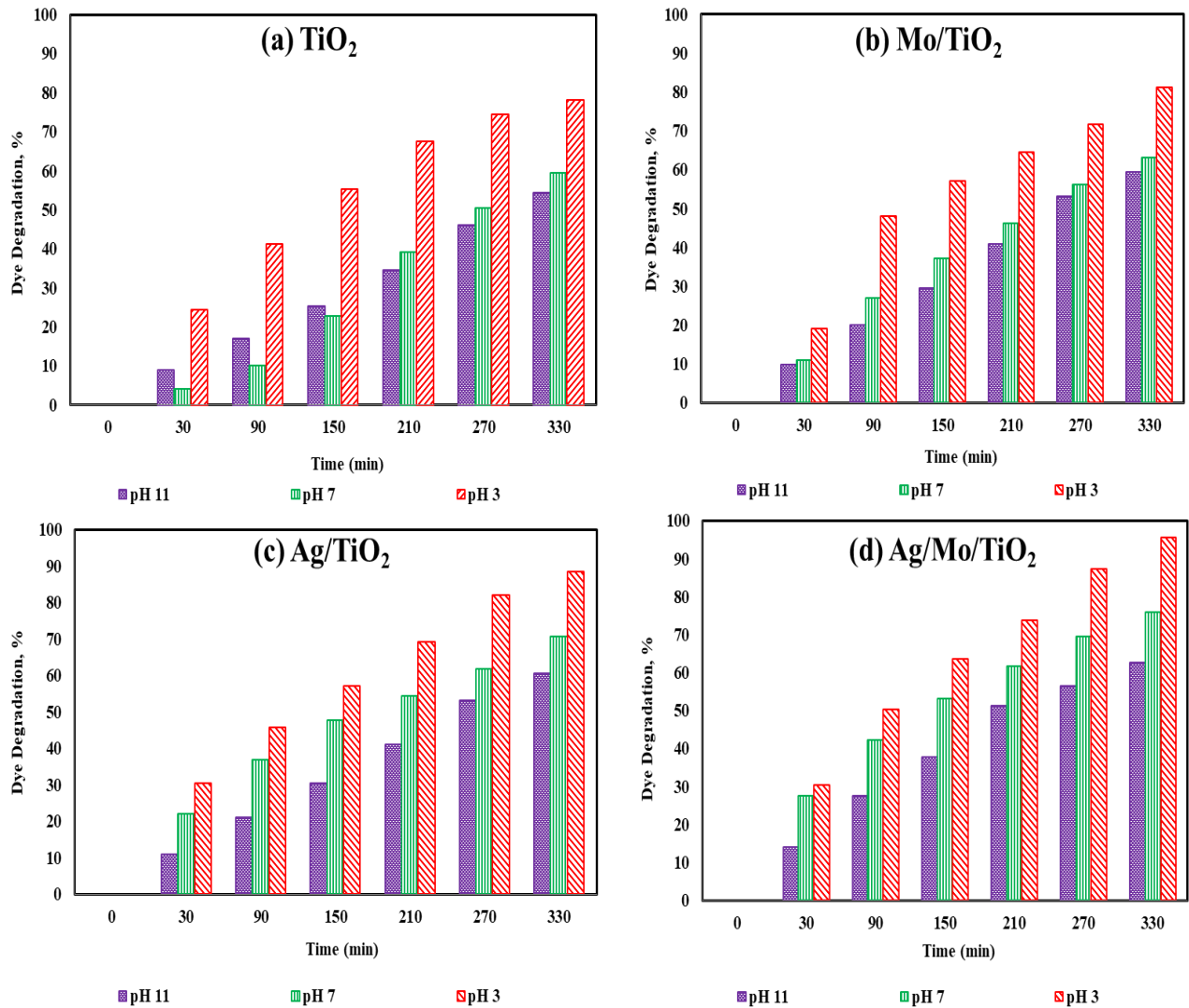


Figure 4.8: Impact of pH on MO degradation efficiency; (a) TiO₂, (b) Mo/TiO₂, (c) Ag/TiO₂, and (d) Ag/MoO₃/TiO₂ nanocomposites under UV-irradiation (Experimental condition: 0.120 g of photocatalyst on immobilized reactor, dye concentration: 10 ppm, pH: 3.0, 7.0 and 11.0)

4.2.4 Impact of Photocatalyst Dose

Assessment of an optimum photocatalyst dose is crucial for the degradation of MO dye from a photocatalytic treatment due to avoid an excess catalyst dose. The impact of doses of Ag/MoO₃/TiO₂ immobilization on BG surface for the degradation of MO dye at a particular dye concentration (10 ppm) and pH (3.0) is shown in Figure 4.9. As shown in Figure 4.9, it was observed that photocatalytic degradation of MO dye were 62.658%, 78.1%, 95.6%, and 98.5% for 0.080, 0.100, 0.120, and 0.140 g of photocatalyst doses, respectively, for Ag/MoO₃/TiO₂

nanocomposite. It can be seen that with an increase of photocatalyst doses in the reactor, the degradation efficiency increases due to a large number of active sites were available to adsorb dye molecules and photons [30,151].

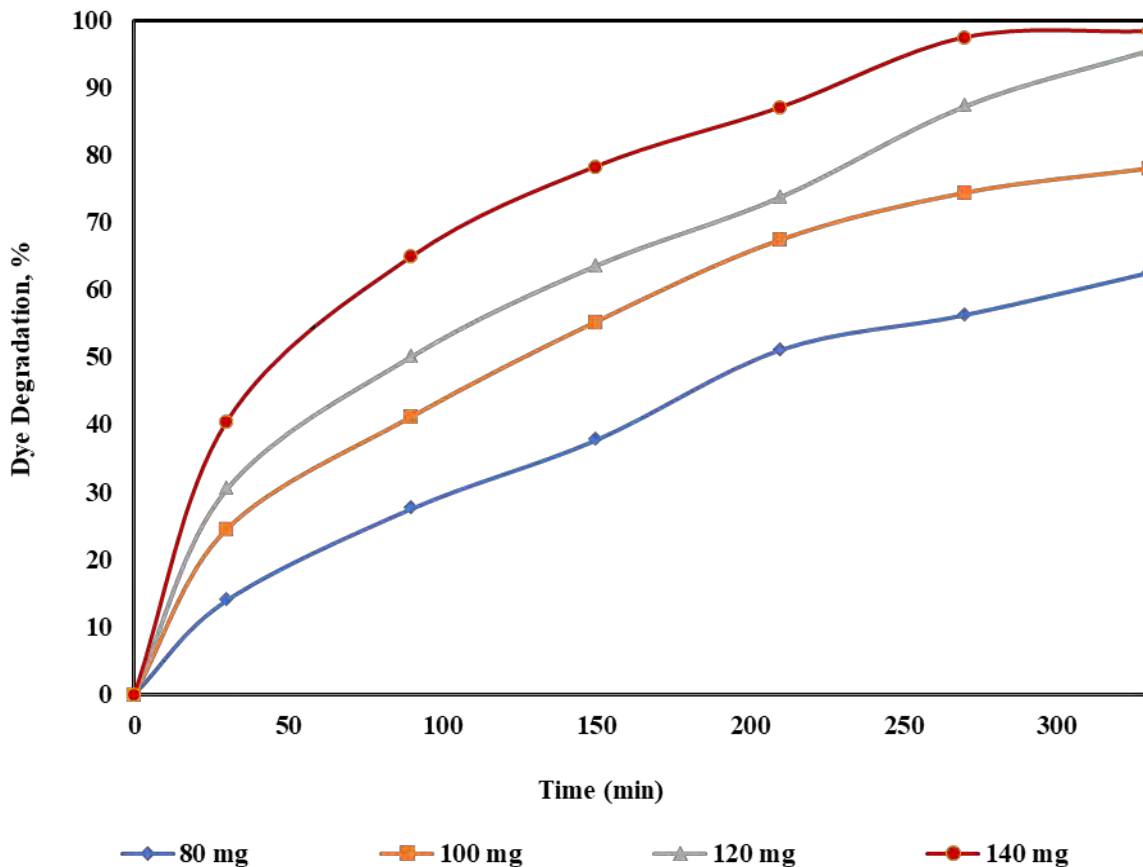


Figure 4.9: MO dye degradation under UV-irradiation (Experimental condition: dose of Ag/MoO₃/TiO₂ immobilized on BG reactors: 120 mg, pH: 3.0, initial MO dye conc.: 10 ppm)

According to literature, it can be seen that by increasing the photocatalyst loading with the substrate, the degradation efficiency increases, but further increasing of photocatalyst loading will decrease the dye degradation efficiency due to the aggregation of photocatalyst on the substrate surface which results in lowering of the surface area [176]. Previously, it has been reported that a sufficient amount of catalysts with coatings/dopings is required for effective dye degradation from the photocatalytic system [177], however, light scattering and the reduction of light penetration into the solution may be executed with an excess amount of photocatalyst loading [178]. It was reported that the surface modification of Ag and MoO₃ into TiO₂ structure enhances the absorption intensity in the visible light (redshift) region and improves the electronic

structure through harvesting UV-irradiation [179]. The photogenerated e^-/h^+ pair and bandgap energy were formed by the incorporation of MoO_3 which effectively suppressed the charge recombination and promoted the charge transfer within TiO_2/Ag nanocomposite [180]. The presence of Ag nanoparticles boosting the photocatalytic activity was ascribed to the redshift of the wavelength response due to the SPR effect and consequently increase the e^-/h^+ recombination rate [2]. It was observed that degradation efficiency was increased with doping due to increasing the anatase phase that suppresses the crystalline size of TiO_2 and consequently, increases the surface area. However, the higher surface area can address more dye molecules adsorption onto the TiO_2 active site and thus, increases MO dye degradation [179]. Therefore, $\text{Ag}/\text{MoO}_3/\text{TiO}_2$ immobilization dose with a degradation efficiency of MO dye of 95.6% was considered as an optimum catalyst dose.

4.3 Impact of Dye Concentration and Hydrogen Peroxide Concentration on Reactor Performance

More than 95% of MO dye degradation was obtained for 10 ppm concentration using $\text{Ag}/\text{MoO}_3/\text{TiO}_2$ nanocomposite within 5.5 h of UV-irradiation, and therefore, the photocatalytic activity was tested at a higher dye concentration such as 30 and 50 ppm. Besides, in this section, we also studied the impact of the addition of H_2O_2 in the reactor to observe the change of reactor performance. The photocatalyst dose (0.120 g $\text{Ag}/\text{MoO}_3/\text{TiO}_2$ nanocomposite) and solution pH (3.0) were kept constant to prepare a $\text{Ag}/\text{MoO}_3/\text{TiO}_2$ -immobilized BG reactor. Two doses (0.1 mL and 0.25 mL) of H_2O_2 concentrations were used to investigate the impact of H_2O_2 on the reactor performance.

4.3.1 Impact of Dye Concentration

The impact of dye concentration on $\text{Ag}/\text{MoO}_3/\text{TiO}_2$ nanocomposite performance is shown in Figure 4.10. As shown in Figure 4.10, the MO dye degradations were 95.6%, 70.77%, and 46.12% after 5.5 h of UV-irradiation for the initial MO concentrations of 10, 30, and 50 ppm, respectively, indicating the decrease of removal efficiency with the increase of dye concentration in the reactor. This was formed due to the higher amount of adsorbed dye in contact with a lower amount of free $\cdot\text{OH}$ or superoxide radical anions and thus, consequently leads to decrease of dye degradation [30,152,179]. Also, a high concentration of MO dye might interfere with

the penetration of UV-irradiation in the solution [2, 16, 49]. However, the constant active site of the photocatalyst surface was occupied by the high concentration of dye molecules, which results in a large number of dye molecules remained in the solution [30,37,152]. To address this challenge, it is required longer irradiation, higher photocatalyst dosages, and addition of oxidant externally into the reactor's to attain a better reactor performance.

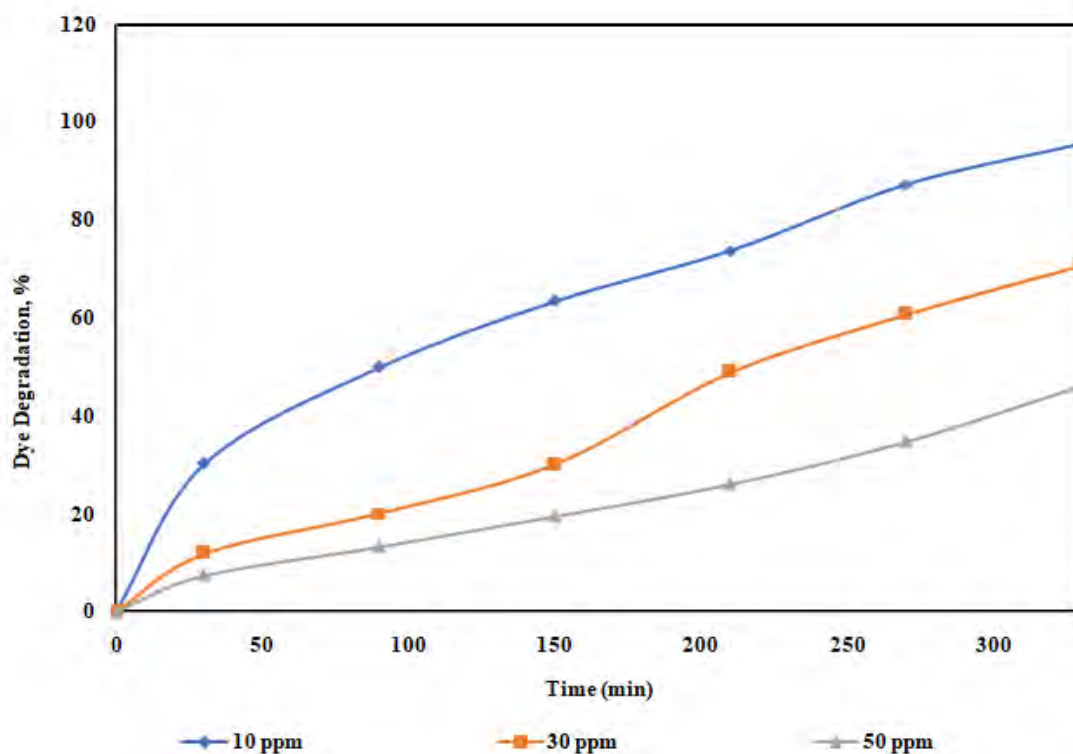
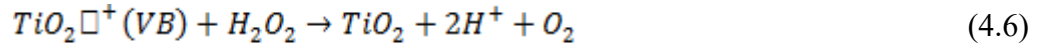
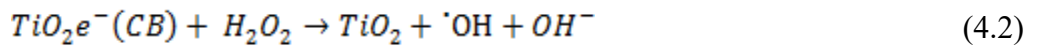


Figure 4.10: Impact of initial MO concentration on the degradation efficiency (Experimental condition: dose of Ag/MoO₃/TiO₂ immobilized on BG reactors: 120 mg, pH: 3.0, initial MO dye conc.: 10, 30, and 50 ppm)

4.3.2 Impact of Hydrogen Peroxide (H₂O₂) Concentration

H₂O₂ acts as a strong oxidant and electron scavengers that can enhance the photocatalytic activity of nanocomposites by increasing the generation of ·OH radicals [181]. The impact of the addition of H₂O₂ (two doses: 0.1 mL and 0.25 mL containing 0.5 M concentration) on the reactor performance were also studied. As shown in Figure 4.11a, more than 99% dye removal was obtained for both additions of 0.1 and 0.25 mL of H₂O₂ doses indicating 0.1 mL H₂O₂ dose was enough to degrade all the dye in 10 ppm solution.

For 30 ppm dye concentration (Figure 4.11b), the addition of H₂O₂ into the reactor has a pronounced impact on MO dye removal, and the removal efficiency was increased from 70.77% to 84.67% and 94.57%, respectively, after the addition of 0.1 and 0.25 mL of H₂O₂ into the reactor. A similar impact was also observed for 50 ppm dye concentration (Figure 4.11c), the removal efficiency was increased from 46.12% to 70.22% and 81.86%, respectively. The removal efficiency was enhanced as the concentration of H₂O₂ was increased from 0.1 to 0.25 mL for a higher dye concentration. There was no effect of H₂O₂ when the reaction was carried out in the absence of photocatalyst as H₂O₂ itself cannot generate ·OH radicals [182]. Two important things might be executed with the addition of H₂O₂; (i) increase the amount of superoxide radical anions which might suppress the recombination of e⁻/h⁺ that acts as an external electron scavenger is stated by Eqn. (4.1) and (ii) increase the charge separation by accepting conduction band electron to generate free ·OH radicals, as represented in Eqns. (4.2-4.3) [37]. The degradation efficiency was decreased at a higher H₂O₂ dose due to the formation of a hydroperoxy radical (less reactive) by the reaction of free ·OH radicals and excess H₂O₂ as expressed in Eqns. (4.4-4.5). Additionally, the H₂O₂ may consume the valance band holes and a competitive reaction must be exhibited due to radical-radical reaction as stated in Eqns. (4.6-4.7) [183].



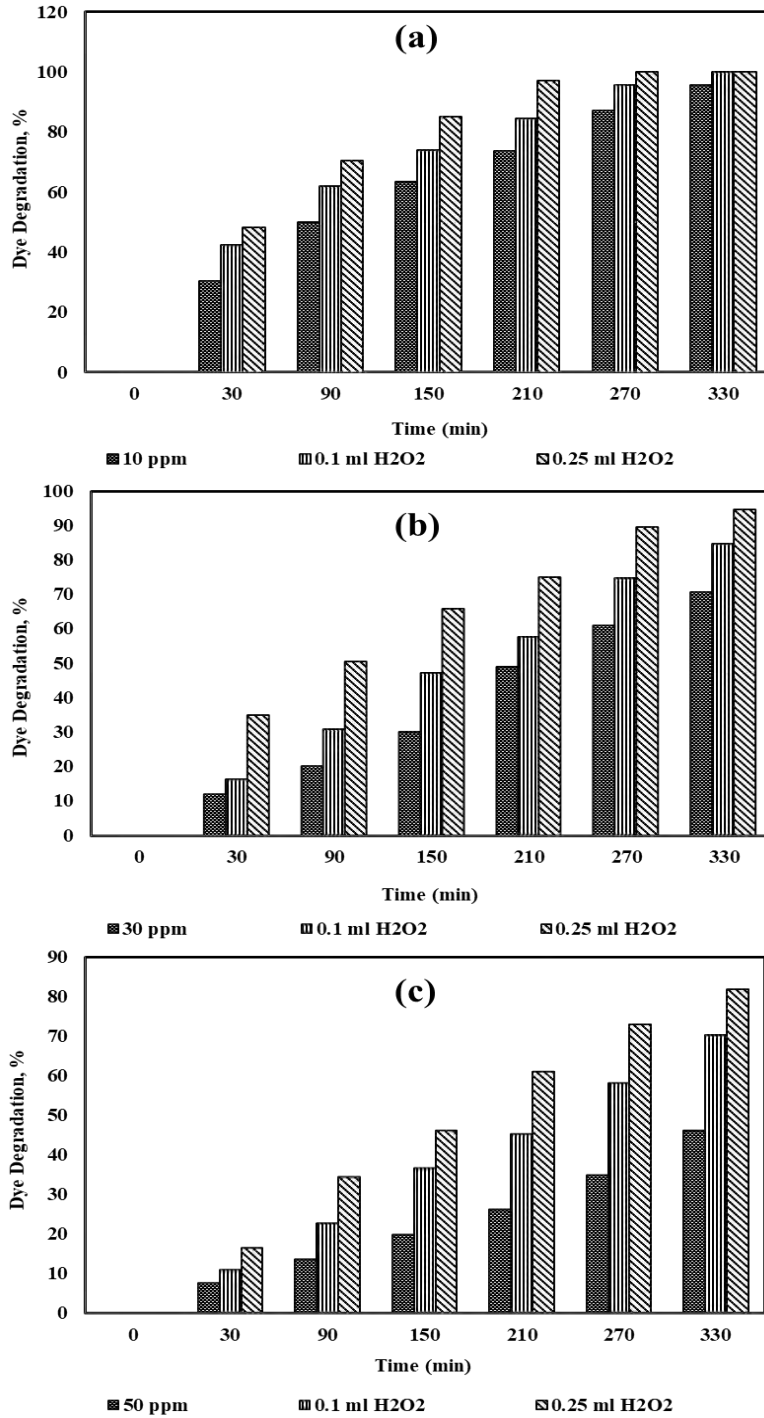


Figure 4.11: Impact of H₂O₂ concentration on the degradation efficiency (Experimental condition: dose of Ag/Mo/TiO₂ immobilized on BG reactors: 120 mg, pH: 3.0). (a) 10 ppm initial dye concentration with addition of 0.1 and 0.25 mL H₂O₂ concentration, (b) 30 ppm initial dye concentration with addition of 0.1 and 0.25 mL H₂O₂ concentration, and (c) 50 ppm initial dye concentration with addition of 0.1 and 0.25 mL H₂O₂ concentration.

CHAPTER 5

CONCLUSION

5.1 Conclusion

The following conclusions can be drawn from the current study:

- (i) The XRD results showed that the synthesized TiO₂ nanoparticles as well as TiO₂ based nanocomposites were preferentially anatase. The average particle size of photocatalysts were significantly decreased from 11.52 nm (TiO₂) to 4.25 nm (Ag/MoO₃/TiO₂) due to addition of dopants. The crystalline size was reduced due to the lattice distortion that was employed with interface tension along with the stress field.
- (ii) The SEM images showed higher surface roughness of dopant assisted photocatalysts and the average particle diameter of photocatalysts were decreased to 16 nm (Ag/MoO₃/TiO₂) from 80 nm of MoO₃/TiO₂ as we observed from the SEM images. The modification of MoO₃ and Ag into TiO₂ photocatalyst indicates an increased ruggedness, roughness and thus yielded a more porous surface area.
- (iii) The FT-IR results showed peaks around 1370-1400 cm⁻¹ and 500-600 cm⁻¹ (less than 1000 cm⁻¹) were attributed to Ti-O-Ti stretching vibration and Ti-O bond in the TiO₂ lattice, respectively. It was reported that the higher surface content of Ti-O-Ti bond subsequently enhances the dispersion and photocatalytic performance of dye degradation.
- (iv) UV-Vis results showed that dopant assisted TiO₂ photocatalysts employed to shift absorption edge towards longer wavelength. The estimated bandgap energies (E_g) were calculated to be 3.24 eV, 3.15 eV, 2.95 eV, and 2.89 eV for TiO₂, MoO₃/TiO₂, Ag/TiO₂, and Ag/MoO₃/TiO₂ photocatalysts, respectively. The E_g values were relatively lower for nanocomposites due to the incorporation of dopants MoO₃ and Ag which attributed to the visible light absorption by surface plasmon resonance (SPR) and suppression of the charge separation, thus resulting in the easier formation of e⁻/h⁺ pair.

- (v) BET surface analysis suggested that the specific area and pore volume of Ag/MoO₃/TiO₂ nanocomposite was around 8 times higher than pure TiO₂. The higher surface area and pore volume can be useful in the formation of photogenerated e⁻/h⁺ pairs in photocatalyst.
- (vi) Photocatalytic treatment of MO dye revealed that the photocatalyst TiO₂, MoO₃/TiO₂, Ag/TiO₂, and Ag/MoO₃/TiO₂ were very effective in presence of 100 W UV-irradiation. The dye degradation results were 59.5%, 63.1%, 70.6%, and 75.8% for 0.12 g of TiO₂, MoO₃/TiO₂, Ag/TiO₂, and Ag/MoO₃/TiO₂ immobilized on BG surfaces, respectively.
- (vii) The degradation rate constants were measured by using pseudo-first-order steady reaction kinetics and the results were 0.003 min⁻¹, 0.002 min⁻¹, 0.003 min⁻¹, and 0.004 min⁻¹ for TiO₂, MoO₃/TiO₂, Ag/TiO₂, and Ag/MoO₃/TiO₂, respectively, for a particular dose of photocatalyst of 0.120 g. The regression values (R²) were 0.998, 0.968, 0.980, and 0.981 for TiO₂, MoO₃/TiO₂, Ag/TiO₂, and Ag/MoO₃/TiO₂, respectively.
- (viii) The photocatalytic degradation of dye was increased with the decrease of pH from 11.0 to 3.0. The degradation of 10 ppm MO dye was 62.6% at pH 11 which was increased to 96.5% at pH 3 for 0.12 g of Ag/MoO₃/TiO₂ dose under 5.5 h of UV-irradiation.
- (ix) The photocatalytic degradation was increased with the increase of photocatalyst dose (Ag/MoO₃/TiO₂) and found 95.6%, and 98.5% for 0.120 g and 0.140 g of photocatalyst doses, respectively, at a fixed pH (3.0). The optimum photocatalyst dose was considered to 0.120 g.
- (x) The dye degradation was decreased with the increase of dye concentration. The degradation was decreased from 95.6% to 46.12% when the MO dye concentration was increased from 10 ppm to 50 ppm, respectively.
- (xi) The addition of H₂O₂ into the reactor has increased the MO dye removal efficiency from 70.77% to 84.67% and 94.57%, respectively, after the addition of 0.1 and 0.25 mL of H₂O₂ into the reactor.

REFERENCES

- [1] Saini, K., and Malhotra, S., “Environmental Pollution,” *J. Eng. Res. Appl.*, vol. 6, pp. 70-74, 2016.
- [2] Islam, M. S., Zhang, Y., McPhedran, K. N., Liu, Y., and Gamal El-Din, M., “Mechanistic investigation of industrial wastewater naphthenic acids removal using granular activated carbon (GAC) biofilm based processes,” *Sci. Total Environ.*, vol. 541, pp. 238-246, 2016.
- [3] Al-Mamun, M., R., Karim, M., N., Afroj, N., Kader, S., Islam, M., S., and Khan, M. Z. H., “Photocatalytic performance assessment of GO and Ag co-synthesized TiO₂ nanocomposite for the removal of methyl orange dye under solar irradiation,” *Environ. Technol. and Innov.*, vol. 22, pp. 101537, 2021.
- [4] Al-Mamun, M. R., Islam, M. S., Hossain, M. R., Kader, S., Islam, M. S., and Khan, M. Z. H., “A novel and highly efficient Ag and GO co-synthesized ZnO nano photocatalyst for methylene blue dye degradation under UV irradiation,” *Environ. Nanotechnol. Monit. Manag.*, vol. 16, pp. 100495, 2021.
- [5] Pourrezaei, P., Afzal, A., Ding, N., Islam, M. S., Moustafa, A., Drzewicz, P., Chelme-Ayala, P., and Gamal El-Din, M., “Physico-chemical processes,” *Water Environ. Res. Literature Rev.*, vol. 82(10), pp. 997-1072, 2010.
- [6] Al-Mamun, M. R., Kader, S., Islam, M. S., and Khan, M. Z. H., “Photocatalytic activity improvement and application of UV-TiO₂ photocatalysis in textile wastewater treatment: A review,” *J. Environ. Chem. Eng.*, vol. 7, pp. 103248, 2019.
- [7] Wesley, M. J., Lerner, R. N., Kim, E-S, Islam, M. S., and Liu, Y., “Biological fixed film,” *Water Environ. Res. Literature Rev.*, vol. 83 (10), pp. 1150-1186, 2011.
- [8] Suhan, M. B. K, Shuchi, S. B., Anis, A., Haque, Z., and Islam, M. S., “Comparative degradation study of remazol black B dye using electro-coagulation and electro-Fenton process: Kinetics and cost analysis,” *Environ. Nanotechnol. Monit. Manag.*, vol. 14, pp. 100335, 2020.
- [9] Islam, M., T., Jahan, T., and Islam., M. S., “A study on the efficiency of fatted and defatted *Moringa oleifera* seed extract (MOSE) on indigo carmine dye removal,” *J. Funct. Mater. Chem. Eng.*, vol. 1(1), pp. 97-102, 2019.

- [10] Carmen, Z. and Daniela, S. (2012). Textile Organic Dyes – Characteristics, Polluting Effects and Separation/Elimination Procedures from Industrial Effluents – A Critical Overview, Organic Pollutants Ten Years After the Stockholm Convention - Environmental and Analytical Update. InTech.
- [11] Shuchi, S. B., Suhan, M. B. K., Humayun, S. B., Haque, M. E., and Islam, M. S., “Heat-activated potassium persulfate treatment of Sudan Black B dye: Degradation kinetic and thermodynamic studies,” *J. Water Process Eng.*, vol. 39, pp. 101690, 2021.
- [12] Al-Mamun, M. R., Kader, S., and Islam, M. S., “Solar-TiO₂ immobilized photocatalytic reactors performance assessment in the degradation of methyl orange dye in aqueous solution,” *Environ. Nanotechnol. Monit. Manag.*, vol. 16, pp. 100514, 2021.
- [13] Dey, P. C., and Das, R., “Enhanced photocatalytic degradation of methyl orange dye on interaction with synthesized ligand free CdS nanocrystals under visible light illumination,” *Spectrochim. Acta-Part A Mol. Biomol. Spectrosc.*, vol. 231, pp. 118122, 2020.
- [14] Quraishi, I. A., Pawar, R. A., Shinde, D. R., and Chaskar, M. G., “Parametric Study on Photocatalytic Dye Degradation under Visible Light in Flat Slurry Reactor with nano-ZnO Photocatalyst,” *Mater. Today Proc.*, vol. 23, pp. 410-422, 2020.
- [15] Wang, W., Lee, G. J., Wang, P., Qiao, Z., Liu, N., and Wu, J. J., “Microwave synthesis of metal-doped ZnS photocatalysts and applications on degrading 4-chlorophenol using heterogeneous photocatalytic ozonation process,” *Sep. Purif. Technol.*, vol. 237, pp. 116469, 2020.
- [16] Ahmed, M. A., Messih, M. F. A., El-Sherbeny, E. F., El-Hafez, S. F., and Khalifa, A. M. M., “Synthesis of metallic silver nanoparticles decorated mesoporous SnO₂ for removal of methylene blue dye by coupling adsorption and photocatalytic processes,” *J. Photochem. Photobiol. A Chem.*, vol. 346, pp. 77-88, 2017.
- [17] Wu, Y., Du, X., Kou, Y., Wang, Y., and Teng, F., “Mesoporous SiO₂ nanostructure: Light-induced adsorption enhancement and its application in photocatalytic degradation of organic dye,” *Ceram. Int.*, vol. 45, pp. 24594-24600, 2019.
- [18] Zarubica, A., Ljupković, R., Papan, J., Vukoje, I., Porobić, S., Ahrenkiel, S. P., and Nedeljković, J. M., “Visible-light-responsive Al₂O₃ powder: Photocatalytic study,” *Opt. Mat.*, vol. 106, pp. 110013, 2020.

- [19] Prabhakar Rao, N., Chandra, M. R., and Rao, T. S., "Synthesis of Zr doped TiO₂/reduced Graphene Oxide (rGO) nanocomposite material for efficient photocatalytic degradation of Eosin Blue dye under visible light irradiation," *J. Alloy. Compd.*, vol. 694, pp. 596-606, 2017.
- [20] Adhikari, S., Chandra, K. S., Kim, D. H., Madras, G., and Sarkar, D., "Understanding the morphological effects of WO₃ photocatalysts for the degradation of organic pollutants," *Adv. Powd. Technol.*, vol. 29, pp. 1591-1600, 2018.
- [21] Ljubas, D., Smoljanić, G., and Juretić, H., "Degradation of Methyl Orange and Congo Red dyes by using TiO₂ nanoparticles activated by the solar and the solar-like radiation," *J. Environ. Manage.*, vol. 161, pp. 83-91, 2015.
- [22] Grabowska, E., Reszczyńska, J., and Zaleska, A., "Mechanism of phenol photodegradation in the presence of pure and modified-TiO₂: A review," *Water. Res.*, vol. 46, pp. 5453-5471, 2012.
- [23] Brindha, A., and Sivakumar, T., "Visible active N, S co-doped TiO₂/graphene photocatalysts for the degradation of hazardous dyes," *J. Photochem. Photobiol. A Chem.*, vol. 340, pp. 146-156, 2017.
- [24] Khan, H., Jiang, Z., and Berk, D., "Molybdenum doped graphene/TiO₂ hybrid photocatalyst for UV/visible photocatalytic applications," *Sol. Eneq.*, vol. 162, pp. 420-430, 2018.
- [25] Patil, S. B., Basavarajappa, P. S., Ganganagappa, N., Jyothi, M. S., Raghu, A. V., and Reddy, K. R., "Recent advances in non-metals-doped TiO₂ nanostructured photocatalysts for visible-light driven hydrogen production, CO₂ reduction and air purification," *Int. J. Hydro. Eneq.*, vol. 44, pp. 13022-13039, 2019.
- [26] Wattanawikkam, C., and Pecharapa, W., "Structural studies and photocatalytic properties of Mn and Zn co-doping on TiO₂ prepared by single step sonochemical method," *Radiat. Phys. Chem.*, vol. 171, pp. 108714, 2020.
- [27] Mancuso, A., Sacco, O., Sannino, D., Pragliola, S., and Vaiano, V., "Enhanced visible-light-driven photodegradation of Acid Orange 7 azo dye in aqueous solution using Fe-N co-doped TiO₂," *Arab. J. Chem.*, vol. 13, pp. 8347-8360, 2020.
- [28] Basavarajappa, P. S., Patil, S. B., Ganganagappa, N., Reddy, K. R., Raghu, A. V., and Reddy, C. V., "Recent progress in metal-doped TiO₂, non-metal doped/codoped TiO₂ and

- TiO₂ nanostructured hybrids for enhanced photocatalysis,” *Int. J. Hydro. Eneq.*, vol. 45, pp. 7764-7778, 2020.
- [29] Tian, H., Shen, K., Hu, X., Qiao, L., and Zheng, W., “N, S co-doped graphene quantum dots-graphene-TiO₂ nanotubes composite with enhanced photocatalytic activity,” *J. Ally Compd.*, vol. 691, pp. 369-377, 2017.
- [30] Hasan Khan Neon, M., and Islam, M. S., “MoO₃ and Ag co-synthesized TiO₂ as a novel heterogeneous photocatalyst with enhanced visible-light-driven photocatalytic activity for methyl orange dye degradation,” *Environ. Nanotechnol. Monit. Manag.*, vol. 12, pp. 100244, 2019.
- [31] Wang, P., Huang, B., Dai, Y., and Whangbo, M., “Plasmonic photocatalysts: harvesting visible light with noble metal nanoparticles,” *Phys. Chem. Chem. Phys.*, vol. 14, pp. 9813, 2012.
- [32] El-Mekkawi, D., and Galal, H. R., “Removal of a synthetic dye “Direct Fast Blue B2RL” via adsorption and photocatalytic degradation using low cost rutile and Degussa P25 titanium dioxide,” *J. Hydro-Environ. Res.*, vol. 7, pp. 219–226, 2013.
- [33] Chen, Y., and Dionysiou, D. D., “TiO₂ photocatalytic films on stainless steel: The role of Degussa P-25 in modified sol-gel methods,” *Appl. Catal. B Environ.*, vol. 62, pp. 255–264, 2006.
- [34] Valtierra, J. E., García, J. S., Frausto, C. R., and Calixto, S., “The photocatalytic application and regeneration of anatase thin films with embedded commercial TiO₂ particles deposited on glass microrods,” *Appl. Surf. Sci.*, vol. 252, pp. 3600–3608, 2006.
- [35] Bouarioua, A., and Zerdaoui, M., “Photocatalytic activities of TiO₂ layers immobilized on glass substrates by dip-coating technique toward the decolorization of methyl orange as a model organic pollutant,” *J. Environ. Chem. Eng.*, vol. 5, pp. 1565–1574, 2017.
- [36] Ashraf, M. A., Liu, Z., Peng, W. X., Jermstittiparsert, K., Hosseinzadeh, G., and Hosseinzadeh, R., “Combination of sonochemical and freeze-drying methods for synthesis of graphene/Ag-doped TiO₂ nanocomposite: A strategy to boost the photocatalytic performance via well distribution of nanoparticles between graphene sheets,” *Ceram. Int.*, vol. 46, pp. 7446-7452, 2020.

- [37] Adly, M. S., El-Dafrawy, S. M., and El-Hakam, S. A., "Application of nanostructured graphene oxide/titanium dioxide composites for photocatalytic degradation of rhodamine B and acid green 25 dyes," *J. Mater. Res. Technol.*, vol. 8, pp. 5610-5622, 2019.
- [38] Hossain, L., Sajib, M. and Enamul, H. (2017) *Readymade garment industries going green*. The Financial Express. International Publications Ltd.
- [39] Saggiaro, E. M., "Use of Titanium Dioxide Photocatalysis on the Remediation of Model Textile Wastewaters Containing Azo Dyes," *Molecules*, vol. 16, pp. 10370-10386, 2011
- [40] Chen, Y., and Dionysiou, D. D., "Effect of calcination temperature on the photocatalytic activity and adhesion of TiO₂ films prepared by the P-25 powdermodified sol-gel method," *J. Molec. Cataly. A: Chem.*, vol. 244, pp. 73-82, 2006b.
- [41] Babuponnusami, A., and Muthukumar, K., "A review on Fenton and improvements to the Fenton process for wastewater treatment," *J. Environ. Chem. Eng.*, vol. 2, pp. 557-572, 2014.
- [42] Pignatello, J. J., Oliveros, E. and MacKay, A., "Advanced Oxidation Processes for Organic Contaminant Destruction Based on the Fenton Reaction and Related Chemistry," *Crit. Rev. Environ. Sci. Tech.*, vol. 36, pp. 1-84, 2006.
- [43] Liu, S. Q., "Magnetic semiconductor nano-photocatalysts for the degradation," *Environ. Chem. Lett.*, vol. 10, pp. 209-216, 2012.
- [44] Herrmann, J., "Heterogeneous photocatalysis: fundamentals and applications to the removal of various types of aqueous pollutants," *Catal. Tod.*, vol. 53, pp. 115-129, 1999.
- [45] Herrmann, J., "Fundamentals and misconceptions in photocatalysis," *J. Photochem. Photobiol. A*, vol. 216, pp. 85-93, 2010.
- [46] Ohtani, B., "Titania photocatalysis beyond recombination: a critical review," *Catal.*, vol. 3, pp. 942-953, 2013.
- [47] Akpan, U. G., and Hameed, B. H., "Parameters affecting the photocatalytic degradation of dyes using TiO₂-based photocatalysts: A review," *J. Hazard. Mater.*, vol. 170, pp. 520-529, 2009.
- [48] Bhatkhande, D. S., Pangarkar, V. G., and Beenackers, A. A. C. M., "Photocatalytic degradation for environmental applications – a review," *J. Chem. Technol. Biot.*, vol. 77, pp. 102-116, 2002.

- [49] Shwarsstein, A. K., Hu, Y. S., Forman, A. J., Stucky, G. D., and Farland, E. M., "Electrodeposition of α -Fe₂O₃ doped with Mo or Cr as photoanodes for photocatalytic water splitting," *J. Phys. Chem. C*, vol. 112, pp. 15900–15907, 2008.
- [50] Hagfeldt, A., and Graetzel, M., "Light-induced redox reactions in nanocrystalline systems," *Chem. Rev.*, vol. 95, pp. 49-68, 1995.
- [51] Diebold, U., "The surface science of titanium dioxide," *Surf. Sci. Repts.*, vol. 48, pp. 53-229, 2003.
- [52] Kitano, M., Matsuoka, M., Ueshima, M. and Anpo, M., "Recent developments in titanium oxide-based photocatalysts," *Appl. Cataly. A: Gen.*, vol. 325, pp. 1-14, 2007.
- [53] Carp, O., Huisman, C. L., and Reller, A., "Photoinduced reactivity of titanium dioxide," *Prog. Sol. Sta. Chem.*, vol. 32, pp. 33-177, 2004.
- [54] King, D. S., and Nix, R. M., "Thermal Stability and Reducibility of ZnO and Cu/ZnO Catalysts", *J. Catal.*, vol. 76, pp. 160, 1996.
- [55] Yao, N., Xiong, G., Zhang, Y., He, M., and Yang, W., "Preparation of novel uniform mesoporous alumina catalysts by the sol–gel method," *Cataly. Tod.*, vol. 68, pp. 97-109, 2001.
- [56] Corradi, A. B., "Conventional and Microwave-hydrothermal Synthesis of TiO₂ Nanopowders," *J. Am. Ceram. Soc.*, vol. 88, pp. 2639-2641, 2005.
- [57] Kajitvichyanukul P., Ananpattarachai J., and Pongpom S., "Sol–gel preparation and properties study of TiO₂ thin film for photocatalytic reduction of chromium (VI) in photocatalysis process", *Sci. Technol..Adv. Mater.*, 6, pp. 352–358, 2005.
- [58] Kwon, C. H., Shin, H., Kim, J. H., Choi, W. S., and Yoon, K. H., "Degradation of methylene blue via photocatalysis of titanium dioxide," *Mater. Chem. Phys.*, vol. 86, pp. 78-82, 2004.
- [59] Akkari F. C., Kanzaria M., and Rezig B., "Preparation and characterization of obliquely deposited copper oxide thin films", *Eur. Phys. J. Appl. Phys.*, vol. 40, pp. 49–54, 2007.
- [60] Chen, X., and Mao, S. S., "Synthesis of Titanium Dioxide (TiO₂) Nanomaterials," *J. Nanosci. Nanotech.*, vol. 6, pp. 906-925, 2006.
- [61] Brinker, C. and Scherer, G., (2014) Sol-Gel Science. Saint Louis: Elsevier Science.
- [62] Brinker, C. J., Frye, G. C., Hurd, A. J., and Ashley, C. S., "Fundamentals of sol-gel dip coating," *Thi. Sol. Fil.*, vol. 201, pp. 97-108, 1991.

- [63] Su, C., Hong, B. Y., and Tseng, C. M., "Sol-gel preparation and photocatalysis of titanium dioxide," *Cataly. Tod.*, vol. 96, pp. 119-126, 2004.
- [64] Ohtani, B., Ogawa, Y., and Nishimoto, S. I., "Photocatalytic Activity of Amorphous-Anatase Mixture of Titanium(IV) Oxide Particles Suspended in Aqueous Solutions," *J. Phys. Chem. B*, vol. 101, pp. 3746-3752, 1997.
- [65] Chen, X., and Mao, S. S., "Titanium Dioxide Nanomaterials: Synthesis, Properties, Modifications, and Applications," *Chem. Rev.*, vol. 107, pp. 2891-2959, 2007.
- [66] Huang, D. G., Liao, S. J., Liu, J. M., Danga, Z., and Petrik, L., "Preparation of visible-light responsive N-F-codoped TiO₂ photocatalyst by a sol-gel-solvothermal method," *J. Photochem. Photobi. A: Chem.*, vol. 184, pp. 282-288, 2006
- [67] Tachikawa, T., Fujitsuka, M., and Majima, T., "Mechanistic Insight into the TiO₂ Photocatalytic Reactions: Design of New Photocatalysts," *J. Phys. Chem. C*, vol. 111, pp. 5259-5275, 2007.
- [68] Blackburn, J. L., Selmarten, D. C., and Nozik, A. J., "Electron Transfer Dynamics in Quantum Dot/Titanium Dioxide Composites Formed by in Situ Chemical Bath Deposition," *J. Phys. Chem. B*, vol. 107, pp. 14154-14157, 2003.
- [69] Kumbhar, A., and Chumanov, G., "Synthesis of Iron (III)-Doped Titania Nanoparticles and its Application for Photodegradation of Sulforhodamine-B Pollutant," *J. Nanopa. Res.*, vol. 7, pp. 489-498, 2005.
- [70] Chong, M., Jin, B., Chow, C., and Saint, C., "Recent developments in photocatalytic water treatment technology: A review," *W. Res.*, vol. 44, pp. 2997- 3027, 2010.
- [71] Dong, H., Zeng, G., Tang, L., Fan, C., Zhang, C., He, X., and He, Y., "An overview on limitations of TiO₂-based particles for photocatalytic degradation of organic pollutants and the corresponding countermeasures," *W. Res.*, vol. 79, pp. 128-146, 2015.
- [72] Spanhel, L., Weller, H., and Henglein, A., "Photochemistry of semiconductor colloids. Electron ejection from illuminated cadmium sulfide into attached titanium and zinc oxide particles," *J. Am.Chem. Soc.*, vol. 109, pp. 6632-6635, 1987.
- [73] Bai, S., Liu, H., Sun, J., Tian, Y., Chen, S., and Song, J., "Improvement of TiO₂ photocatalytic properties under visible light by WO₃/TiO₂ and MoO₃/TiO₂ composites," *Appl. Surf. Sci.*, vol. 338, pp. 61-68, 2015.

- [74] Gnatyuk, Y. I., Yatskiv, V. I., Smirnova, N. P., Granchak, V. M., Eremenko, A. M., “Photocatalytic properties of mesoporous TiO₂/ZrO₂ films in gas-phase oxidation of alcohols,” *Theore. Experim. Chem.*, vol. 41, pp. 371-376, 2005.
- [75] Umebayashi, T., Yamaki, T., Itoh, H., and Asai, K., “Analysis of electronic structures of 3d transition metal doped TiO₂ based on band calculations,” *J. Phys. Chem. Sol.*, vol. 63, pp. 1909, 2002.
- [76] Paleologou, A., Marakas, H., Xekoukoulotakis, N. P., Moya, A., Vergara, Y., Kalogerakis, N., Gikas, P., and Mantzavinos, D., “Disinfection of water and wastewater by TiO₂ photocatalysis, sonolysis and UV-C irradiation,” *Catal. Tod.*, vol. 129, pp. 136-142, 2007.
- [77] Pouloupoulos, S., and Philippopoulos, C., “Photo-assisted oxidation of chlorophenols in aqueous solutions using hydrogen peroxide and titanium dioxide,” *J. Environ. Sci. Heal.*, vol. 39, pp. 1385-1397, 2004.
- [78] Ahmad, R., Ahmad, Z., Khan, A. U., Mastoi, N. R., Aslam, M., and Kim, J., “Photocatalytic systems as an advanced environmental remediation: Recent developments, limitations and new avenues for applications,” *J. Environ. Chem. Eng.*, vol. 4, pp. 4143-4164, 2016.
- [79] Chong, M., Jin, B., Chow, C. and Saint, C., “Recent developments in photocatalytic water treatment technology: A review,” *W. Res.*, vol. 44, pp. 2997-3027, 2010.
- [80] Kuang, D., Ito, S., Wenger, B., Klein, C., Moser, J., Humphry-baker, R., Zakeeruddin, S. M., and Gra, M., “High molar extinction coefficient heteroleptic ruthenium complexes for thin film dye-sensitized solar cells,” *J. Am. Chem. Soc.*, vol. 128, pp. 4146-4154, 2006.
- [81] Ray, A. K., and Beenackers, A. A. C. M., “Development of a new photocatalytic reactor for water purification,” *Cataly. Tod.*, vol. 40, pp. 73-83, 1998.
- [82] Pozzo, R. L., Giombi, J. L., Baltanás, M. A., and Cassano, A. E., “Performance in a fluidized bed reactor of photocatalysts immobilized onto inert supports,” *Cataly. Tod.*, vol. 62, pp. 175-187, 2000.
- [83] Zhang, W., Ding, L., Luo, J., Jaffrin, M. Y., and Tang, B., “Membrane fouling in photocatalytic membrane reactors (PMRs) for water and wastewater treatment: a critical review,” *Chem. Eng. J.*, vol. 302, pp. 446-458, 2016.

- [84] Byrne, J. A., Eggins, B. R., Brown, N. M. D., McKinney, B., and Rouse, M., “Immobilisation of TiO₂ powder for the treatment of polluted water,” *Appl. Catal. B: Environ.*, vol. 17, pp. 25-36, 1998.
- [85] Fretwell, R., and Douglas, P., “An active, robust and transparent nanocrystalline anatase TiO₂ thin film —preparation, characterisation and the kinetics of photodegradation of model pollutants,” *J. Photochem. Photobiol. A: Chem.*, vol. 143, pp. 229-240, 2001.
- [86] Yagub, M. T., Sen, T. K., Afroze, S. and Ang, H. M., “Dye and its removal from aqueous solution by adsorption: a review”, *Adv. Colloid Interface Sci.*, vol. 209, pp. 172–184, 2014.
- [87] Carmen, Z. and Daniela, S. (2012). Textile Organic Dyes – Characteristics, Polluting Effects and Separation/Elimination Procedures from Industrial Effluents – A Critical Overview, Organic Pollutants Ten Years After the Stockholm Convention - Environmental and Analytical Update. InTech
- [88] Reemtsma, T. (2008) Organic pollutants in the water cycle. Weinheim: Wiley-VCH.
- [89] Brüsweiler, B. J., Küng, S., Bürgi, D., Muralt, L., and Nyfeler, E., “ Identification of non-regulated aromatic amines of toxicological concern which can be cleaved from azo dyes used in clothing textiles,” *Regul. Toxicol. Pharmacol.*, vol.69, pp. 263-272, 2014.
- [90] Deepak, R., Vandana, M., and Radhey, S. S., “Detoxification of azo dyes in the context of environmental processes,” *Chemosp.*, vol. 155, pp. 591-605, 2016.
- [91] Wai, S., Chi, W. K., Yuen, C. W. M., Shun, W. C., and Kim, H. L., “Effective Photodegradation of Methyl Orange Using Fluidized Bed Reactor Loaded with Cross-Linked Chitosan Embedded Nano-CdS Photocatalyst,” *Int. J. Chem. Eng.*, vol. 2014, pp. 270946, 2014.
- [92] Konstantinou, I., and Albanis, T., “TiO₂-assisted photocatalytic degradation of azo dyes in aqueous solution: kinetic and mechanistic investigations,” *Appl. Catal. B: Environ.*, vol. 49, pp. 1-14, 2004.
- [93] Brickner, P. W., Vincent, R. L., First, M., Nardell, E., Murray, M., Kaufman, W., “The application of ultraviolet germicidal irradiation to control transmission of airborne disease: bioterrorism countermeasure,” *Pub. Heal. Rep.*, vol. 118, pp. 99, 2003.
- [94] Meiting, G., Hong, Y. H., James, R. B., and Mohamed, G. E. D., “Comparison of Low- and Medium-Pressure Ultraviolet Lamps: Photoreactivation of Escherichia Coli and Total

- Coliforms in Secondary Effluents of Municipal Wastewater Treatment Plants,” *Water Res.*, vol. 43, pp. 815-21, 2009.
- [95] Halen, W., and Waltar, H., “A very large stereoelectronic effect on acetal cleavage,” *Am. Chem. Soc.*, vol. 104, pp. 4630-4, 1982.
- [96] Fenton, H. J. H., “Oxidation of tartaric acid in presence of iron,” *Chem. Soc.*, vol. 65, pp. 899-910, 1894.
- [97] Tia, G., “3D hierarchical flower-like TiO₂ nanostructure: morphology control and its photocatalytic property,” *Cryst. Eng. Comm.*, vol. 13, pp. 2994-3000, 2011.
- [98] Xia, X. H., “Synthesis and photocatalytic properties of TiO₂ nanostructures. Materials,” *Res. Bull.*, vol. 43, pp. 2187-2195, 2008.
- [99] Gogate, P. R., and Pandit, A. B., “A review of imperative technologies for wastewater treatment I: oxidation technologies at ambient conditions,” *Adv. Environ. Res.*, vol. 8, pp. 501-551, 2004.
- [100] Mills, A., Morris, S., and Davies, R., “Photomineralisation of 4-chlorophenol sensitised by titanium dioxide: a study of the intermediates. Journal of Photochemistry and Photobiology,” *A: Chem.*, vol. 70, pp. 183-191, 1993.
- [101] Harraz, F. A., “Magnetic nanocomposite based on titania– silica/cobalt ferrite for photocatalytic degradation of methylene blue dye,” *Cera. Int.*, vol. 40, pp. 375–384, 2014.
- [102] Toor, A. P., “Photocatalytic degradation of direct yellow 12 dye using UV/TiO₂ in a shallow pond slurry reactor,” *Dy. Pig.*, vol. 68, pp. 53-60, 2005.
- [103] Epling, G. A., and Lin, C., “Photo assisted bleaching of dyes utilizing TiO₂ and visible light,” *Chemosphere*, vol. 46, pp. 561-570, 2002.
- [104] Yu, J., “Enhanced photocatalytic activity of TiO₂ powder (P25) by hydrothermal treatment,” *J. Mole. Catal. A: Chem.*, vol. 253, pp. 112-118, 2006.
- [105] Watson, S., Beydoun, D., and Amal, R., “Synthesis of a novel magnetic photocatalyst by direct deposition of nanosized TiO₂ crystals onto a magnetic core,” *J. Photochem. Photobi. A: Chem.*, vol. 148, pp. 303-313, 2002.
- [106] Beydoun, D., and Amal, R., “Implications of heat treatment on the properties of a magnetic iron oxide/titanium dioxide photocatalyst,” *Mater. Sci. Eng.*, vol. 94, pp. 71-81, 2002.

- [107] Herney, J. R., Vicente, M. A., and Madeira, L. M., "Heterogeneous photo-Fenton oxidation with pillared clay-based catalysts for wastewater treatment: A review," *Appl. Catal. B: Environ.*, vol. 98, pp. 10-26, 2010.
- [108] Casbeer, E., Sharma, V. K., and Li, X. Z., "Synthesis and photocatalytic activity of ferrites under visible light: A review," *Sep. Purifi. Techn.*, vol. 87, pp. 1-14, 2012.
- [109] Ji, T., Yang, F., Lv, Y., Zhou, J., and Sun, J., "Synthesis and visible-light photocatalytic activity of Bi-doped TiO₂ nanobelts," *Mater. Lett.*, vol. 63, pp. 2044-2046, 2009.
- [110] Fan, H., "ZnO-graphene composite for photocatalytic degradation of methylene blue dye," *Catal. Commun.*, vol. 29, pp. 29-34, 2012.
- [111] Saien, J., Delavari, H., and Solymani, A.R., "Sono-assisted photocatalytic degradation of styrene-acrylic acid copolymer in aqueous media with nano titania particles and kinetic studies," *J. Hazar. Mater.*, vol. 177, pp. 1031-1038, 2010.
- [112] Subramanian, V., Pangarkar, G., and Beenackers, A. A., "Photocatalytic degradation of PHBA: relationship between substrate adsorption and photocatalytic degradation," *Clean Prod. Pro.*, vol. 2, pp. 149, 2000.
- [113] Piscopo, A., Robert, D., and Weber, J. V., "Influence of pH and chloride anion on the photocatalytic degradation of organic compounds. Part I. Effect on the benzamide and para-hydroxybenzoic acid in TiO₂ aqueous solution," *Appl. Catal. B: Environ.*, vol. 35, pp. 117-124, 2001.
- [114] Ollis, D. F., Pelizzetti, E., and Serpone, N., "Photocatalyzed Destruction of Water Contaminants", *Environ. Sci. Technol.*, vol. 25, pp. 1523, 1991.
- [115] Xu, N., "Effects of Particle Size of TiO₂ on Photocatalytic Degradation of Methylene Blue in Aqueous Suspensions," *Ind. Eng. Chem. Res.*, vol. 38, pp. 373-379, 1999.
- [116] Shi, Z., Fan, Y., Xu, N., and Shi, J., "Kinetics of Photocatalytic Degradation of Methylene Blue over TiO₂ Particles in Aqueous Suspensions," *Chin. J. Chem. Eng.*, vol. 8, pp. 15-19, 2000.
- [117] Xuan, S., "Magnetically Separable Fe₃O₄/TiO₂ Hollow Spheres: Fabrication and Photocatalytic Activity," *J. Phys. Chem. C*, vol. 113, pp. 553-558, 2009.
- [118] Ayrat, M. D., and James, M. T., "Mechanism of graphene oxide formation", *ACS Nan.*, vol. 8, pp. 3060-3068, 2014.

- [119] Rengaraj, S., and Li, X., “Enhanced photocatalytic activity of TiO₂ by doping with Ag for degradation of 2,4,6-trichlorophenol in aqueous suspension,” *J. Mole. Catal. A: Chem.*, vol. 243, pp. 60-67, 2006.
- [120] Saleh, I. M., Ruyter, I. E., Haapasalo, M. P., Orstavik, D., “Adhesion of endodontic sealers: scanning electron microscopy and energy dispersive spectroscopy,” *J. Endod.*, vol. 29, pp. 595-601, 2003
- [121] Umer, A., Naveed, S., Ramzan, N., Rafique, M. S., “Selection of a suitable method for the synthesis of copper nanoparticles,” *Wor. Sci. Publ. Comp.*, vol. 7(5), pp. 1793-2920, 2012.
- [122] Brinker, C. J. and Scherer, G. W., “Sol-Gel Science: The Physics and Chemistry of Sol-Gel Processing”, Academic, San Diego, 1990.
- [123] Stuart, B. H. (2004). *Infrared Spectroscopy: Fundamentals and Applications (Analytical Techniques in the Sciences)*. John Wiley and Sons Ltd., UK.
- [124] Heera, P. and Shanmugam, S., “Nanoparticle Characterization and Application: An Overview,” *Int. J. Curr. Microbiol. App. Sci.*, vol. 4(8), pp. 379-386, 2015.
- [125] Songfeng, P., and Hui, C. M., “The reduction of graphene oxide”, *Carb.*, vol. 50, pp. 3210-3228, 2012.
- [126] Ebraheem, S., and El-Saied, A., “Band Gap Determination from Diffuse Reflectance Measurements of Irradiated Lead Borate Glass System Doped with TiO₂ by Using Diffuse Reflectance Technique,” *Mater. Sci. Appl.*, vol. 5, pp. 324-329, 2013.
- [127] Sing, K., “The use of nitrogen adsorption for the characterization of porous materials,” *Coll. Surf. A: Physicochem. Eng. Asp.*, vol. 187-188, pp. 3-9, 2001.
- [128] Yang, H., Zhang, K., Shi, R., Li, X., Dong, X., and Yu, Y., “Sol-gel synthesis of TiO₂ nanoparticles and photocatalytic degradation of methyl orange in aqueous TiO₂ suspensions,” *J. Alloy Compd.*, vol. 413, pp. 302-306, 2006.
- [129] Venkatachalam, N., Palanichamy, M., and Murugesan, V., “Sol-gel preparation and characterization of nanosize TiO₂: Its photocatalytic performance,” *Mater. Chem. Phys.*, vol. 104, pp. 454-459, 2007.
- [130] Jasbi, N. E., and Dorrnian, D., “Effect of aging on the properties of TiO₂ nanoparticle,” *J. Theor. Appl. Phys.*, vol. 10, pp. 157-161, 2016) 157–161.

- [131] Yang, X., Ma, F., Li, K., Guo, Y., Hu, J., and Li, W., "Mixed phase titania nanocomposite co doped with metallic silver and vanadium oxide: new efficient photocatalyst for dye degradation," *J. Hazard. Mater.*, vol. 175, pp. 429–438, 2010.
- [132] Girginov, C., Stefchev, P., Vitanov, P., and Dikov, H., "Silver doped TiO₂ photocatalyst for methyl orange degradation," *J. Eng. Sci. Tech. Rev.*, vol. 5, pp. 14–17, 2012.
- [133] Bai, S., Liu, H., Sun, J., Tian, Y., Chen, S., and Song, J., "Improvement of TiO₂ photocatalytic properties under visible light by WO₃/TiO₂ and MoO₃/TiO₂ composites," *Appl. Surf. Sci.*, vol. 338, pp. 61–68, 2015.
- [134] Sakthivel, S., Shankar, M. V., Palanichamy, M., Arabindoo, B., Bahnemann, D. W., and Murugesan, V., "Enhancement of photocatalytic activity by metal deposition: characterisation and photonic efficiency of Pt, Au and Pd deposited on TiO₂ catalyst," *W. Res.*, vol. 38, pp. 3001-3008, 2004.
- [135] Kotani, Y., Matoda, T., Marsuda, A., Kogure, T., Tatsumisago, M., and Minami, T., "Anatase nanocrystal-dispersed thin films via sol–gel process with hot water treatment: effects of poly(ethylene glycol) addition on photocatalytic activities of the films," *J. Mater. Chem.*, vol. 11, pp. 2045-2048, 2001.
- [136] Yahia, C. L., Yahiaoui, I., Aissani, B. F., Madi, K., Benmehdi, N., Fourcade, F., and Amrane, A., "Heat Attachment Method for the Immobilization of TiO₂ on Glass Plates: Application to Photodegradation of Basic Yellow Dye and Optimization of Operating Parameters, Using Response Surface Methodology," *Ind. Eng. Chem. Res.*, vol. 53, pp. 3813-3819, 2014.
- [137] Vaez, M., Moghaddam, A. Z., Mahmoodi, N. M., and Alijani, S., "Decolorization and degradation of acid dye with immobilized titania nanoparticles," *Pro. Saf. Environ. Protect.*, vol. 90, pp. 56-64, 2012.
- [138] Simonsen, M. E., Jensen, H., Li, Z., and Sogaard, E. G., "Surface properties and photocatalytic activity of nanocrystalline titania films," *J. Photochem. Photobiol. A: Chem.*, vol. 200, pp. 192-200, 2008.
- [139] kte, A. N., and Yılmaz, ., "Photodecolorization of methyl orange by yttrium incorporated TiO₂ supported ZSM-5," *Appl. Catal. B: Environ.*, vol. 85, pp. 92-102, 2008.

- [140] Jiang, W., Joens, J. A., Dionysiou, D. D., and O'Shea, K. E., "Optimization of photocatalytic performance of TiO₂ coated glass microspheres using response surface methodology and the application for degradation of dimethyl phthalate," *J. Photochem. Photobiol. A: Chem.*, vol. 262, pp. 7-13, 2013.
- [141] Tipparach, U., Wongwanwatthana, P., Sompan, T., and Saipin, T., "Preparation and Characterization of Nano-TiO₂ Thin Films by Sol-gel Dip-coating Method," *Nanotechnol.*, vol. 7, pp. 129-136, 2008.
- [142] Šegota, S., Čurković, L., Ljubas, D., Svetličić, V., Houra, I. F., and Tomašić, N., "Synthesis characterization and photocatalytic properties of sol-gel TiO₂ films," *Ceram. Int.*, vol. 37, pp. 1153–1160, 2011.
- [143] Park, N. G., Van, D. L. J., and Frank, A. J., "Comparison of dye-sensitized rutile- and anatase-based TiO₂ solar cells," *J. Phys. Chem. B*, vol. 104, pp. 8989–8994, 2000.
- [144] Behnajady, M. A., Eskandarloo, H., Modirshahla, N., and Shokri, M., "Investigation of the effect of sol-gel synthesis variables on structural and photocatalytic properties of TiO₂ nanoparticles," *Desalin.*, vol. 278, pp. 10–17, 2011.
- [145] Xin, B., Jing, L., Ren, Z., Wang, B., and Fu, H., "Effects of simultaneously doped and deposited Ag on the photocatalytic activity and surface states of TiO₂," *J. Phys. Chem. B*, vol. 109, pp. 2805–2809, 2005.
- [146] Yoldas, B. E., "Hydrolysis of titanium alkoxide and effects of hydrolytic polycondensation parameters," *J. Mater. Sci.*, vol. 21, pp. 1087-1092, 1986.
- [147] Seok, J., Lee, J., Cho, S., Ji, B., Kim, H. W., Kwon, M., and Yang, H., "Active hydrogen evolution through lattice distortion in metallic MoTe₂," *2d Mat.*, vol. 4, pp. 025061, 2017.
- [148] Kuznetsov, A. Y., MacHado, R., Gomes, L. S., Achete, C. A., Swamy, V., Muddle, B. C., and Prakapenka, V., "Size dependence of rutile TiO₂ lattice parameters determined via simultaneous size, strain, and shape modeling," *Appl. Phys. Lett.*, vol. 94, pp. 2–5, 2009.
- [149] Rengaraj, S., and Li, X., "Enhanced photocatalytic activity of TiO₂ by doping with Ag for degradation of 2,4,6-trichlorophenol in aqueous suspension," *J. Mol. Catal. A Chem.*, vol. 243, pp. 60–67, 2006.
- [150] Karkare, M., "Choice of precursor not affecting the size of anatase TiO₂ nanoparticles but affecting morphology under broader view," *Int. Nano Lett.*, vol. 4, pp. 111, 2014.

- [151] Kurniawan, T. A., Mengting, Z., Fu, D., Yeap, S. K., Othman, M. H. D., Avtar, R., and Ouyang, T., "Functionalizing TiO₂ with graphene oxide for enhancing photocatalytic degradation of methylene blue (MB) in contaminated wastewater," *J. Environ. Manage.*, vol. 270, pp. 110871, 2020.
- [152] Matiullah, K., Zeng, Y., Fawad, U., Wazir, M., Abdul, N., Muhammad, I. Z., and Asad, U., "Enhancing the photoactivity of TiO₂ by codoping with silver and molybdenum: the effect of dopant concentration on the photoelectrochemical properties," *Mater. Res. Expr.*, vol. 4, pp. 045023, 2017.
- [153] Song, K. Y., Park, M. K., Kwon, Y. T., Lee, H. W., Chung, W. J., and Lee, W. I., "Preparation of transparent particulate MoO₃/TiO₂ and WO₃/TiO₂ films and their photocatalytic properties," *Chem. Mater.*, vol. 13, pp. 2349–2355, 2001.
- [154] Jegadeeswaran, P., Rajiv, P., Vanathi, P., Rajeshwari, S., and Venckatesh, R., "A novel green technology: Synthesis and characterization of Ag/TiO₂ nanocomposites using *Padina tetrastromatica* (seaweed) extract," *Mater. Lett.*, vol. 166, pp. 137-139, 2016.
- [155] Khan, H., Jiang, Z., and Berk, D., "Molybdenum doped graphene/TiO₂ hybrid photocatalyst for UV/visible photocatalytic applications," *Sol. Enege.*, vol. 162, pp. 420-430, 2018.
- [156] Rab, N., Chong, F. K., Mohamed, H. I., and Lim, W. H., "Preparation of TiO₂ nanoparticles by hydrolysis of TiCl₄ using water and glycerol solvent system," *J. Phys. Conf. Ser.*, vol. 1123, pp. 012065, 2018.
- [157] Zhang, T., Wang, X., and Zhang, X., "Recent Progress in TiO₂-Mediated Solar Photocatalysis for Industrial Wastewater Treatment," *Int. J. Photoeneg.*, vol. 2014, pp. 1–12, 2014.
- [158] Sugapriya, S., Sriram, R., and Lakshmi, S., "Effect of annealing on TiO₂ nanoparticles," *Opt.*, vol. 124, pp. 4971–4975, 2013.
- [159] Zhang, L., Ni, C., Jiu, H., Xie, C., Yan, J., and Qi, G., "One-pot synthesis of Ag-TiO₂/reduced graphene oxide nanocomposite for high performance of adsorption and photocatalysis," *Ceram. Int.*, vol. 43, pp. 5450-5456, 2017.
- [160] Li, Y., Wu, W., Dai, P., Zhang, L., Sun, Z., Li, G., and Chen, C., "WO₃ and Ag nanoparticle co-sensitized TiO₂ nanowires: preparation and the enhancement of photocatalytic Activity," *RSC Adv.*, vol. 4, pp. 23831–23837, 2014.

- [161] Alsharaeh, E. H., Bora, T., Soliman, A., Ahmed, F., Bharath, G., Ghoniem, M. G., Abu, K. M. S., and Dutta, J., "Sol-gel-assisted microwave-derived synthesis of anatase Ag/TiO₂/GO nanohybrids toward efficient visible light phenol degradation," *Cataly.*, vol. 7, pp. 1-11, 2017.
- [162] Khalid, N. R., Ahmed, E., Hong, Z., Zhang, Y., Ullah, M., and Ahmed, M., "Graphene modified Nd/TiO₂ photocatalyst for methyl orange degradation under visible light irradiation," *Ceram. Int.*, vol. 39, pp. 3569-3575, 2013.
- [163] López, R., and Gómez, R., "Band-gap energy estimation from diffuse reflectance measurements on sol-gel and commercial TiO₂: A comparative study," *J. Sol-Gel Sci. Technol.*, vol. 61, pp. 1-7, 2012.
- [164] Yang, X., Ma, F., Li, K., Guo, Y., Hu, J., Li, W., Huo, M., and Guo, Y., "Mixed phase titania nanocomposite codoped with metallic silver and vanadium oxide: New efficient photocatalyst for dye degradation," *J. Hazard. Mater.*, vol. 175, pp. 429-438, 2010.
- [165] Wang, T., Tang, T., Gao, Y., Chen, Q., Zhang, Z., and Bian, H., "Hydrothermal preparation of Ag-TiO₂-reduced graphene oxide ternary microspheres structure composite for enhancing photocatalytic activity," *Phys. E Low-Dimensi. Syst. Nanostru.*, vol. 112, pp. 128-136, 2019.
- [166] Nolan, N., Seery, M., and Pillai, S., "Spectroscopic investigation of the anatase-to-Rutile transformation of sol-Gel-Synthesized TiO₂ photocatalysts," *J. Phys. Chem. C*, vol. 113, pp. 16151-16157, 2009.
- [167] Kim, S. W., Khan, R., Kim, T. J., and Kim, W. J., "Synthesis, characterization, and application of Zr, S Co-doped TiO₂ as visible-light active photocatalyst," *Bull. Kor. Chem. Soc.*, vol. 29, pp. 1217-1223, 2008.
- [168] He, K., Zhao, C., Zhao, G., and Han, G., "Effects of pore size on the photocatalytic activity of mesoporous TiO₂ prepared by a sol-gel process," *J. Sol-Gel Sci. Technol.*, vol. 75, pp. 557-563, 2015.
- [169] Li, J., Xu, J., Dai, W. L., Li, H., and Fan, K., "Direct hydro-alcohol thermal synthesis of special core-shell structured Fe-doped titania microspheres with extended visible light response and enhanced," *Appl. Catal. B: Environ.*, vol. 85, pp. 162-170, 2009.
- [170] Noorjahan, M., Pratap, R. M., Durga, K. V., Lavédrine, B., Boule, P., and Subrahmanyam, M., "Photocatalytic degradation of H-acid over a novel TiO₂ thin Film

- fixed bed reactor and in aqueous suspensions,” *J. Photochem. Photobiol. A: Chem.*, vol. 156, pp. 179-187, 2003.
- [171] Valtierra, J. M., Servín, J. G., Reyes, C. F., and Calixto, S., “The photocatalytic application and regeneration of anatase thin films with embedded commercial TiO₂ particles deposited on glass microrods,” *Appl. Surf. Sci.*, vol. 252, pp. 3600-3608, 2006.
- [172] Kaur, J., and Singhal, S., “Heterogeneous photocatalytic degradation of rose bengal: Effect of operational parameters,” *Phys. B Condens. Mat.*, vol. 450, pp. 49–53, 2014.
- [173] Lu, D., Yang, M., Fang, P., Li, C., and Jiang, L., “Enhanced photocatalytic degradation of aqueous phenol and Cr (VI) over visible-light-driven TbxOy loaded TiO₂-oriented nanosheets,” *J. Appl. Surf. Sci.*, vol. 399, pp. 167-184, 2017.
- [174] Huang, M., Xu, C., Wu, Z., Huang, Y., Lin, J., and Wu, J., “Photocatalytic discolorization of methyl orange solution by Pt modified TiO₂ loaded on natural zeolite,” *J. Dy. Pigm.*, vol. 77, pp. 327-334, 2008.
- [175] Li, F., Sun, S., Jiang, Y., Xia, M., Sun, M., and Xue, B., “Photodegradation of an azo dye using immobilized nanoparticles of TiO₂ supported by natural porous mineral,” *J. Hazar. Maters.*, vol. 152, pp. 1037-1044, 2008.
- [176] Elmira, P., Mehdi, R., and Mokhtar, A., “Carbon and CNT fabricated carbon substrates for TiO₂ nanoparticles immobilization with industrial perspective of continuous photocatalytic elimination of dye molecules,” *J. Indus. Eng. Chem.*, vol.55, pp. 149-163, 2017.
- [177] Sampaio, M. J., Silva, C. G., Silva, A. M. T., Vilar, V. J. P., Boaventura, R. A. R., and Faria, J. L., “Photocatalytic activity of TiO₂-coated glass raschig rings on the degradation of phenolic derivatives under simulated solar light irradiation,” *Chem. Eng. J.*, vol. 224, pp. 32–38, 2013.
- [178] Toor, A. P., Verma, A., Singh, V., Jotshi, C. K., and Bajpai, P. K., “Treatment of bleaching effluents from the pulp and paper industry by photocatalytic oxidation,” *Tap. J.*, vol. 6, pp. 9–13, 2007.
- [179] Shende, T. P., Bhanvase, B. A., Rathod, A. P., Pinjari, D. V., and Sonawane, S. H., “Sonochemical synthesis of Graphene-Ce-TiO₂ and Graphene-Fe-TiO₂ ternary hybrid photocatalyst nanocomposite and its application in degradation of crystal violet dye,” *Ultrason. Sonochem.*, vol. 41, pp. 582-589, 2018.

- [180] Hsieh, S. H., Chen, W. J., and Wu, C. T., "Pt-TiO₂/graphene photocatalysts for degradation of AO7 dye under visible light," *Appl. Surf. Sci.*, vol. 340, pp. 9-17, 2015.
- [181] Nadimi, M., Saravani, A. Z., Aroon, M. A., and Pirbazari, A. E., "Photodegradation of methylene blue by a ternary magnetic TiO₂ /Fe₃O₄ /graphene oxide nanocomposite under visible light," *Mater. Chem. Phys.*, vol. 225, pp. 464-474, 2019.
- [182] Dionysiou, D. D., Suidan, M. T., Bekou, E., Baudin, I., and Lainé, J. M., "Effect of ionic strength and hydrogen peroxide on the photocatalytic degradation of 4-chlorobenzoic acid in water," *Appl. Catal. B Environ.*, vol. 26, pp. 153-171, 2000.
- [183] Maruthamani, D., Divakar, D., and Kumaravel, M., "Enhanced photocatalytic activity of TiO₂ by reduced graphene oxide in mineralization of Rhodamine B dye," *J. Ind. Eng. Chem.*, vol. 30, pp. 33-43, 2015.

APPENDIX

Appendix A: Experimental UV Reactor with Apparatus

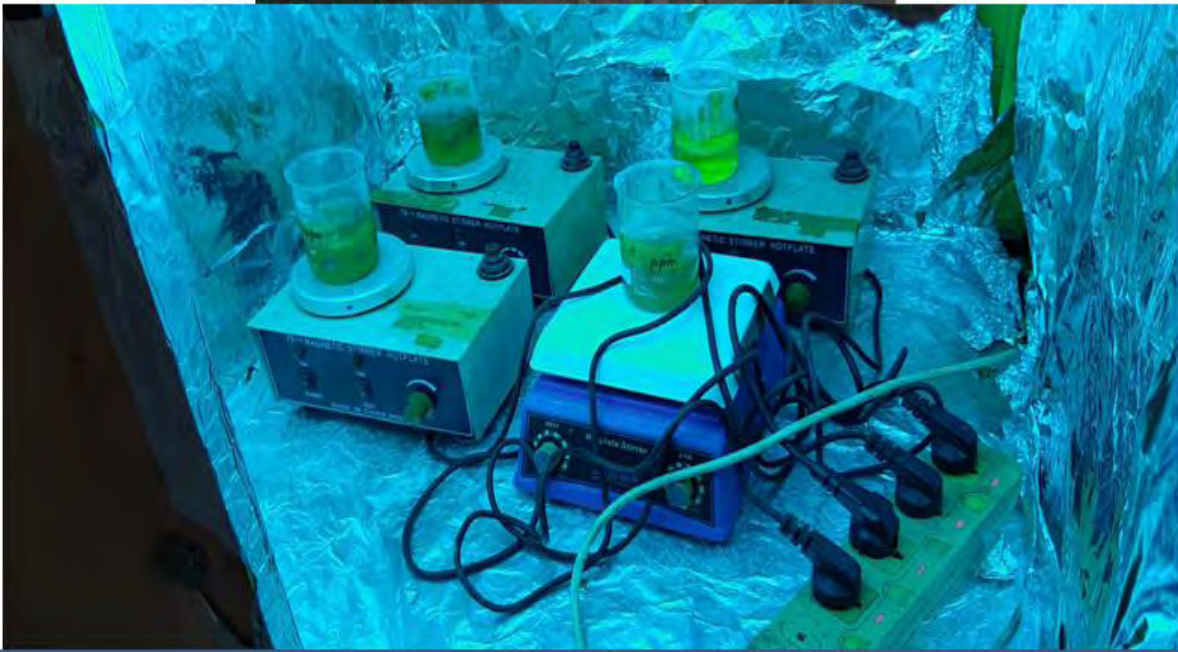


Figure A-1: Experimental UV Reactor with Apparatus

Appendix B: BET Isotherm Study

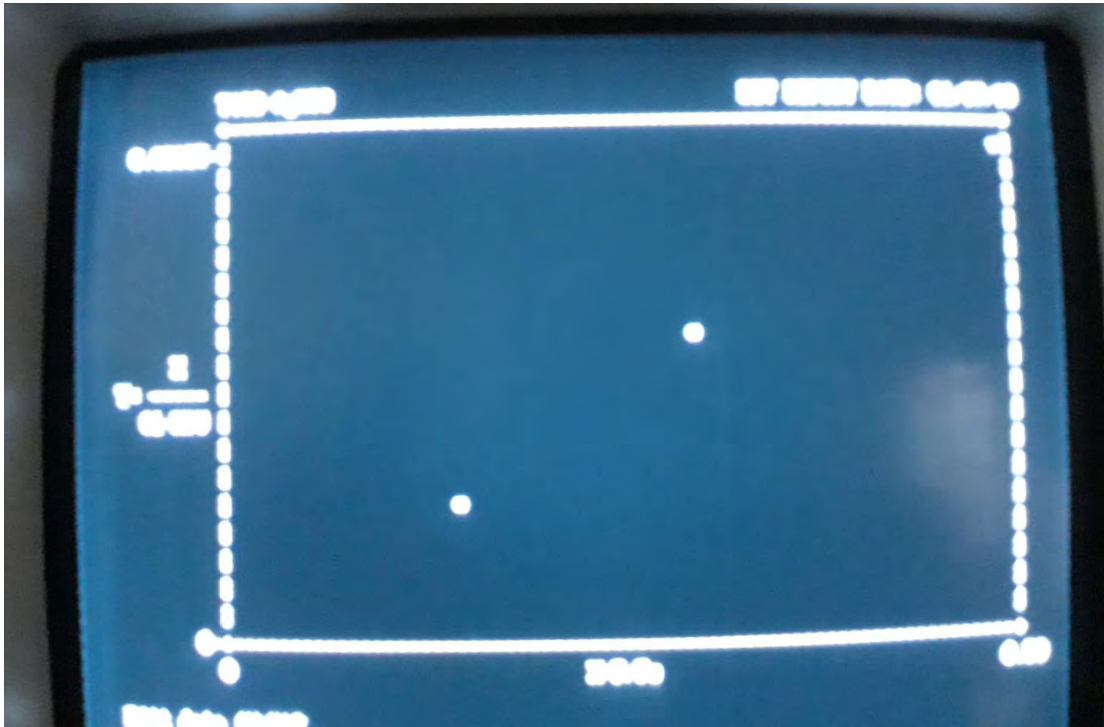


Figure B-1: Plot of BET isotherm of TiO₂ nanoparticle

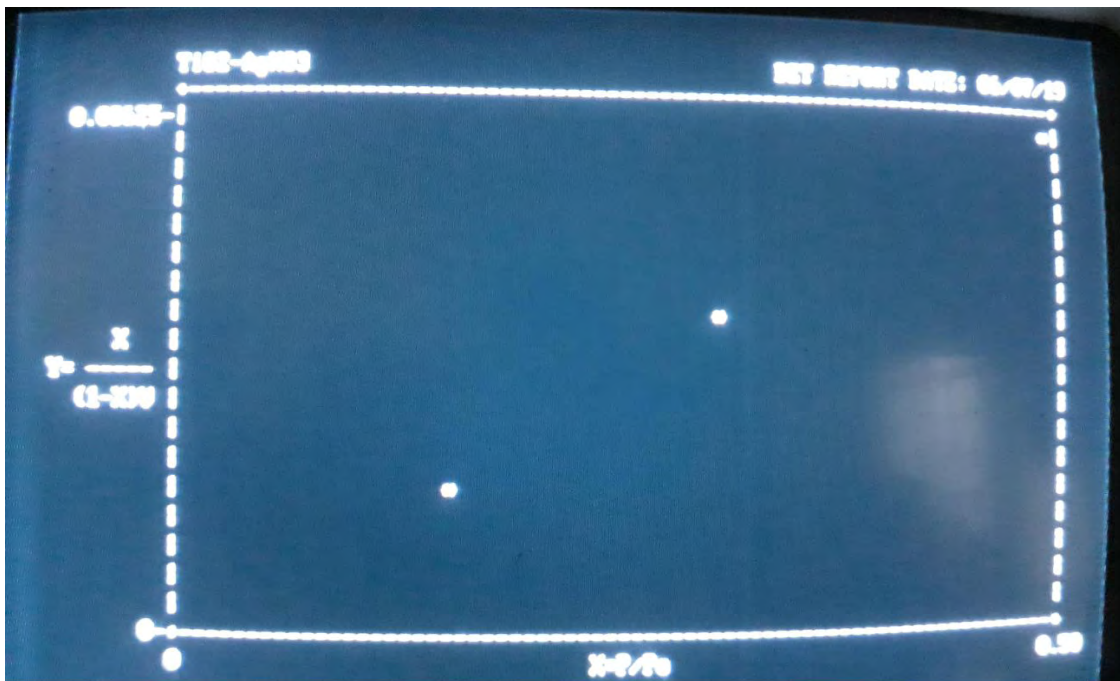


Figure B-2: Plot of BET isotherm of MoO₃/TiO₂ nanocomposite

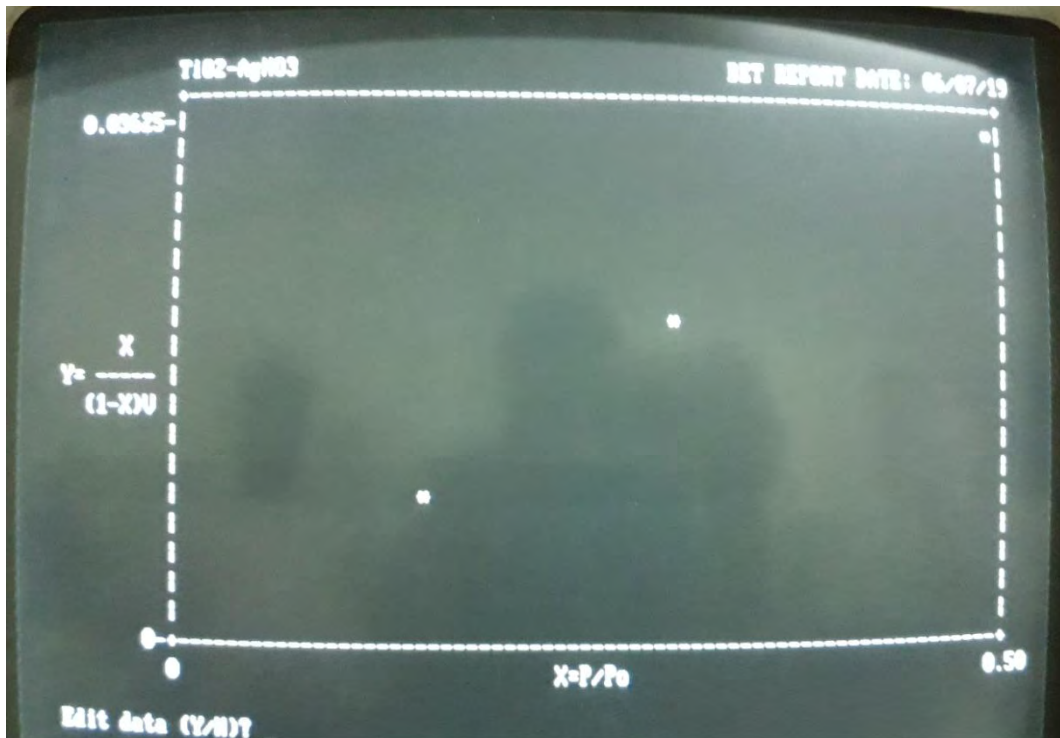


Figure B-3: Plot of BET isotherm of Ag/TiO₂ nanocomposite

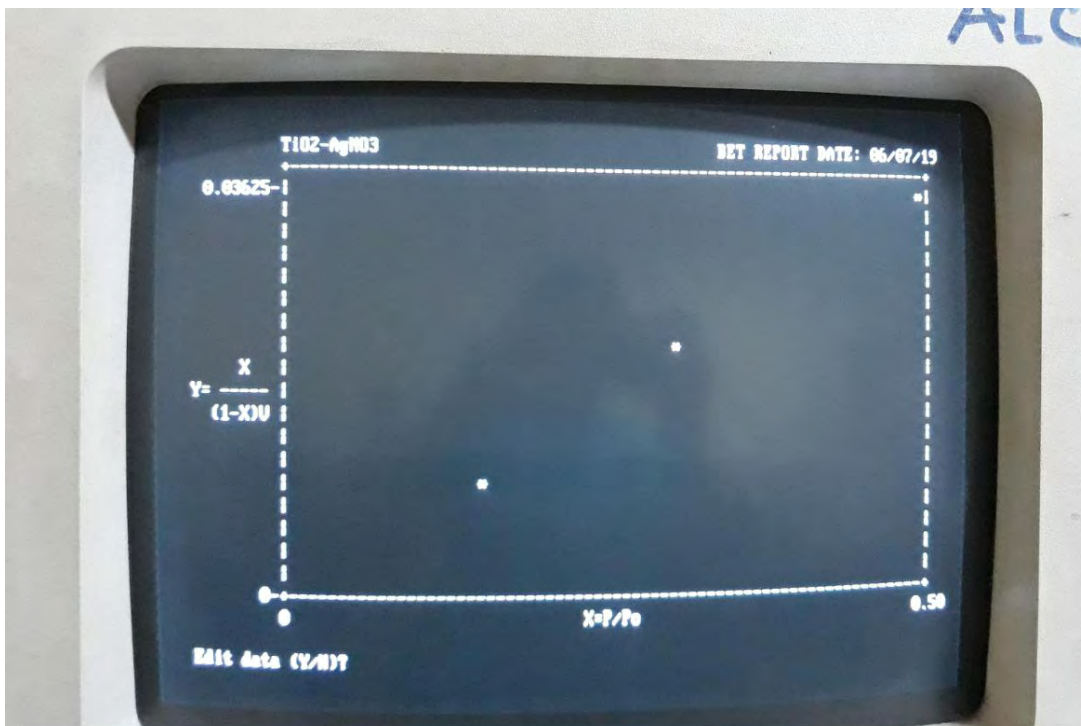


Figure B-4: Plot of BET isotherm of MoO₃/Ag/TiO₂ nanocomposite

Appendix C: Reaction Kinetic Study

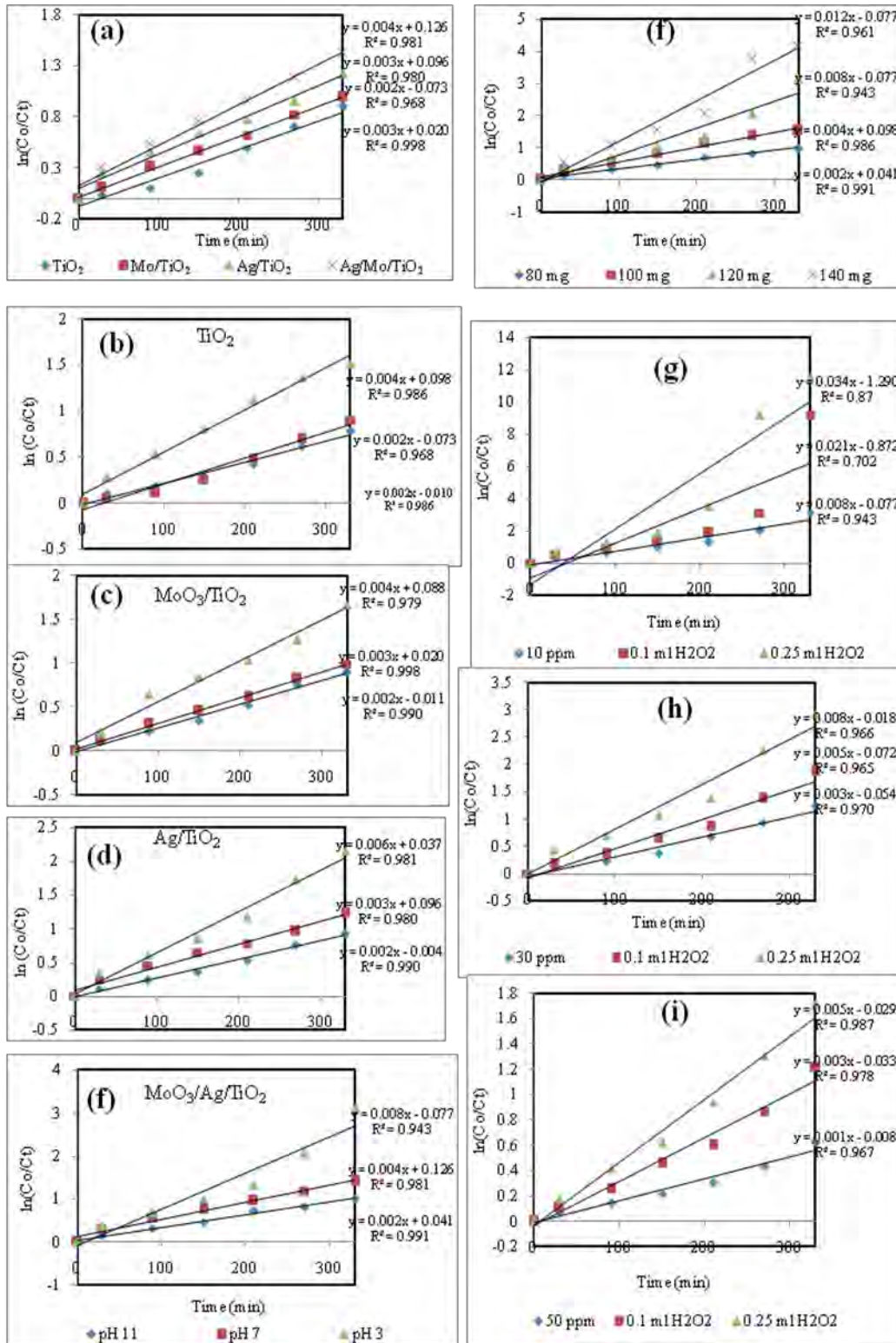


Figure C-1: Pseudo-first-order reaction kinetics of MO dye removal in presence of UV irradiation

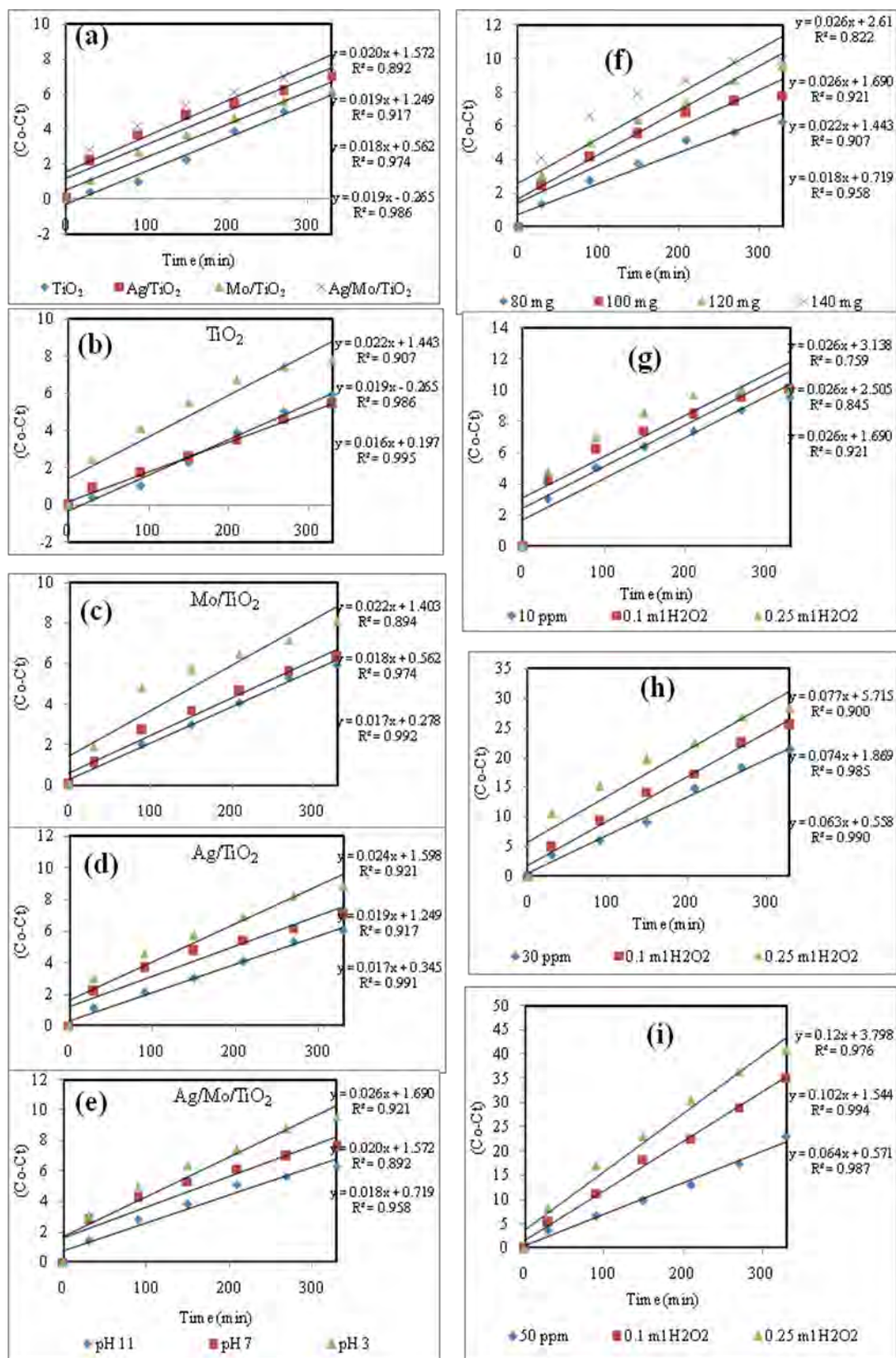


Figure C-2: Zero-order reaction kinetics of MO dye removal in presence of UV irradiation

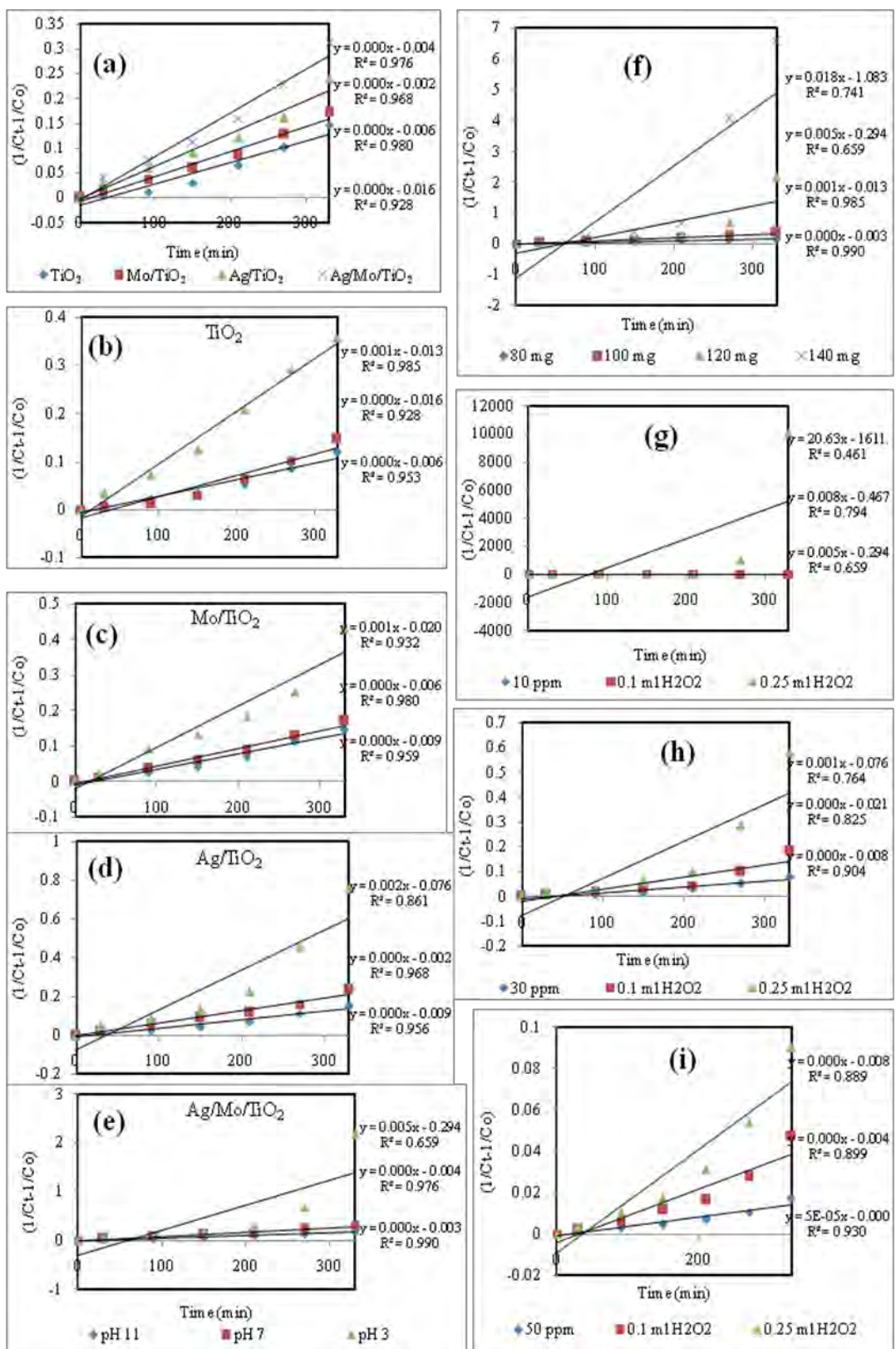


Figure C-3: Second-order reaction kinetics of MO dye removal in presence of UV irradiation